MOTIONAL STATES OF NO_2^- AND OTHER IONS IN KI SINGLE CRYSTALS

SUKHDEO SINGH KHATRI

DEPARTMENT OF PHYSICS
SCHOOL OF PHYSICAL SCIENCES

SUBMITTED IN FULFILMENT OF THE REQUIREMENT OF
THE DEGREE OF
DOCTOR OF PHILOSOPHY
TO

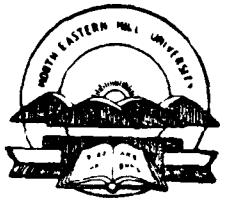

The North-Eastern Hill University
SHILLONG-793001
INDIA
APRIL, 1983

Professor A.L. Verma.
Department of Physics
School of Physical Sciences
North-Eastern Hill University
Laitumkhrah, Shillong-793003.
INDIA

phone : 4558
Grams : NEHU

CERTIFICATE

I certify that the thesis entitled "Motional states of NO_2^- and other ions in KI single crystals" submitted by Shri Sukhdeo Singh Khatri for the Degree of Doctor of Philosophy of the North-Eastern Hill University, Shillong embodies the record of original investigation carried out by him under my supervision. He has been duly registered and the thesis presented is worthy of being considered for the Award of Ph.D. Degree. This work has not been submitted for any Degree of any other University.

A.L. Verma
28.4.83
(A.L. Verma)
Supervisor

Dated: April 1983
Shillong.

Department of Physics
School of Physical Sciences
North-Eastern Hill University
Laitumkhrah, Shillong-793003.

phone : 4558
Grams : NEHU

CERTIFICATE

This is certified that Shri S.S. Khatri has cleared the following four Pre-Ph.D. courses obtaining 'A' grade (on seven point scale) in all of them.

	Course	G.P.A.	Grade
(1).	Laser Physics	5.23	A
(2).	Statistical mechanics-I (Phase Transitions)	5.00	A
(3).	Numerical methods	5.05	A
(4).	Molecular physics and Group theory-I	5.45	A

A.L. Verma
28.4.83
(A.L. Verma)
Professor and Head
of the Department.

ACKNOWLEDGEMENTS

I should like to express my deep sense of gratitude to Prof. A.L. Verma for suggesting me the research problem, his constant guidance, advice, encouragement and help throughout the entire course of my Ph.D. programme. I am also grateful to Prof. J. Van der Elsken of the University of Amsterdam, Amsterdam, in whose laboratory most of the experimental work was done by Prof. A.L. Verma. I am thankful to all the faculty members for their encouragement and help during the course of the work.

I would like to express my thanks to all my friends and colleagues for their help during the course of this work. Thanks are also due to Mr. R. Sadhu for his adept typing and Mr. MacDonald Lakiang for cyclostyling.

I am extremely grateful to my parents for their patience, help and encouragement during the entire period of my research.

S. S. Khatri

(S.S. Khatri)

CONTENTS

Page

CHAPTER VI

Temperature Dependence of Half-Width and Frequency Shift of the Gap Mode of the NO_3^- Ion in KI.

SYNOPSIS

MOTIONAL STATES OF NO_2^- AND OTHER IONS IN KI SINGLE CRYSTALS

This thesis deals with the behaviour of polyatomic molecular impurities in alkali halide crystals, their localized and reorientational states and the interaction effects among impurities. The thermal, mechanical and many other properties of solids are strongly dependent on the orientational degree of freedom of its constituents and impurities. Therefore a systematic study of different orientational motions of ions in solids may lead to better understanding of the properties of solids containing molecular impurities.

A number of small ions or dipolar impurities dissolved as solid solution in alkali halide single crystals in small concentrations are known to occupy substitutional positions with discrete orientations in the lattice (Barker and Sievers 1975). The equilibrium orientations of dipoles are determined by the directions of potential energy minima within the lattice site they occupy. The dipolar impurities at low temperatures can reorient themselves among the equivalent potential wells due to

overlapping of wave functions of the oriented dipolar states leading to tunnel splitting of the orientational degeneracy. The tunnel splitting is extremely sensitive to the details of crystal field due to the host lattice. Another interesting problem is that of modes due to pairs and triplet clusters of impurities in alkali halide crystals. At relatively higher concentrations, formation of pairs and triplet cluster of impurities are favoured. The coupling between the impurities in a pair or triplet cluster gives rise to localized modes.

We have studied the tunneling modes, and modes due to pairs and triplet clusters of the NO_2^- ions doped in KI single crystals at 1.7 K. The nitrite ion is a bent dipolar ion. When it is doped in potassium iodide crystal it replaces the iodide ion such that its dipole moment points in the [110] direction with its O-O axis along the [001] direction in the KI lattice. It has a dipole moment of 0.97 Debye in KI (Sack and Moriarty 1965). This large dipole moment indicates that it is off-centred and is displaced along the $\langle 110 \rangle$ direction. Hence it has twelve equilibrium orientations. At very low concentrations of the impurity ($\sim 10^{17}$ ions cm^{-3}), the ν_3 vibration (antisymmetric stretch) of the NO_2^- ion shows multiplet structure. We have explained this structure as resulting from the tunneling

of the ion among the twelve $\langle 110 \rangle$ equivalent potential wells for the ion in the KI lattice (Khatri and Verma 1983a). The tunneling of the ion in KI has been explained in terms of the Gomez, Bowen and Krumhansl model (Gomez et al 1967). From these studies we have found that the probability for the tunneling of the ions among the next nearest-neighbour wells is largest whereas nearest-neighbour tunneling probability is small. From the observed splittings, we have estimated the potential barrier heights for different types of tunneling motions of the NO_2^- ion in KI. At relatively higher concentrations ($\sim 10^{19}$ ions cm^{-3}), the infrared spectra of the KI:NO_2^- crystals at 1.7 K in the ν_3 fundamental vibration region of the NO_2^- ion shows many distinct side bands on both sides of the main ν_3 absorption peak. The intensities of these side bands show non-linear (roughly quadratic) dependence on concentration. The structure on the low frequency side is more pronounced than that on the high frequency side. These side bands have been explained as arising from the electrostatic coupling between the transition dipole moments of the NO_2^- ions occuring in pairs and triplet clusters. We have considered different types of pairs and triplet clusters of the ions in KI and their calculated mode frequencies are in reasonable agreement with the experimental observations (Khatri and Verma 1983b). The calculations are based on a

coupled harmonic oscillator model (De Souza and Luty 1973) where the coupling is provided by the interaction between the transition dipole moments of the NO_2^- ions during their ν_3 vibrations. From these studies we have estimated the magnitude of the transition dipole moment of the NO_2^- ion in KI.

Temperature dependent studies of the localized modes can provide useful information about the interaction between the local mode and lattice phonons. There have been numerous studies, both experimental and theoretical (Barker and Sievers 1975) on the temperature dependence of the width, position and intensity of local modes and resonant modes of several substitutional impurities in alkali halide hosts but hardly any study on infrared active gap mode has yet been possible. The reason is that the difference band absorption of the host lattice dominates the spectral region near the gap and thus masks the impurity induced absorption in the gap above around 10 K. It would be of considerable interest to study the temperature dependence of the gap modes in a suitable system and see whether similar mechanism can explain the temperature dependent effects for the gap mode which have been so successful in understanding the temperature dependent effects for the local and resonant modes.

The NO_3^- ion substituted in KI induces two gap modes at $\sim$73 cm^{-1} and $\sim$88 cm^{-1} (Metselaar and Van der Elsken 1968, Eijnthoven 1970) and they appear as side bands to the ν_3 fundamental vibration of the NO_3^- ion in KI. We have investigated the temperature dependence of the half-width and centre frequency of the ν_3 fundamental and its combination with the 73 cm^{-1} gap mode from 1.7 to 77 K. Information about the variation of half-width and centre frequency of the gap mode as a function of temperature is extracted from this study which can be satisfactorily explained in terms of anharmonic interactions of the gap mode with lattice phonons (Khatri and Verma 1982).

This thesis consists of seven chapters. Chapter I introduces the problem and outlines the controversies and confusing interpretations given by earlier workers about the motional states of the NO_2^- and NO_3^- ions doped in KI.

Chapter II presents the theoretical background to understand the different kind of motional states and localized modes of ions substituted in alkali halides. A brief review on the tunneling states, pair modes and temperature dependence of localized modes of various impurities in alkali halide hosts is also given in this chapter.

Chapter III deals with the experimental techniques like sample preparation, modified instrumental arrangement to attain higher resolution and helium cooled detector etc.

In chapter IV the tunneling motion of the NO_2^- ions in KI has been discussed. Studies made by earlier workers on the NO_2^- ion doped in alkali halides have been briefly described. From the observed splitting of the ν_3 fundamental vibration of the NO_2^- ion in KI, we have calculated various tunneling matrix elements. We have also calculated potential barrier heights for different types of tunneling motions of the NO_2^- ion in KI. From the magnitudes of these matrix elements and barrier heights, conclusions have been drawn about the nature of tunneling motions performed by the ion.

Chapter V contains the discussion of the modes arising due to pairs and triplet clusters of the NO_2^- ions in KI. In this chapter we have calculated the interaction energies between the permanent dipole moments of the NO_2^- ions and also between the induced dipole moments of the ions during their ν_3 vibration when the NO_2^- ions form pairs and triplet clusters in KI. From this we have calculated the position of various satellite bands observed in the vicinity of ν_3 vibration of the NO_2^- ion. We have also estimated the value of the induced (transition) dipole moment of the ion during its ν_3 vibration.

In chapter VI we have discussed the temperature dependence of the half-width and frequency shift of the 73 cm^{-1} gap mode of the NO_3^- ion in KI. From this study we have estimated the values of the effective Debye temperatures θ_C and θ_D, and coupling coefficients β , δ and $\alpha(A_{1g})$, which provide clues to the nature of coupling of the gap mode with lattice phonons.

The last chapter presents the conclusions derived from the present work.

REFERENCES

1. Barker A.S. Jr. and Sievers A.J. 1975 Rev. Mod. Phys. 47, Suppl. 2, S1.

2. De Souza M. and Luty F. 1973 Phys. Rev. B8, 5866.

3. Eijnthoven R.K. 1970 Ph.D. thesis, University of Amsterdam, Amsterdam.

4. Gomez, M., Bowen S.P. and Krumhansl J.A. 1967 Phys. Rev. 153, 1009.

5. Khatri S.S. and Verma A.L. 1982 J. Phys. C: Solid State Phys. 15, 1143.

6. Khatri S.S. and Verma A.L. 1983a J. Phys. C: Solid State Phys. 16 (in press).

7. Khatri S.S. and Verma A.L. 1983b Phys. Lett. (accepted for publication)

8. Metselaar R. and Van der Elsken J. 1968 Phys. Rev. 165, 359.

9. Sack H.S. and Mariarty M.C. 1965 Solid State Commun. 3, 93.

CHAPTER - I

INTRODUCTION

If an atom in a pure crystal lattice is replaced by another atom or molecular group, the crystal is said to contain impurities. Presence of impurities in pure crystalline solids changes their properties like dielectric constant specific heat, thermal conductivity etc. The thermal, mechanical, electrical and many other properties of solids are strongly dependent on the orientational degree of freedom of the constituents of the solids and on the presence of impurities. Introduction of impurities in crystal destroys the periodicity of the lattice and affects its potential energy function leading to modifications in the vibrational characteristics of the host crystals. Weakly coupled or lighter impurities may induce non-propagating vibrational modes at frequencies where the normal lattice vibrations of the host crystal may not occur. Depending on the nature and coupling of impurities with the host lattice, they may induce localized modes, gap modes, resonant modes and reorientational or tunneling modes if the concentration of impurities is small. Coupled modes due to interactions among impurities themselves may also arise if the concentration of impurities is large.

The frequencies of these exceptional modes are determined mainly by the intermolecular forces between the impurity and the surrounding lattice and hence their study has become an important means of investigation of the interaction potential between the impurities and the host lattice. The knowledge of this potential is also of importance for a better understanding of the properties of pure crystals themselves. Moreover, the orientational freedom of molecular groups or impurities in solids depends on four parameters: The height and symmetry of the potential in which the impurity ion moves, the rotational moment of inertia of the impurity and the temperature of system. In order to understand all these phenomenon associated with the motion of impurities, a definite knowledge of the potential in which the impurity ion performs different types of motion is important.

The potential energy for a crystal containing impurities can be expressed as:

$$H_i = H_i^o + H_i' + \sum_j H_{ij} + H_{Li} \qquad \ldots \qquad (1.1)$$

where H_i^o is the potential energy of the impurity in free state, i.e., the unperturbed part, H_i' is the perturbation due to crystal field and it is a static field effect. This term gives the effect of surrounding lattice in its

equilibrium configuration on impurity. In the case of a complex ion, it gives rise to shift in the internal vibration frequencies of the impurities. This term may also give rise to a number of possible equilibrium configurations of impurities in crystals which may or may not be situated on the normal lattice site. In that case a tunneling from one configuration to another may take place. The term $\sum_{J} H_{ij}$ is the dynamic field effect which is responsible for the coupling between the impurities in crystals giving rise to pair modes and modes due to clustering of impurities. The last term H_{Li} in the expansion represents the interaction between the host lattice and impurities. This term is responsible for giving rise to various types of localized modes which are non-propagatory modes. In the case of complex ions, interaction between the internal vibrations of the ion and the lattice modes can lead to combination bands in the mid-infrared region. Therefore, the knowledge of the potential is necessary in order to understand the effect of these interaction terms on the properties of the system.

Most of such studies have been made in ionic crystal hosts such as alkali halides. This is because of their simpler crystal structure and they are easier to grow and purify. Moreover, these crystals have been studied extensively and their lattice dynamics has been understood quite thoroughly. Consequently, alkali halide

crystals have become ideal hosts for the study of impurity modes. There has been considerable amount of work, theoretical as well as experimental, in case of monatomic impurities substituted in alkali halide crystals. The far-infrared spectra of alkali halides doped with monatomic impurities involving localized states, reorientational or tunneling states etc have been understood quite satisfactorily. Polyatomic impurities, however, present more difficulties due to their complex structures as compared to the monatomic impurities. But there is an advantage with polyatomic impurities that various types of modes can be observed as side bands to internal vibrations of the impurities in the mid-infrared absorption where high resolution can be attained rather easily. In the present work the behaviour of polyatomic impurities like nitrite and nitrate ions in potassium iodide single crystals has been studied. We have chosen these particular defect-host systems because the motional states of the NO_2^- ion in KI by earlier workers were not understood properly mainly due to inadequate resolution and proper choice of samples. Moreover, KI has a well-defined gap between its acoustical and optical phonon branches, which most of the other alkali halides do not have. Therefore potassium iodide is a suitable host for studying gap modes due to impurities. We have studied the temperature dependence of the gap mode of the NO_3^- ions in KI.

Many atomic or molecular impurities substituted in crystals are known to produce isolated dipoles. Such impurities can be divided into two groups: (1) those having intrinsic dipole moments such as NCO^-, CN^- or NO_2^- and (2) those in which the defect-host combination itself produces an effective dipole such as Li^+ in KCl, F^- in NaBr, Ag^+ in RbCl etc. Both of these types of defects are called paraelectric defects and are characterized by their dipole orientations in crystals, ie, the off-centre displacement direction for a monatomic impurity or the direction of dipolar axis for polyatomic impurities. The molecular impurities may also be off-centred because it is possible that the normal lattice site may not be a stable equilibrium position, the impurity ion then will move off-centre until it finds a new equilibrium position.

When a small impurity ion replaces a large host ion in an alkali halide, the large decrease in the repulsive potential can lead to an instability at the normal lattice site. The actual position of the ion depends primarily upon a delicate balance of repulsive and polarization energies. A large repulsive interaction tends to keep the ion in place, while a high polarizability will tend to move it off the normal lattice site. The equilibrium orientations of the dipoles at low temperatures are determined by the directions of the potential energy minima within the multiwell potential

produced by the crystalline field of the host lattice at the substitutional site. In either case, the motion of the impurity occurs in a local potential well of lower symmetry than the octahedral symmetry of the lattice. In order to agree with the symmetry of the lattice surrounding the impurity, the dipolar direction can be along the six $\langle 100 \rangle$ directions, the eight $\langle 111 \rangle$ directions or the twelve $\langle 110 \rangle$ directions having C_{4v}, C_{3v} or C_{2v} as local symmetries respectively. The dipolar impurities substituted in alkali halides have an interesting possibility of reorienting themselves at very low temperatures ($KT \ll Vo$) along several equilibrium directions of the host lattice by tunneling among the equivalent potential wells in crystalline lattice. The overlapping of the oriented dipolar states leads to a periodic motion of the ion among multiwell potential with a characteristic tunnel splitting which is extremely sensitive to the details of the crystal field of the host lattice. There has been a great deal of experimental and theoretical work on low-lying motional states of dipolar impurities substituted in alkali halide crystals (Narayanamurti et al 1970, Barker and Sievers 1975). A brief review on the work done so far on tunneling states is given in chapter II for completeness.

The KI:NO_2^- system has been investigated previously by several workers (Narayanamurti et al 1966, Evans and Fitchen 1970, Sack and Mariarty 1965, Rebane et al 1974, Avarma and Rebane 1969) in order to understand various types of impurity modes. Narayanamurti et al (1966) observed large band-width associated with the ν_3 fundamental vibration of the NO_2^- ion in KI which showed a stronger temperature dependence than in KCl. Even at 1.7 K we observed large band-width associated with the ν_3 absorption band of the NO_2^- ion in KI. The large band-width which could not be resolved due to inadequate instrumental resolution and relatively large concentrations of the NO_2^- ions used in KI by earlier workers, is interpreted by us as arising due to the tunneling of the NO_2^- ions among several equivalent potential wells. In the present work we have studied motional states of the NO_2^- ions in KI due to tunneling. We have measured the high resolution infrared spectra of the KI:NO_2^- system for both the low and high impurity concentrations at very low temperatures. To study the tunneling behaviour of the ion, it is essential to use thick samples having very low concentrations of the NO_2^- ions to ensure that the ions are isolated from one another. With increasing concentration, the electrostatic coupling between the ions causes new absorption bands close to the vibrational bands of the isolated ions, which will be discussed later in details

At low concentrations ($\sim 10^{17}$ ions cm^{-3}) a very complex and temperature dependent structure, with at least six components, with the antisymmetric stretching vibration ν_3 of the NO_2^- ion is observed which is interpreted as arising from the tunneling of the NO_2^- ion among the twelve $\langle 110 \rangle$ equivalent orientations of the ion at 1.7 K. From the observed unequal tunnel splitting of the ν_3 fundamental vibration, we have estimated potential barriers for reorientation of the ion due to different types of tunneling motions.

Tunneling is purely a quantum mechanical phenomenon. It means penetration of a potential barrier by a particle, which is forbidden in classical mechanics. In classical picture a particle confined by a potential barrier cannot overcome the barrier unless it aquires energy equal to or greater than that of the barrier. But in quantum mechanical picture, where a particle is described by its wave function and is not, strictly confined to the well, it has a finite probability of being found on the other side of the barrier also even though its energy may be less than the barrier height. If the wave function of the particle is extending out side the region of potential barrier, then it has a finite probability of penetrating the barrier and escape, such a motion is known as tunneling. An impurity inside a

solid or molecule may have two or more energetically identical equilibrium orientations, but different configurations. In other words it may have two or more potential wells separated by potential barriers. Now if barrier height is very high compared to kT, the atom can not go to next configuration without getting extra energy. But in quantum mechanical picture the overlapping of the wave function of the atom in different wells leads to tunneling; i.e., the atom can penetrate the potential barrier and go to the next configuration. The resultant wave function of the atom will be time-dependent giving rise to a periodic motion of the atom among different equilibrium configurations. In contrast to the thermally activated processes, this motion is temperature independent. The particle must be localized initially at least in one of the wells otherwise the term tunneling is not meaningful. Tunneling removes the original degeneracy of the ground state and splits it into a number of components. This will be discussed in detail in chapter II.

The tunneling modes constitutes a special group of impurity modes having a number of interesting properties. Their frequencies are small compared to the Debye frequencies of the host whose density of phonon modes is very low in this frequency region. These impurity modes can therefore be considered separately from the motional

states of the host which makes their theoretical treatment particularly simple.

Although tunneling modes are relatively weakly coupled to the host compared to the in-band impurity modes (resonant modes) of higher frequencies, they are still pronounced phonon scatterers. Consequently they lend themselves to the study of phonon-defect interactions. Most of the paraelectric impurities in crystals have net electrical dipole moments and therefore are electrically polarizable. Hence the impurities behave like a gas of electric dipoles. This fact allows the study of the dielectric properties of a gas without the limiting influence of condensation at low temperatures. The tunneling states can be considered as the electrical analogs to the magnetic spin states of impurities and therefore allows one to do a variety of experiments previously restricted to spin states. Analogous to cooling by adiabatic demagnetization, they show paraelectric cooling effect.

The mixed crystals having dipolar impurities capable of performing tunneling motion, may show cooperative phenomenon, i.e., they may show an ordered state when the average dipole-dipole interaction energy exceeds the tunneling energy. This has been examined theoretically (Fischer and Klein 1976) but no experimental evidence on any system has been found.

These properties of tunneling states allow them to be investigated by a number of different techniques. They have been investigated by thermal conductivity measurements, dielectric constant measurements, specific heat measurements, paraelectric resonance, paraelectric cooling, spectroscopic techniques, ultrasonic attenuation, NMR, resonant scattering of tunable phonons, microwave absorption techniques etc. These various techniques will be discussed briefly in chapter II.

During several recent experiments on a number of alkali halide-impurity systems, it has been observed that for higher impurity concentrations interactions between impurity ions become important and modes due to pair of ions have been observed (Templeton and Clayman 1971, Becker and Martin 1972, Moller et al 1970, De Souza and Luty 1973 etc). In case of polyatomic ions, the coupling of internal vibrations of different ions may have a profound influence on the absorption spectrum. This may lead to asymmetric broadening of absorption bands and may give rise to extra features. Narayanamurti et al (1966) observed many broad bands near the ν_3 absorption band but they could not explain the origin of these lines properly. At relatively higher concentrations of the NO_2^- ions in KI, we have observed closely-spaced side bands on the low and high frequency sides of the main ν_3 vibration whose

relative intensities are temperature independent. These side bands are interpreted as arising from electrostatic coupling of the transition dipole moments during ν_3 vibration of the nearby NO_2^- ions in KI. Several configurations of the NO_2^- ions pairs and triplet clusters were detected and their mode frequencies were found in reasonable agreement calculated from a model of coupled harmonic oscillators where the coupling is provided by the electric dipolar interactions. From these studies we have estimated the magnitude of the transition dipole moment of the NO_2^- ions during its ν_3 vibration in KI.

Another aspect of our present work is to study the temperature dependence of the gap mode of the NO_3^- ion in KI. The NO_3^- ion is preferred to the NO_2^- ion for such type of study because the NO_2^- ions in KI has larger tunneling probability whereas the NO_3^- ion in KI has large barrier heights for librational motion and hence for tunneling as suggested by Narayanamurti et al (1966). This is confirmed by the sharp features of the infrared absorption band arising due to internal vibrations of the NO_3^- ions in KI. So the gap mode due to the NO_2^- ions in KI are likely to have broadening due to tunneling creating more complications. To avoid these complications, we have chosen KI:NO_3^- system for such study.

Introduction of impurities in ionic crystals destroys the periodicity of the lattice and this may modify the vibrational characteristics of the host crystal. These impurities may induce non-propagating vibrational modes at frequencies where the normal lattice vibrations of the host crystal may not occur. These are called local modes if they occur at higher frequencies than the highest frequency phonon mode, gap modes if they occur in a forbidden gap between the acoustic and optical phonon branches and resonant or band modes if they fall within an allowed frequency band of lattice phonons. A study of all these localized modes of impurities in host lattice is an important means for investigating the interaction potential between the impurity and the host lattice as well as for better understanding of the properties of pure crystals themselves.

Temperature dependent studies of the localized modes can provide useful information about the interactions between the local mode and lattice phonons. There have been numerous studies, both experimental and theoretical, on the temperature dependence of the width, position and intensities of local and resonant modes of several substitutional impurities in alkali halides using far-infrared absorption techniques as reviewed by Barker and Sievers(1975). In contrast, hardly any temperature dependent measurements

on the infrared active gap modes have yet been possible. The reason is that the difference band absorption of the host lattice dominates the spectral region near the gap and thus masks the impurity-induced absorption in the gap above around 10K. Although there are no phonons in the forbidden gap at very low temperatures, gap mode states due to the impurities appear whose eigen vectors involve the motion of nearest-neighbours along with it. It would be of considerable interest to study the temperature dependence of gap modes in a suitable system and see whether similar mechanisms can explain the temperature dependent effects for gap modes which have been so succssful for explaining these effects for local modes.

In this part of the work we shall investigate the temperature dependence of the band-width and frequency shift of the gap mode of the NO_3^- ion in KI which appears at $\sim 73\ cm^{-1}$. Substitution of impurities in an otherwise perfect crystal changes its symmetry for the vibrational transitions. The symmetry of the molecular impurity is determined, besides by the symmetry of the molecule and the symmetry of the lattice site of the host crystal, also by the orientation of the molecular axis relative to the crystal axes. In case of the NO_3^- ion with D_{3h} symmetry substituted in KI, its three-fold axis coincides with the cube diagonal of the KI unit cell resulting in a C_{3v} site symmetry. The original triply degenerate gap mode in O_h

symmetry splits into A and E components and induces two gap modes at 72.92 ± 0.05 and 87.93 ± 0.05 cm^{-1} in the phonon gap of KI. Due to the anharmonicity of the oscillator potential, these gap modes may appear as side bands to the strong ν_3 internal vibration of the NO_3^- ion in KI. These have been observed in the mid-infrared as sidebands(Metselaar et al 1968) as well as in the far-infrared absorption directly (Eijnthoven 1970, Renk 1965). From an experimental point of view, it is a great advantage that the gap modes can be observed as combination bands in the mid-infrared and are amenable for temperature variation studies without any interference from background absorption. Moreover, the high resolution attainable in this frequency region can allow observations of very small frequency shifts and band-widths rather easily.

The ν_3 fundamental vibration (antisymmetric stretch) of the nitrate ion ($^{14}NO_3^-$) in KI gives rise to a very strong and sharp band at 1372.50 cm^{-1} even at room temperature. We have measured the temperature dependence of the band-width and centre frequency of the ν_3 fundamental of the $^{15}NO_3^-$ isotope in KI in natural abundance and of the combination band of the 73 cm^{-1} gap mode with the ν_3 fundamental of the $^{14}NO_3^-$ isotope in KI. From these studies we have extracted information about the temperature dependence of the gap mode of the $^{14}NO_3^-$ ion in KI and

results are discussed in light of anharmonic interactions between the gap mode and the host lattice phonons.

REFERENCES

1. Avarma R. and Rebane L. 1969. Phys. Status Solidi 35, 107

2. Barker A.S. Jr. and Sievers A.J. 1975 Rev. Mod. Phys. 47, Suppl. 2, S1.

3. Becker C.R. and Martin T.P. 1972 Phys. Rev. B5, 1604.

4. De Souza M., Gongora A., Aegerter M. and Luty F. 1970 Phys. Lett. 25, 1426.

5. Eijnthoven R.K. 1970 Ph.D. Thesis, University of Amsterdam, Amsterdam (unpublished).

6. Evans A.R. and Fitchen D.B. 1970 Phys. Rev. B2, 1074.

7. Fischer B. and Klein M.V. 1976 Phys. Rev. Lett. 37, 756.

8. Metselaar R. and Van der Elsken J. 1968 Phys. Rev. 165, 359.

9. Moller W., Kaiser R. and Bilz H. 1970 Phys. Lett. 32A, 171.

10. Narayanamurti V. and Pohl R.O. 1970 Rev. Mod. Phys. 42, 201.

11. Narayanamurti V., Seward W.D. and Pohl R.O. 1966 Phys. Rev. 148, 481.

12. Rebane L.A., Khal'dre T. Yu., Novik A.E. and Gorokhovskii A.A. 1974 Sov. Phys. Solid State 15, 2129.

13. Renk K.F. 1965 Phys. Lett 14, 281.

14. Sack H.S. and Moriarty M.C. 1965 Solid State Commun. 3, 93.

15. Templeton T.L. and Clayman B.P. 1971 Solid State Commun. 9, 697.

CHAPTER II

2.1. THEORETICAL BACKGROUND AND VARIOUS MODELS FOR TUNNELING STATES

There has been a great deal of theoretical as well as experimental work on tunneling states of atoms and molecules in solids (Narayanamurti and Pohl 1970 and Barker and Sievers 1975). Various theoretical models have been developed in order to understand the tunneling states of atoms and molecules in solids. We shall review the models proposed by Hund (1927), Pauling (1930), Devonshire (1936) and Gomez et al (1967) which have been particularly useful for the understanding of the tunneling states. Hund (1927) described the tunneling of nitrogen atom in ammonia molecule with the help of double well harmonic oscillator. This model was later extended for tunneling of impurities in solids among multiwell potential wells by Gomez et al (1967) which is also known as GBK model. Pauling (1930) developed the model for tunneling of molecules capable of rotating in one plane and having two equivalent potential minima. In such a potential, the rotational states of the molecules are perturbed due to the possibility of tunneling. Later on, Devonshire (1936) calculated the effect of octahadral symmetry on the rotational states of a linear molecule. This is the generalization of the Pauling's (1930) one dimensional model into three dimensional model.

Devonshire potential is a function of the angular coordinates only and does not involve motion of the centre of mass of the impurity.

2.2 HUND'S MODEL

Application of the new quantum mechanics to the theory of molecular spectra by Hund (1927) lead to the following problem: the atoms in a polyatomic molecule can exist in configurations which are different but energetically identical. A well known example is that of sugar molecule which has two optical isomers. These two isomers are mirror images of each other and hence they have equal potential energy. Another example is that of ammonia molecule. The potential energy of nitrogen atom in ammonia is the same whether it is above the plane formed by the three hydrogen atoms or below it. Classically a flip over becomes very unlikely when the energy barrier separating the two configurations is very large compared to kT. In quantum mechanical picture, the particle can penetrate the potential barrier and go to the next configuration. Hund (1927) studied such a problem for ammonia molecule where nitrogen atom is subjected to a two-well harmonic potential and has two equilibrium positions above and below the plane formed by the three hydrogen atoms. He found that the oscillatory states occur in pairs, the separation between the pairs is approximately $\hbar\omega_E$, where ω_E is the harmonic-oscillator

frequency for the single well. Each pair consists of a symmetric state of lower energy and an antisymmetric state of higher energy. The energy difference between these two states is $\hbar\omega_t$ where ω_t is the tunneling frequency of the nitrogen atom. Barker (1929) first suggested the existence of tunneling-splitting in gaseous ammonia. Cleeton and William (1934) measured directly the tunnel splitting in the molecule through microwave absorption experimentally for the first time. This proved the correctness of Hund's prediction. Therefore, the work by Hund represents the first instance of the penetration of potential barrier by a particle.

For a double well harmonic oscillator, the tunneling frequency ω_t between the lowest two states is given, to a very good approximation, by (Merzbacher, 1970).

$$\omega_t = \frac{\Delta E_t}{\hbar} = 2\omega_E \left[\frac{2V_o}{\hbar\omega_E}\right]^{1/2} \exp\left[-\frac{2V_o}{\hbar\omega_E}\right] \quad \ldots \quad (2.1)$$

Because of the exponential form of equation 2.1, if the barrier height $V_o > \hbar\omega_E$, ω_t depends critically on the ratio of barrier height to oscillator energy $\hbar\omega_E$. For a typical $\hbar\omega_E$ = 0.1 eV(1000 cm^{-1}), the tunneling period varied between 10^{-9} sec and 10^9 years if $\frac{2V_o}{\hbar\omega_E}$ varied

between 10 and 70. Consequently, a modest barrier height V_o of few electron volts could produce an essentially infinitely stable molecule.

2.3 TUNNELING OF IMPURITIES IN SOLIDS AND PAULING'S MODEL

The rotational states of free molecules are modified when they crystallize into a lattice. This effect was first studied by Pauling (1930). He approximated the crystal field as seen by a molecule by cosine potential of the form

$$V = V_o (1-\text{Cos } 2\theta) \qquad ..(2.2)$$

where θ is the angular coordinate for rotation occuring in one plane, $2V_o$ is the barrier height. The potential has two minima as shown in the figure 2.1. The Schrodinger equation obtained for such a potential is called Mathew equation. The energies for a free rotor are given by

$$W_J = BJ(J+1) \qquad ... \quad (2.3)$$

where J is the angular momentum quantum number and B is the rotational constant given by

$$B = \frac{\hbar}{2I} \qquad .. \quad (2.4)$$

Here I is the moment of inertia of the molecule about the axis of rotation. As barrier height increases, the free rotor states, particularly the ones with energies below the barrier height $2V_o$, are perturbed. These states are better

described as states of angular oscillations and in order to distinguish them from the oscillator states of internal molecular vibrations, they are called librational states. These librational states form pairs, and the energy splitting within each pair is the tunnel splitting. The states near the top of the barrier are called hindered rotor states as shown in figure 2.1. The states near the bottom of the potential wells are very similar in the model of Hund and Pauling except that the spacial coordinate is translation in the one and rotational in the other case. The difference between the two models becomes apparent only for states near and above the top of the barrier. In Hund's case, these states are oscillator states whereas in Pauling's case they are rotor states.

2.4 DEVONSHIRE MODEL

Devonshire model (1936) is the extension of Pauling's model to three dimensions. He calculated the effect of a crystalline field of octahedral symmetry on rotational states of a linear molecule when substituted in a crystal lattice. For this, he chose a potential of the form of the lowest order surface harmonics having octahedral symmetry which is of degree four. The Devonshire potential can be written as:

$$V_{Dev}(\theta,\phi) = -K\left[P_4^0(\cos\theta) + \frac{1}{168}P_4^4(\cos\theta)\cos 4\phi\right] \quad \cdots \quad (2.5)$$

where

$$P_l^m(\mu) = \frac{1}{l!\,2^l}(1-\mu^2)^{m/2}\frac{\partial^{l+m}}{\partial\mu^{l+m}}(\mu^2-1)^l \quad \cdots (2.6)$$

The expression for $V_{Dev}(\theta, \phi)$ can also be written as

$$V_{Dev}(\theta,\phi) = -K\left[\frac{1}{8}(3-30\cos^2\theta+35\cos^4\theta+5\sin^2\theta\cos 4\phi)\right] \quad \cdots (2.7)$$

where θ and ϕ are polar coordinates and K is the potential barrier parameter. For K positive, V has six minima, equal to -K, in the directions

$$\theta = 0 \text{ or } \pi$$

$$\theta = \tfrac{1}{2}\pi \;,\; \phi = 0,\; \pm\tfrac{1}{2}\pi \text{ or } \pi$$

which correspond to six $\langle 100 \rangle$ directions in the cubic crystal. It has eight maxima, equal to $\frac{2}{3}$ K, which occur in the following directions

$$\theta = \cos^{-1}\left[\pm(1/\sqrt{3})\right] \;,\; \phi = \pm\tfrac{1}{4}\pi \text{ or } \pm\tfrac{3}{4}\pi$$

Such a potential can be used if the molecule has equilibrium orientation pointing along the $\langle 100 \rangle$ direction of a cubic crystal. For K negative the maxima and minima are inverted,

i.e., we get eight minima and six maxima and this potential may be used if the molecule has equilibrium orientation along the eight $\langle 111 \rangle$ directions.

If V=0, which corresponds to the case of free rotation, the solutions are the surface harmonics and are degenerate, but under the influence of octahedral symmetry, the degenracy is partly removed, and they split up. The eigen values of the Schrodinger equation for a molecule of rotational constant B in such a potential are shown in figure 2.2, as computed by Devonshire (1936) and later on by Sauer (1966). With increasing $|K|$, the energies in figure 2.2 change from those of the free rotor to those of a librator, librating in six or eight wells respectively. In the limit of large K, the low lying librator states can also be calculated by starting from the wavefunctions describing the libration of the particle confined to one of the potential wells assumed to be harmonic. The tunnel splitting is then caused by the overlap of these localized wavefunctions. We have seen that the potential function used by Devonshire can account for impurities which have minima in the $\langle 100 \rangle$ or $\langle 111 \rangle$ directions. This potential function does not have minima in the $\langle 110 \rangle$ directions. Later on, this model was extended by Sauer (1967) and was applied to the KCl : NO_2^- system but it was unable to account for the experimental data satisfactorily. Beyler (1972)

extended this model by including higher order spherical harmonics in the expansion of potential function which predicted minima in the $\langle 110 \rangle$ directions but it was not applied to any system. Another shortcoming of applying the Devonshire model in its present form to the tunneling of point mass or off-centre ions is that tunneling through the centre of the unit cell is not allowed. It is possible that a dipolar molecule such as OH^-, CN^- or NO_2^- might have more degrees of freedom than the Devonshire model can account for. The problem becomes more complex if such a molecule is free to move in a potential which is a function not only of orientation, but also of centre of mass coordinates of the ion.

2.5 GOMEZ BOWEN AND KRUMHANSL(GBK) MODEL

The GBK model assumes that a point mass is subjected to a potential produced by the crystalline field of the host lattice having minima at various points. For an impurity substituted in a crystal lattice its Hamiltonian can be expressed as :

$$H = H_L + H_I + H_C \qquad .. \quad (2.8)$$

where H_L is the defect-lattice Hamiltonian. This can be obtained by collecting all the kinetic energy terms of the host lattice and all terms of the potential in the small-oscillation approximation which are independent of the

impurity. H_I is the impurity Hamiltonian and H_C is the coupling term. The term H_C is derived from that part of the total potential energy V_{LI} which involves both the impurity and the host coordinates. V_{LI} is expanded in terms of the displacement coordinates of the host ions, but not with respect to the impurity coordinates. Coefficient in this expansion are explicit functions of impurity coordinates r_{imp}. The expansion for V_{LI} can be written as:

$$V_{LI} = V_{LI}^{(o)}(\{R(l,K)\}, r_{imp}) + \sum_{l,K,\alpha} \frac{\partial V}{\partial R_\alpha(l,K)}(\{R(l,K)\}, r_{imp}) U_\alpha(l,K) \quad \cdots (2.9)$$

Here $\{R(l,K)\}$ indicates evaluation at the equilibrium positions of the host-lattice ions, $U_\alpha(l,K)$ is the αth component of the (l,K) host-lattice ion displacement. The first term in this expansion belongs to impurity Hamiltonian and is due to defect lattice. The rest of the terms constitute the coupling term H_C. Therefore the impurity Hamiltonian can be written as:

$$H_I = T_I + V_{LI}^{(o)}(\{R(l,K)\}, r_{imp}) \quad .. \quad (2.10)$$

$V_{LI}^{(o)}$ is the multiwell potential in which the impurity ion moves. The eigen states of H_I are determined in the approximation of a linear combination of atomic orbitals (LCAO) for the lowest energy multiplets.

The important features of the low lying vibrational states associated with the off-centred ions can be better understood with the help of a simple one-dimensional model in which tunneling between two wells is considered. The impurity is assumed to move in a double well truncated harmonic oscillator potential as shown in figure 2.3. The potential can be expressed as:

$$V = \begin{cases} \frac{1}{2} m\omega^2 (x + x_o)^2 & , x < 0 \\ \frac{1}{2} m\omega^2 (x - x_o)^2 & , x > 0 \end{cases} \qquad \ldots \quad (2.11)$$

where $2x_o$ is the separation between the two minima positions, m is the mass and $\omega = 2\pi\nu$ is the frequency of the particle in the single well and the rest of the lattice is assumed to be rigid. The lowest states can be expressed as linear combinations of the ground state wavefunctions $|a\rangle$ and $|b\rangle$ of the unperturbed harmonic oscillator in the two wells respectively. The energies are determined by the secular equation

$$\begin{vmatrix} E_o - E & \delta - SE \\ \delta - SE & E_o - E \end{vmatrix} = 0 \qquad \ldots \quad (2.12)$$

where $E_o = \langle a|H|a\rangle = \langle b|H|b\rangle$, $\delta = \langle a|H|b\rangle$ and $S = \langle a|b\rangle$. There are two solutions for E corresponding to symmetric and antisymmetric states.

$$E_{\pm} = (E_o \pm \delta)/(1 \pm S) \qquad \ldots \qquad (2.13)$$

If the barrier between the wells is large compared to zero point energy, then $S \ll 1$. Then we get

$$E_{\pm} \approx E_o \pm \delta \qquad \ldots \qquad (2.14)$$

where $$\delta = \hbar\omega\, x_o (m\omega/\pi\hbar)^{\frac{1}{2}} \exp\left(-\frac{m\omega x_o^2}{\hbar}\right) \cdots (2.15)$$

Gomez et al (1967) have generalized this model to the three dimensional problem. For the cubic symmetry of the environment, there are three types of multiwell potentials which are consistent with the octahedral symmetry. These are having: (1) six minima along the six $\langle 100\rangle$ axes (XY_6), (2) eight minima along the eight $\langle 111\rangle$ axes (XY_8) and (3) twelve minima along the twelve $\langle 110\rangle$ axes (XY_{12}). Schematic models for these three types of potential are shown in the figure 2.4. Each well by itself corresponds to a three dimensional harmonic oscillator. A given well can be described by certain parameters such as frequency and well location r_o. These model parameters may be determined either by comparison with experiment or by adjusting the parameters to approximate a theoretical potential calculated

from first principles. For the calculation of the low lying states the model potential can be adjusted to the theoretical one by letting them have the same minima positions and the same curvatures at the bottom of the wells. There is no reason to suppose that the off-centre wells should be isotropic or even to require that they should have inversion symmetry about their minimum positions.

If the wells were infinitely deep then the individual well eigen states would represent the eigen states of the off-centre ion and there would be 6-, 8- or 12-fold degeneracy as the case may be. These individual states are called pocket states. But when the wells are not infinitely deep, ie., when tunneling probability is higher, the actual states of the system will be linear combinations of the pocket states. The energy levels of the lowest lying multiplet are found from the correct linear combination of the pocket states. For the ground state splitting the basis states (pocket states) are normalized simple harmonic oscillator ground state wavefunctions centred at each well minima. The labelling of the basis states for the XY_6, XY_8 and XY_{12} wells are shown in the figure 2.4. The important feature of the three dimensional case is that more energy levels occur than for the one-dimensional case. This model is usually referred to as the 'GBK' model. The correct linear combinations of the pocket states for each of these models are easily determined by group theoretical

methods. The wave functions must transform according to the irreducible representations of the O_h group. The wave functions for each irreducible representation are used to evaluate the energies of that eigen state. The wave functions and energies for the XY_6, XY_8 and XY_{12} cases are given below.

Wavefunctions and energies for the XY_6 model:

$$\psi(A_{1g}) = [6(1 + 4S + S')]^{-\frac{1}{2}} (a + b + c + d + e + f)$$

$$\psi(T_{1u}) = [2(1 - S')]^{-\frac{1}{2}} (a - c)$$

$$\psi(T_{1u}) = [2(1 - S')]^{-\frac{1}{2}} (b - d)$$

$$\psi(T_{1u}) = [2(1 - S')]^{-\frac{1}{2}} (e - f)$$

$$\psi(E_g) = [12(1 - 2S + S')]^{-\frac{1}{2}} (a + b + c + d - 2e - 2f)$$

$$\psi(E_g) = [4(1 - 2S + S')]^{-\frac{1}{2}} (a - b + c - d)$$

$$E\ (A_{1g}) = (E_o + 4\eta + \mu)/(1 + 4S + S')$$

$$E\ (T_{1u}) = (E_o - \mu)/1 - S')$$

$$E\ (E_g) = (E_o - 2\eta + \mu)/(1 - 2S + S')$$

where $E_o = \langle a|H|a\rangle = \langle b|H|b\rangle = \cdots$

$\eta = \langle a|H|b\rangle = \langle a|H|d\rangle = \cdots$

$\mu = \langle a|H|c\rangle = \langle e|H|f\rangle = \cdots$

$S = \langle a|b\rangle = \langle b|c\rangle = \cdots$

$S' = \langle a|c\rangle = \langle b|d\rangle = \cdots$

η and μ are the matrix elements, S and S′ are the overlaps. H is the impurity Hamiltonian. $|a\rangle$, $|b\rangle$, $|c\rangle$, $|d\rangle$, $|e\rangle$, $|f\rangle$, $|g\rangle$ and $|h\rangle$ are the pocket states. Labeling of the pocket states for the XY_6 model are shown in the figure 2.4(A).

Wave functions and energies for the XY_8 model:

$$\psi\ (A_{1g}) = \left[8(1 + 3S + 3S' + S'')\right]^{-1/2} (a + b + c + d + e + f + g + h)$$

$$\psi_x\ (T_{1u}) = \left[8(1 + S - S' - S'')\right]^{-1/2} \left[(a + b + e + f) - (d + c + g + h)\right]$$

$$\psi_y\ (T_{1u}) = \left[8(1 + S - S' - S'')\right]^{-1/2} \left[(b + c + f + g) - (a + d + e + h)\right]$$

$$\psi_z\ (T_{1u}) = \left[8(1 + S - S' - S'')\right]^{-1/2} \left[(a + b + c + d) - (e + f + g + h)\right]$$

$$\psi_{yx}\ (T_{2g}) = \left[8(1 - S - S' + S'')\right]^{-1/2} \left[(b + c + e + h) - (a + d + f + g)\right]$$

$$\psi_{xz}\ (T_{2g}) = \left[8(1 - S - S' + S'')\right]^{-1/2} \left[(a + b + g + h) - (c + d + e + f)\right]$$

$$\psi_{xy}\ (T_{2g}) = \left[8(1 - S - S' + S'')\right]^{-1/2} \left[(b + d + f + h) - (a + c + g + e)\right]$$

$$\psi\ (A_{2u}) = \left[8(1 - 3S + 3S' - S'')\right]^{-1/2} \left[(b + d + e + g) - (a + c + f + h)\right]$$

$$E\ (A_{1g}) = (E_o + 3\eta + 3\mu + \nu)/(1 + 3S + 3S' + S'')$$

$$E\ (T_{1u}) = (E_o + \eta - \mu - \nu)/(1 + S - S' - S'')$$

$$E\ (T_{2g}) = (E_o - \eta - \mu + \nu)/(1 - S - S' + S'')$$

$$E\ (A_{2u}) = (E_o - 3\eta + 3\mu - \nu)/(1 - 3S + 3S' - S'')$$

η, μ and ν are matrix elements and S, S′ and S″ are overlaps

$$E_o = \langle a|H|a\rangle = \langle b|H|b\rangle = \cdots$$
$$\eta = \langle a|H|b\rangle = \langle b|H|c\rangle = \cdots$$
$$\mu = \langle a|H|c\rangle = \langle a|H|h\rangle = \cdots$$
$$\nu = \langle a|H|g\rangle = \langle b|H|h\rangle = \cdots$$
$$S = \langle a|b\rangle = \langle b|c\rangle = \cdots$$
$$S' = \langle a|c\rangle = \langle a|h\rangle = \cdots$$
$$S'' = \langle a|g\rangle = \langle b|h\rangle = \cdots$$

The figure 2.4(B) shows the labeling of the pocket states for the XY_8 model.

Wavefunctions and energies for the XY_{12} model:

$$\Psi(A_{1g}) = [12(1 + 4S + 2S' + 4S'' + S''')]^{-1/2} (a + b + c + d + e + f + g + h + k + l + m + n)$$

$$\Psi_1(E_g) = [24(1 - 2S + 2S' - 2S'' + S''')]^{-1/2} [(a + b + c + d + n + k + l + m - 2(e + f + g + h)]$$

$$\Psi_2(E_g) = [8(1 - 2S + 2S' - 2S'' + S''')]^{-1/2} [(a + b + c + d) - (n + k + l + m)]$$

$$\Psi_1(T_{1u}) = [8(1 + 2S - 2S'' - S''')]^{-1/2} [(a + b + k + n) - (c + d + l + m)]$$

$$\Psi_2(T_{1u}) = [8(1 + 2S - 2S'' - S''')]^{-1/2} [(a + d + e + h) - (b + c + f + g)]$$

$$\psi_3(T_{1u}) = \left[8(1 + 2S - 2S'' - S''')\right]^{-1/2}\left[(g + h + m + n) - (e + f + k + l)\right]$$

$$\psi_1(T_{2g}) = \left[4(1 - 2S' + S''')\right]^{-1/2}\left[(a + c - b - d)\right]$$

$$\psi_2(T_{2g}) = \left[4(1 - 2S' + S''')\right]^{-1/2}\left[(h + f - e - g)\right]$$

$$\psi_3(T_{2g}) = \left[4(1 - 2S' + S''')\right]^{-1/2}\left[(n + l - m - k)\right]$$

$$\psi_1(T_{2u}) = \left[8(1 - 2S' + 2S'' - S''')\right]^{-1/2}\left[(e + f + n + m) - (h + g + k + l)\right]$$

$$\psi_2(T_{2u}) = \left[8(1 - 2S' + 2S'' - S''')\right]^{-1/2}\left[(b + c + e + h) - (d + a + g + f)\right]$$

$$\psi_3(T_{2u}) = \left[8(1 - 2S' + 2S'' - S''')\right]^{-1/2}\left[(c + d + n + k) - (b + a + m + l)\right]$$

$$E(A_{1g}) = (E_o + 4\eta + 2\mu + 4\nu + \sigma)/(1 + 4S + 2S' + 4S'' + S''')$$

$$E(E_g) = (E_o - 2\eta + 2\mu - 2\nu + \sigma)/(1 - 2S + 2S' - 2S'' + S''')$$

$$E(T_{1u}) = (E_o + 2\eta - 2\nu - \sigma)/(1 + 2S - 2S'' - S''')$$

$$E(T_{2g}) = (E_o - 2\mu + \sigma)/(1 - 2S' + S''')$$

$$E(T_{2u}) = (E_o - 2\eta + 2\nu - \sigma)/(1 - 2S + 2S'' - S''')$$

η, μ, ν, and σ are matrix elements and S, S', S'', and S'''overlaps.

$$E_o = \langle a|H|a\rangle = \langle b|H|b\rangle = \cdots$$

$$\eta = \langle a|H|n\rangle = \langle a|H|k\rangle = \cdots$$

$$\mu = \langle a|H|b\rangle = \langle a|H|d\rangle = \cdots$$

$$\nu = \langle a|H|g\rangle = \langle a|H|f\rangle = \cdots$$

$$\sigma = \langle a|H|c\rangle = \langle b|H|d\rangle = \cdots$$
$$S = \langle a|n\rangle = \langle a|k\rangle = \cdots$$
$$S' = \langle a|b\rangle = \langle a|d\rangle = \cdots$$
$$S'' = \langle a|g\rangle = \langle a|f\rangle = \cdots$$
$$S''' = \langle a|c\rangle = \langle b|d\rangle = \cdots$$

The labeling of the pocket states for the XY_{12} model is shown in the figure 2.4 (C)

In all these cases the matrix elements are negative quantities. An interesting physical significance can be associated with the overlap integrals and the tunnel-splitting matrix elements. For the XY_8 model, for instance, the overlap integrals S, S′and S″, and the tunnel-splitting matrix elements η , μ , and ν are characterized by the location of the two basis states in each matrix elements. S and η represent overlap and tunneling along the cube edges. S′and μ represent overlap and tunneling across the cube faces. S″and ν represent overlap and tunneling through the cube along a body diagonal. The expressions for wavefunctions and energies are completely independent of the actual shape of the potential function and depend only on the XY_6, XY_8, or XY_{12} symmetry of the Hamiltonian, provided the basis functions, $|a\rangle$, $|b\rangle$,$|c\rangle$, etc., are chosen properly. The basis states must be complete in the sense that the tunneling states can be represented by linear combinations of the basis states. This condition is seen to be easily satisfied in

the case of wells where the overlap integrals are small. The basis states, a, b, c, etc., can be taken to be the ground-state wavefunctions found for the individual wells as if they were isolated. The tunneling may be calculated for some simple types of potentials such as harmonic oscillator potentials.

The relative magnitude of the matrix elements depends on the nature of tunneling motion performed by the impurity ion. The dependence of the matrix elements on the well separation $2x_o$ and barrier height V_o can be seen from the one dimensional double well model (equation 2.15). It has an exponential dependence of the form $\exp\left(-\frac{m\omega x_o^2}{\hbar}\right)$ or $\exp\left(-\frac{2V_o}{\omega\hbar}\right)$ (since $V_o = \frac{1}{2} m x_o^2 \omega^2$ for $x = 0$ from equation 2.11). For large well separation or large barrier height the matrix elements will be small.

Referring to the XY_8 model once again, one can see that if ion tunnels along the cube edge, the tunneling parameter η will be large. In case of tunneling along a face diagonal, μ will be large, and for tunneling through the body diagonal ν will be large. Conclusions about the relative magnitude of tunneling parameters can be drawn if the spacing of the energy levels are known accurately.

The wavefunctions in GBK model are found by the linear combinations of the basis states which are supposed

to be complete, ie., they should be independent of each other. This condition can be satisfied only when the overlap integrals are very small which can be obtained for large barrier heights. So, the GBK model is basically applicable for larger barrier heights compared to the energy of the oscillator. For large barrier height limit, the energy levels are determined by the matrix elements found in the numerators of the expressions for energies, since the overlap integrals can be neglected.

Dreyfus (1969) has correlated the Devonshire model and the GBK model for lowest level structure observed for impurities substituted in crystals. The GBK model is applicable to large and to some extent to medium potential barriers whereas the Devonshire model is applicable to small and medium potential barriers. Another difference is that the parabolic curve utilized in the GBK model has a cusp halfway between the potential minima, while the Devonshire model utilizes a potential which has a saddle point in the same position. In the Devonshire model, the rotating molecule is constrained to lie on a sphere, whereas, in the GBK model, the ion tunnels through the barrier by the shortest path. Despite the above differences, this correlation method gives satisfactory results.

In GBK model the tunnel splitting can be expressed in terms of the matrix elements. If the moment of inertia I for rotation of the ion about the lattice site and its

librational frequency ω about the lattice site are known then the matrix elements can be expressed in terms of I and ω . ω can be related to the barrier parameter K from the Devonshire model. The tunnel splitting can be predicted if K or ω is known or from the known tunnel splitting, the libration frequency or potential barrier parameter K can be calculated. Since Devonshire has solved only for the $\langle 100 \rangle$ and $\langle 111 \rangle$ models, the relationship between ω and K is not easy to establish for the $\langle 110 \rangle$ model. This method was applied by Dreyfus (1969) for the KCl : Li^+ system. Recently it has been applied for the calculation of barrier heights for the reorientation of the CN^- ion in KCl and KBr matrices (Verma 1980).

For an impurity substituted in a crystal lattice it is very likely that the impurity will distort the lattice in its initial position. An impurity capable of performing tunneling motion when reorients, the distortion also changes and follows the impurity motion. This effect modifies the tunneling matrix elements. The matrix elements given by the GBK model are only the effective matrix elements. For some systems (e.g. the Ag^+ ion in RbCl and RbBr, Kapphan and Luty 1972) it was found that the nearest-neighbour tunneling is not important. The reason for this may be the large distortion of the lattice around the impurity ion which may not be able to follow the nearest-neighbour tunneling motion. Therefore this effect should be taken into account

in treating the tunneling of impurities in crystals and the tunneling matrix elements must be renormalized. Shore and Sander (1975) have discussed this effect and they could explain the dominance of the 90° tunneling over the 60° tunneling of the $\langle 110 \rangle$ oriented Ag^+ ions in RbCl and RbBr crystals (Kapphan and Luty 1972).

2.6 VARIOUS EXPERIMENTAL TECHNIQUES USED FOR STUDYING TUNNELING STATES.

Impurities in crystals capable of performing tunneling motion produce states of definite energy. These states may scatter phonons resonantly if their energies match with that of the tunneling states. A study of this scattering may provide information about the tunneling states. A convenient method of studying this scattering is to measure the phonon or lattice thermal conductivity at low temperatures. The scattering of phonons by the tunneling states causes a depression in the thermal conductivity at temperatures around $\frac{\hbar \omega_t}{k}$ where ω_t is the frequency of the tunneling state. The selective phonon scattering suggests the existance of discrete states which are coupled to the phonons and hence scatter them resonantly. These discrete states may be due to tunneling or other types of modes which couple to the lattice phonons. Therefore the measurement of low temperature thermal conductivity can

reveal the existance of tunneling states. In contrast to optical spectroscopy, the phonon spectroscopy via thermal conductivity is a broad band technique. It cannot resolve different resonant states if they are closely spaced.

The tunneling states can be observed in the far-infrared absorption along with resonant modes. In the absence of tunneling, the resonant modes due to impurities in crystals will not show broadening or additional absorption peaks near them, but in the presence of tunneling broadening or splitting of the original absorption peaks due to resonance modes may occur. Since the resonant modes are strong scatterer of phonons, they are thermally broadened and may show broad absorption peaks with tunneling levels hidden within them. Therefore, even with high instrumental resolution, it may not be possible to resolve them in distinct peaks so easily.

In mid-infrared absorption region tunneling states can be seen as side bands to the internal vibrations of the molecular impurities. Monatomic impurities cannot be studied by this method because they do not have internal vibrations. Internal vibrations of molecular impurities generally fall far beyond the lattice vibration region and hence they couple very weakly to the lattice phonons and have negligible broadening due to scattering of phonons. Therefore, closely-spaced tunneling levels may be possible to resolve

with the high resolution attainable in this region.

The tunneling behaviour of dipolar impurities can be studied by a method analogous to electron paramagnetic resonance (EPR). The microwave spectroscopy of such impurities has come to be known as "Paraelectric resonance (PER)". The dipolar impurities are paraelectric in nature. In a PER experiment, electric field is applied to a sample containing paraelectric impurity and absorption of microwave radiation of fixed frequency is observed as a function of applied electric field. The analogy with paramagnetic resonance is obvious. Effect of electric field on paraelectric molecular impurities can also be studied in the mid-infrared or near-infrared absorption, ie., in the internal vibration region of molecular impurities.

Paraelectric impurities capable of aligning themselves by tunneling can produce cooling effect by adiabatic depolarization method similar to the adiabatic demagnetization of magnetic spins. This effect is known as paraelectric cooling. Paraelectric cooling is a very sensitive test for establishing the existance of tunneling states of atomic and molecular impurities in solids.

Using optical and IR absorption techniques the effect of uniaxial stress on tunneling states has been studied. The application of stress makes the equivalent potential wells unequal, and thus causing drastic changes in

the structure of tunneling levels and sometimes splitting them further. This effect can be observed in the far-infrared, mid-infrared, near-infrared, visible and UV absorption etc.

Tunneling states can be directly measured by resonant scattering of tunable monochromatic phonons, generated by superconducting tunnel junction. Eisenmenger and Dayen (1967) used a symmetric superconducting tunnel junction as a source of monochromatic phonons in the range above 100 GHz. The phonons originate on recombination of quasiparticles which are excited in the junction by single-particle tunneling. The recombination process produces phonons at a fixed frequency equal to the energy gap of the superconductor. Narayanamurti and Dynes (1971) attempted to tune the energy gap using a magnetic field but it broadened the spectrum of emitted phonons. Later on Kinder (1972) using phonon bremsstrahlung of a superconducting tunnel junction produced monochromatic phonons which can be tuned simply by adjusting the battery voltage. This was used to study the tunnel splitting due to the OH^- ions in NaCl (Windheim and Kinder 1975) and the CN^- ion in KCl (Windheim 1976).

Apart from these, tunneling properties of dipolar impurities have been studied by the dielectric constant measurements, specific heat measurements, NMR, ultrasonic attenuation measurements etc.

2.7 TUNNELING STATES OF VARIOUS MONATOMIC AND MOLECULAR IMPURITIES IN ALKALI HALIDES.

The Li^+ doped KCl is the most extensively studied system. It was Lombardo and Pohl (1965) who observed an electrocaloric effect in the KCl : Li^+ system which suggested that the Li^+ ion in KCl performs tunneling motions. Lombardo and Pohl (1965) and Sack and Moriarty (1965) suggested that the Li^+ ion might not be stable at the normal lattice site and might take off-centre position. This hypothesis was confirmed by Narayanamurti and Pohl (1970). Diens et al (1966), Wilson et al (1967) and Quigley and Das (1969) indicated an off-centred position for the Li^+ ion in KCl along the [111] direction.

Matthew (1965) showed qualitatively that when a small ion like the Li^+ ion replaces a large host ion in an alkali halide (KCl) the induced electric dipole interaction together with the decreased repulsive forces could cause highly asymmetric equilibrium configuration for the Li^+ ion in the lattice. The actual position of the ion will depend upon a delicate balance of repulsive and polarization energies. A large repulsive interaction would tend to keep the ion in place while a high polarizability would tend to move it off the normal lattice site.

Stress-induced quadrupole splitting of NMR signal due to the Li^+ ion doped in KCl by Alderman and Cotts (1970)

and electric field induced quadrupole splitting of the ^{7}Li NMR signal are in agreement with the [111] tunneling model of Gomez et al (1967) with eight equivalent off-centre potential minima. From stress effects in the paraelectric resonance spectrum (Larson and Silsbee 1972) and Kirby et al (1970) from far-infrared absorption spectrum of the ^{6}Li and ^{7}Li in KCl for applied electric fields found that the tunneling levels are well described by the model of Gomez et al (1967). Hetzler and Walton (1970, 1973a, 1973b) have measured the energy spacing of the four-level tunneling multiplet with a phonon spectrometer and found unequal spacings. They concluded that this is due to the presence of body diagonal tunneling in addition to the nearest-neighbour tunneling where as earlier workers considered only nearest-neighbour tunneling.

The NaBr:F^- system: The NaBr crystal doped with F^- ions was studied by Rollefson (1972) using specific heat, paraelectric cooling, thermal conductivity and dielectric relaxation measurements. From the measurements of the dielectric constant under applied stress they concluded that the fluorine ion tunnels between the potential minima displaced from lattice site in the $\langle 110 \rangle$ directions. The low temperature specific heat contribution is found to be much broader in temperature than that given by the GBK model (Gomez et al 1967). In addition the relaxation rate

of the impurity ion in NaBr is much slower than what had been observed in the KCl : Li^+ system (Narayanamurti and Pohl 1970). Thus NaBr:F^- represents a tunneling system in the limit of small tunneling probability while the KCl:Li^+ is characteristic of a system with large tunneling probability.

The RbCl: Ag^+ system: Drybodt and Fussgaenger (1966) first suggested that the Ag^+ impurity in RbCl could be displaced from the normal lattice site. They concluded this from their temperature dependent studies on the Ag^+ UV absorption band in RbCl. Nolt (1967) measured the infrared absorption spectrum of the RbCl:Ag^+ system and observed stress-induced dichroism, which were consistent with an off-centred Ag^+ defect. Paraelectric cooling was first observed in the RbCl:Ag^+ by Kapphan and Luty (1968). They concluded that the defect was displaced along the [111] direction . Bridges (1972) observed the paraelectric resonance spectrum and found that the tunnel-splitting was very small $\sim$ 0.1 cm^{-1}. The far-infrared dichroism associated with the stress and electric fields were studied and analysed by Kirby et al (1970) and found to be compatible with the displacement of the defect along the [110] direction. They found that the system can be understood in terms of the classical limit of GBK model. Kapphan and Luty (1972) have studied the detailed dynamics of the Ag^+

defect in RbCl and RbBr using the electrodichroism in UV absorption region. Their results lead to the [110] oriented dipoles for Ag^+ in both the systems. Electrodichroism experiments showed the existence of two relaxation processes whose relaxation rates differed by several orders of magnitude. This complex relaxation behaviour suggested that the next nearest-neighbour tunneling dominates over the nearest-neighbour tunneling.

The OH^- ion in alkali halides : Klein (1961) observed unusual decrease in the thermal conductivity of the NaCl crystals at very low temperatures. He attributed this to the OH^- impurities in NaCl which scatter the lattice phonons. He attempted to explain the strong phonon scattering as a result o. resonance interaction with some rotational tunneling states of the molecular impurity. Brugger and Mason (1961) and Brugger et al (1967) observed attenuation of ultra sound in KCl and NaCl due to the OH^- ions and explained this due to reorientation of the impurity ion via a relaxation process. Observation of electrocaloric effect (Kunh and Luty 1965, Shepherd and Feher 1965) and measurements of electric field (Kuhn and Luty 1964) and stress-induced dichroism of UV absorption in several OH^- doped alkali halides (Hartel and Luty 1965) gave the direct evidence of the high rotational mobility of the OH^- ions at low temperatures. These measurements further showed that the OH^-

ion has six equilibrium orientations pointing along the six ⟨100⟩ directions. Luty (1974a) measured the effect of electric field on the vibrational absorption of the KCl crystals doped with OH^- ions and their results were consistent with the ⟨100⟩ dipolar model. The first direct evidence for the tunneling states of the OH^- ion was obtained from measurements of the paraelectric resonance (Bron and Dreyfus 1966) and the results were explained on the basis of the Devonshire potential in the high barrier limit. From thermal conductivity measurements at very low temperatures of the $NaCl:OH^-$ and $KCl:OH^-$ (Chau et al 1967, Rosenbaum et al 1969) it was found that tunnel splitting for the $NaCl:OH^-$ was larger than that for the $KCl:OH^-$. Hartel and Luty (1968) have studied the electric field-induced dichroism of the OH^- stretching vibration using very high resolution at 5 K but could not observe any tunnel splitting which was a very puzzling situation because specific heat measurements strongly supported the tunneling model. The tunneling states of the $KCl:OH^-$ and $NaCl:OH^-$ systems (Scott and Flygare 1969) have also been studied by microwave absorption. The absorption bands were explained in the framework of the Devonshire potential with an additional perturbing potential. Scott and Flygare (1969) assumed that the centre of mass of the OH^- ion does not coincide with the cavity centre, but is displaced in a [100] direction. An almost similar model was proposed by Shore (1966) and by Pompi and Narayanamurti

(1968). In the NaCl:OH^- system (Scott and Flygare 1969), the tunnel splitting appeared to be larger than in the KCl:OH^- system. Windheim and Kinder (1975) directly measured the tunnel-splitting by resonant scattering of monochromatic phonons and the splitting was found rather large for the NaCl:OH^- system. From the studies on the statics and dynamics of dipolar alignment of the OH^- ions in various alkali halide hosts (Kapphan and Luty 1973 and Kapphan 1974) it was found that the OH^- ions has $\langle 111 \rangle$ orientation in the CsBr and $\langle 110 \rangle$ orientation in the KI lattices. The $\langle 110 \rangle$ orientation of the OH^- ion in KI was confirmed by Bridges(1973).

The CN^- ion in alkali halides: The first evidence of tunneling of the CN^- ion in alkali halides like KCl was found by thermal conductivity measurements (Seward and Narayanamurti 1966). They observed the infrared absorption due to CN^- ions doped in KCl crystals at 300 K and found a broad band with a double hump which was explained as arising due to the rotational motions of the CN^- ion in the KCl lattice. But at low temperatures below 60 K the spectrum showed drastic changes. A narrow absorption band, between the two maxima observed at high temperatures, rises rapidly which was explained to arise due to librational motions of the ions (tunnel splitting was ignored for simplicity). They calculated the potential barriers for librations of the ion using Pauling's model (1930). The phonon resonant

scattering and infrared spectra of the CN^- ions in the KBr and KI lattices are similar to those in the KCl lattice. On the basis of stress-induced dichroism of the CN^- stretching vibration at low temperatures, they found [100] orientation for the CN^- ion in the KCl, KI and KBr lattices, which is incorrect from the recent findings of Luty (1974b) and Verma (1980). Later on, Windheim (1976) directly measured the energy separation between the low-lying states in the KCl:CN^- system by resonant scattering of tunable monochromatic phonons and his data proved that the CN^- ion is oriented along the [111] direction. Recently tunnel splitting was observed with the stretching vibration of the CN^- ion in the KBr single crystals in high resolution infrared absorption spectra (Verma 1980) and the results were compatible with the [111] model for the ion.In this study, the potential barriers for reorientation of the CN^- ion in KCl and KBr lattices were calculated as 28.7 and 36.5 cm^{-1} respectively. The larger barrier height in the KBr matrix compared to that in KCl is contrary to expectations on the basis of bigger cavity dimensions of KBr. From this comparative study, an extremely important conclusion was drawn (Verma 1980) that the anisotropic part of the interionic potential giving rise to a barrier for reorientation is determined by the attractive part rather than by the repulsive part of the potential. More

precisely, one might say that it is not the repulsive interaction with the neighbouring K^+ ions which gives rise to maxima, but rather the longer range polarization effects with the next nearest-neighbour halide ions which give rise to minima in the potential with the rotational coordinates.

The NO_2^- ion in alkali halides : There has been considerable amount of work done on reorientational degree of freedom of the NO_2^- ion in various alkali halide crystals. This will be discussed in chapter IV.

2.8 PAIR MODES AND THEORETICAL BACKGROUND

For impurities dissolved in small concentrations in crystals, mutual interaction effects among them are not prominent. But there comes a stage when pairing or clustering of impurities becomes important with increasing concentrations. Then the mutual interactions among the impurities cannot be neglected. The pairing or clustering gives rise to localized modes and they are reflected in the infrared, Raman or EPR spectra. Intensities of such absorption bands are quadratically dependent on the concentration of impurities. In alkali halides, many impurity pairs have been studied and detected by various techniques which will be discussed later. In most of the cases the pairs were obtained by high level of doping of impurities and making use of statistical probability of pair formation. But de Souza et al (1970) have obtained pairing of U-centres

in KCl by a controlled technique with low concentration of impurities and could produce isolated pairs.

There have been a large number of theoretical formulations to understand these modes. They have been studied by molecular models (Jaswal 1965, 1972), Green's function techniques (Gupta and Mathur 1976, 1980, Kalyani and Haridasan 1976) and coupled harmonic oscillator model (de Souza and Luty 1973). In molecular model approach, impurity and their nearest-neighbours only are assumed to take part in the motion while rest of the crystal lattice is assumed to be at rest. In Green's function technique a complete knowledge of the eigen states and eigen vectors of the host lattice is required and the method in principle yields an exact solution of the problem. The molecular model should give good results for impurities whose motions are highly localized so that the assumption of neglecting the motion of rest of the lattice other than the impurities is valid. De Souza and Luty (1973) have proposed a model of two coupled harmonic oscillators for a pair of impurities. They (De Souza and Luty 1973) have applied this model to U-centre pairs in KCl with quite satisfactorily results. The coupling between the two harmonic oscillators is provided by the electric dipole-electric dipole interactions between the two impurities due to induced dipole moments

during their vibrations. If the motion of individual impurity is highly localized than the motion of lattice relative to the impurity can be neglected and the rest of the lattice can be considered to be rigid. The Hamiltonian for two coupled harmonic oscillators can be written as:

$$H = \frac{1}{2}(m_1\dot{q}_1^2 + m_2\dot{q}_2^2 + m_1 q_1^2\omega_1^2 + m_2 q_2^2\omega_2^2) + B q_1 q_2 \quad \cdots (2.16)$$

where m_1 is the mass of the first impurity, m_2 that of the second, q_1 is the displacement of the first impurity and q_2 that of the second. ω_1 and ω_2 are the localized frequencies of the individual impurities. The last term is the interaction between the two localized harmonic oscillators which is responsible for giving rise to side bands to the localized vibration. B is the coupling constant. If the impurities during their vibrations have induced electric dipole moments μ_1 and μ_2 respectively than the last term can be written in terms of dipole-dipole interactions as :

$$B q_1 q_2 = \frac{\mu_1 \mu_2}{R_{12}^3}\left[\hat{\mu}_1 \cdot \hat{\mu}_2 - 3(\hat{\mu}_1 \cdot \hat{R}_{12})(\hat{\mu}_2 \cdot \hat{R}_{12})\right] \cdots (2.17)$$

$\hat{\mu}_1$ and $\hat{\mu}_2$ are the unit vectors along $\vec{\mu}_1$ and $\vec{\mu}_2$ respectively and $\hat{R}_{12}$ is the unit vector along $\vec{R}_{12}$. which is the distance between the two dipoles. This interaction predicts the correct shifts. The sign of this interaction decides the position of side bands. If the sign of the interaction is negative the side band will appear on the low frequency side and if it is positive then the side band will appear on the high frequency side of the localized vibration. A pair due to two dipoles in crystals will show infrared absorption when the net dipole moment of the system is non zero. In crystal lattices the two dipoles can be in the same plane or in different planes. When the dipoles vibrate in the same plane two types of situations may arise : (1) the two dipoles can vibrate in the same directions; i.e., they are in phase, or (2) they may vibrate in the opposite directions; i.e., they are out of phase. In the first case the pairs may show/up in infrared absorption. But in the second case because of the cancellation of dipole moments, they will not show infrared absorption. However, they may give/rise to Raman scattering.

In treating dipole-dipole interactions for large distances ($R \gg a$) the dipolar interaction would be screened by the polarization of the host lattice and dielectric constant of the medium giving rise to a correction factor. But for alkali halides for small distances, the

corrections from screening by dielectric constant and local field effects are very much close to unity (De Souza and Luty 1973).

2.9 PAIR MODES DUE TO VARIOUS IMPURITIES IN ALKALI HALIDES

The first experimental evidance for pair modes was obtained from Raman scattering from Ag^+ pairs in NaCl by Moller et al (1970). Ag^+ ions induced a peak at 47 cm^{-1} in NaCl which remained unexplained theoretically by earlier workers. The intensity of this band was found to increase nearly quadratically with the Ag^+ concentration. Moller et al (1970) have calculated the frequency of a vibrating Ag^+ pair occupying second nearest-neighbour site in the [110] directions, on the basis of the assumption that only the nearest-neighbour Cl^- ions contribute to the pair vibration. They obtained 47.5 cm^{-1} as the frequency of the pair mode which was in excellent agreement with the experimentally observed value. Templeton and Clayman (1971) have observed pair mode in KCl : Na^+ system whose intensity showed quadratic dependence on the Na^+ ion concentration. Jaswal (1972) used molecular model to explain the pair mode. It was shown that the defect produces a very large softening of short range force constants around itself. De Jong et al (1973) observed a series of closely-spaced absorption lines

in the KI : Rb^+ system. The origin of these lines has been explained as arising due to the Rb^+ pairs in KI by Ward and Clayman (1974a). Using a molecular model, they have calculated the resonant mode frequencies of the Rb^+ pairs in KI. Later on, Ward and Clayman (1974b, 1974c) have observed pair modes due to Na^+, Cl^- and Br^- impurities in KI. The intensities of these bands were found to vary quadratically with the concentration of impurities. The experiments of Becker and Martin (1972) on infrared absorption of the NaCl:F^- system revealed six peaks. The quadratic concentration dependence of the strength of these lines indicated that they arise due to the pairs of fluorine impurities. They suggested two types of pairs the nearest-neighbour and the second nearest-neighbour pairs responsible for these modes. Haridasan et al (1973) employed Green's function techniques to explain the pair modes observed by Becker and Martin (1972). This model could explain all the infrared resonant modes due to pairs of impurities, at least in a qualitative way. Ishigama et al (1972) observed infrared absorption at 16.5 cm^{-1} due to K-F impurity pairs in NaCl containing large concentration of potassium and fluorine ions. This line was not present in samples with high concentration of only fluorine or only potassium ions. A careful analysis by them indicated that the strength of the absorption line was proportional to the product

of the concentrations of the fluorine impurity and that of potassium impurity. The most extensively studied pair mode system is the U-centre pairs in alkali halides. This has been studied experimentally as well as theoretically by de Souza et al (1970, 1973) and Robert and de Souza (1974). Several other workers have studied this system theoretically (Kalyani and Haridasan 1976, Gupta and Mathur 1976, 1980) by using Green's function technique. De Souza et al (1970) achieved U- centre pairs in KCl by thermal reaction of mobile interstitial H_2 molecules with F-centre pairs (M-centres). The observed pair modes due to U-centre pairs in KCl were satisfactorily explained by a model of coupled harmonic oscillators where the coupling between two oscillators is provided by electric dipole-electric dipole interactions (de Souza and Luty 1973). Later on, Robert and de Souza (1974) observed pair modes due to U-centres in many other alkali halides, viz., KBr, KI, NaCl and RbCl. They confirmed that the main coupling between the H^- or D^- harmonic oscillators in various hosts was provided by the dipole-dipole interactions. Some vibrational lines were identified due to $\langle 200 \rangle$, $\langle 211 \rangle$ and $\langle 220 \rangle$ neighbouring $H^- H^-$, $D^- D^-$ or $H^- D^-$ pairs in the crystals.

Infrared spectra of the KI:NO_2^- system has been studied previously by Narayanamurti et al (1966) for relatively large concentration of the NO_2^- ions in KI.

We have also made a detailed study of this system for large concentration of the NO_2^- ions in KI. This will be discussed in chapter V.

2.10 THE LOCALIZED MODES AND EFFECTS OF ANHARMONICITY.

A localized mode is a vibrational state associated with a crystal defect having frequency out side the frequency band or bands of the perfect crystal lattice. Unlike lattice phonons, localized modes are non-propagatory modes. For such modes amplitude of displacement at the impurity site is maximum and it decays exponentially at subsequent lattice sites. Depending upon the frequencies, these modes can occur at frequencies higher than the highest frequency phonon state and such type of modes are called local modes. If their frequencies fall within the allowed bands of unperturbed lattice than they are called resonant modes or band modes. Some crystals have a gap in between their optical and acoustical phonon branches where there are no phonons in the host lattice. If the modes due to defects have frequencies which lie in the forbidden gap then they are called gap modes. They are shown schematically in figure 2.5. The appearance of these modes can be understood qualitatively by considering the modification of mass at the lattice site due to impurity and changes in the force constants between the host atoms and impurities. A local

mode occurs if a light host ion is replaced by a lighter impurity or the impurity is coupled to its sorroundings more strongly than the host ion. The replacement of the light host ion by a heavier impurity or softening of force constant around the impurity ion may produce a gap mode. If a heavier ion of the host crystal is replaced by a lighter impurity ion it may give rise to a gap mode. Softening of force constant around a heavier impurity does not give any mode out side the band of phonons of the host lattice but within the band only, giving rise to resonant modes.

In harmonic approximation, the normal modes of vibration of a perfect or imperfect crystal are independent of each other. They are exact eigen states of the crystal Hamiltonain and are therefore infinitely long-lived. However, no crystal is perfectly harmonic. If one goes beyond the harmonic approximation to the crystal Hamiltonian and retains the third-, fourth- and higher order terms in the expansion of the crystal potential energy and the impurity host potential energy in powers of the atomic displacements, the exact eigen-states of the harmonic approximation are no longer exact eigen states of the anharmonic crystal. In the presence of anharmonicity the normal coordinate transformation, which diagonalizes the harmonic part of the crystal Hamiltonian, leads to a coupling

between the formerly independent normal modes of the harmonic approximation. This coupling allows the exchange of energy between the normal modes of the harmonic approximation and gives rise to a number of interesting and observable effects such as thermal expansion of lattice, temperature-dependent band-width and frequency shift of localized modes etc. The band-width of local mode is, in general, very small because they are very weakly coupled to lattice phonons. The life time of such a localized oscillator is determined by indirect coupling to lattice modes due to anharmonic terms. Absorption due to resonant modes is generally very broad. In some cases the excited resonant state can loose energy by exciting phonons of the same frequency. This will cause damping of the oscillations. Sometimes damping may be weak, eg., when the number of phonon states at frequencies near the resonant mode frequency is small, or when the impurity is only weakly coupled to the phonon states.

The potential energy of an anharmonic crystal containing a substitutional point defect can be expanded in powers of the normal coordinates of the lattice phonons and the impurity modes. In the expansion there will be cubic and quartic terms involving normal coordinates of localized mode Q_g, such as Q_g^3 and Q_g^4. These terms affect the energy levels of the localized state, but not of the

other lattice modes and thus induce higher harmonics and side bands etc. The terms involving only the lattice mode normal coordinates such as $q_i q_j q_k$ give rise to thermal expansion (Peierls 1974). So, the anharmonic terms containing normal coordinates associated with only localized modes or only with lattice phonons are not responsible for the exchange of energy between the localized modes and lattice phonons. Excluding these contributions, the Hamiltonian for the local mode oscillator involving coupling between the localized mode and lattice phonons can be written as (Bauerle 1973):

$$H = H_0 + H_3 + H_4 \ldots \qquad (2.18)$$

where H_0 is the harmonic part of the Hamiltonian for the localized mode, H_3 and H_4 are the cubic and quartic terms respectively of the Hamiltonian containing mixed terms responsible for temperature dependent band-width and frequency shift of localized modes. In terms of normal coordinates of the localized mode Q_g and lattice phonons q_i, q_j etc, they can be expressed as :

$$H_3 = \frac{1}{6}\left[\sum_{g,i,j} \frac{\partial^3 V}{\partial Q_g q_i q_j} Q_g q_i q_j + \sum_{g,i} \frac{\partial^3 V}{\partial^2 Q_g \partial q_i} Q_g^2 q_i\right] + \ldots$$

and

$$H_4 = \frac{1}{24}\left[\sum_{g,i,j,k} \frac{\partial^4 V}{\partial Q_g \partial q_i \partial q_j \partial q_k} Q_g q_i q_j q_k + \sum_{g,i,j} \frac{\partial^4 V}{\partial^2 Q_g \partial q_i \partial q_j} Q_g^2 q_i q_j\right] + \cdots \quad \cdots (2.19)$$

which can be written in terms of creation and annihilation operators (Bauerle 1973) as:

$$H_3 = \frac{1}{6}\left[\sum_{g,i,j} V_3(g,i,j)(a_g + a_g^\dagger)(q_i + a_i^\dagger)(a_j + a_j^\dagger) + \sum_{g,i} V_3(g,i)(a_g + a_g^\dagger)^2 (a_i + a_i^\dagger)\right] + \ldots.$$

and

$$H_4 = \frac{1}{24}\left[\sum_{g,i,j,k} V_4(g,i,j,k)(a_g + a_g^\dagger)(a_i + a_i^\dagger)(a_j + a_j^\dagger)(a_k + a_k^\dagger) + \sum_{g,i,j} V_4(g,i,j)(a_g + a_g^\dagger)^2(a_i + a_i^\dagger)(a_j + a_j^\dagger)\right] + \cdots \quad \cdots (2.20)$$

where g refers to the eigen vectors of the localized modes and i,j,k those of lattice phonons. V_3 and V_4 represent the coupling coefficients of the cubic and quartic terms in the potential energy, coupling localized modes with lattice

phonons. Since these processes depend on thermal occupation number $n_i = \exp\left[\left(\frac{h\nu}{kT} - \right) - 1\right]^{-1}$ of phonons involved in the interactions, temperature dependence is contained in this factor.

2.11 HALF-WIDTH

As the terms H_3 and H_4 in the equation 2.18 are small compared to H_0, the contributions of these anharmonic terms to the energy and damping of the localized modes can be calculated using perturbation techniques. The differen processes contributing to the width and shift of energy levels can be divided into two broad categories: decomposition processes and scattering processes. Both of these processes modify the lifetime of the excited localized state and consequently affect the width of the level by limiting its life time, ie, through uncertainity principle (Alexander et al 1970). In the decomposition mechanism, the excited local mode state decays into two or more lattice phonons, the overall energy being conserved. The excited resonant mode can lose energy by exciting phonons of the same frequency. This will cause damping of oscillations. But for local modes and gap modes such possibility does not exist because at these frequencies, phonon states are not there. They can lose energy by decaying into two or more lattice phonons causing damping. The two-phonon decay is

brought about by terms $V_3\ (g,i,j)\ a_g a_i^\dagger a_j^\dagger$. Similarly a three-phonon decay takes place through the terms $V_4(g,i,j,k)$ $a_g a_i^\dagger a_j^\dagger a_k^\dagger$. The temperature dependent half-width due to two-phonon decay will have the form (Bauerle 1973):

$$(n_i + 1)(n_j + 1) - n_i n_j \quad \ldots \qquad (2.21)$$

where n_i and n_j are the thermal occupation numbers. This predicts a constant value at low temperatures and a linear dependence on temperature at higher temperatures. The half-width due to a three-phonon decay will have a temperature dependent form as (Bauerle 1973):

$$(n_i + 1)(n_j + 1)(n_k + 1) - n_i n_j n_k \ldots \qquad (2.22)$$

This predicts a constant half-width at low temperatures and quadratic dependence on temperature at higher temperatures. Higher order anharmonic terms other than cubic and quartic can give multiphonon decay but such contributions are negligibly small. For the processes in which the localized mode decays into two phonons, we must have

$$\Omega < 2\omega_m$$

and for three-phonon decay we must have $\Omega < 3\omega_m$, where Ω is the localized mode frequency and ω_m is the maximum phonon frequency of the host crystal.

The other mechanism giving rise to width is the scattering mechanism, often called Raman mechanism, and involves the scattering of lattice phonons at the localized excitations. It does not casue a decay of the excited localized excitation, but it broadens the localized mode by limiting the lifetime of a given overall state consisting of localized excitation plus phonons, since phonons are changing due to the scattering. The effect of scattering on the localized excitation part of the overall wavefunction is to produce a fluctuating phase shift or, what is the same thing, a fluctuating frequency and hence a broadening. The process can be expressed as (Alexander et al 1970):

$$|g\rangle|\cdots n_i,\ n_j,\ \cdots\rangle \longrightarrow |g\rangle|\cdots n_i \pm 1,\ n_j \mp 1,\ \cdots\rangle \qquad (2.23)$$

This process can be brought about by anharmonic terms like $V_3(g,i)(a_g + a_g^+)^2\ (a_i + a_i^+)$(taken to second order in perturbation theory) or $V_4(g,i,j)\ (a_g + a_g^+)^2\ (a_i + a_i^+)$ $(a_j + a_j^+)$ (taken to first order). In the Debye Approximation for phonon distribution, both of these processes give a contribution to half-width which can be expressed as (Bauerle 1973):

$$\Delta\Gamma = \beta\left(\frac{T}{\theta_D}\right)^7 \int_0^{\theta_D/T} \frac{x^6 e^x}{(e^x-1)^2}\, dx \quad \cdots \quad (2.24)$$

where β is a coupling constant and is positive, $X = \frac{h\nu}{kT}$ and $\frac{k\theta_D}{h}$ is the effective Debye cut off frequency. This process predicts a T^2 dependence in the high temperature limit and a T^7 dependence at low temperatures.

2.12 FREQUENCY SHIFT

The temperature dependent frequency shift of localized modes may arise from direct anharmonic coupling to lattice phonons and the thermal expansion of the lattice. The thermal expansion of the lattice is caused by the anharmonicity of the lattice modes. It leads to softening of the force constants and thereby to a decrease in frequency. The major contribution to the shift in the centroid frequency of a localized mode with temperature can be attributed to the elastic scattering of lattice phonons by the localized excitation. In the Debye approximation this can be expressed as (Alexander 1970):

$$\Delta\nu_{SC} = \delta\left(\frac{T}{\theta_c}\right)^4 \int_0^{\theta_c/T} \frac{x^3}{e^x - 1}\, dx \quad \cdots \quad (2.25)$$

where δ is a coupling coefficient and θ_c an effective Debye temperature. This gives the limiting behaviour as

$\Delta\nu_{sc} \propto T^4$ for low T

$\Delta\nu_{sc} \propto T$ for high T

The frequency shift from the thermal expansion effect can be written as

$$\Delta\nu_{th} = \frac{3\Delta a}{a(0)} \alpha(A_{1g})$$

a(o) is the lattice parameter at 0 K, a(T) that at temperature T and $\Delta a = a(T) - a(o)$, $\alpha(A_{1g})$ is the hydrostatic strain coupling constant related to the uniform dialation of the lattice and is responsible for the shift of the energy level of the localized mode. This can be estimated from the uniaxial stress experiments on crystals containing impurities.

2.13 EARLIER STUDIES ON THE TEMPERATURE DEPENDENCE OF THE HALF-WIDTH AND FREQUENCY SHIFT OF LOCALIZED MODES.

Temperature dependent studies on localized modes have been made by several workers experimentally as well as theoretically (Maradudin 1966, Elliot et al 1965, Alexander et al 1970). Experimentally nearly all of the work has been done with infrared spectroscopy. Elliot et al (1965) made a detailed analysis of the temperature

dependence of localized vibrations of H^- and D^- ions in the alkaline earth fluorides such as CaF_2, SrF_2 and BaF_2. The temperature dependent half-widths and frequency shifts associated with various localized modes were explained satisfactorily in terms of anharmonic interactions giving rise to decomposition of localized modes into lattice phonons, and scattering of phonons by localized modes.

Temperature dependent studies on the localized modes due to U-centres (H^- and D^- ions) in various alkali halides have been made by Fritz (1968). He explained the temperature dependent width in terms of decomposition processes. For the H^- ions in all the alkali halide hosts studied, $\nu_{Loc} > 2\nu_m$ where ν_{Loc} is the localized vibration and ν_m is the highest band mode frequency. The H^- local mode quantum cannot decay into two phonons but must decay into at least three. The absence of a two-phonon decay contribution explains the longer lifetime and thus small half-width of the H^- band. For the D^- local mode, $\nu_{Loc} < 2\nu_m$ and its lifetime is mostly governed by a decay into two lattice phonons. The causes of frequency shifts of these modes were attributed to the direct anharmonic contributions and the influence of the thermal expansion. Such measurements by Dotsch (1969) on the LiF and NaF containing H^- and D^- impurities illustrate two possible limiting examples.

Because of the small mass of lithium, the local mode frequency in the $LiF:H^-$ system is close enough to the maximum frequency of LiF, i.e., a two-phonon decay process is possible. The damping is found to be very large. For the $LiF:H^-$, $LiF:D^-$ and $NaF:D^-$ systems, $\nu_{Loc} < 2\nu_m$. But for the $NaF:H^-$ system where $\nu_{Loc} > 2\nu_m$, a three-phonon decay scheme is necessary. The absence of two-phonon decay explains small half-width of the H^- band in NaF. Although the three-phonon decay scheme has the correct limiting temperature dependence ($\propto T^2$) at higher temperatures, the scattering process is believed to play the dominant role here.

Alexander et al (1970) have measured the temperature dependent absorption spectrum associated with resonant modes in the $KBr:Li^+$, $NaCl:Cu^+$, $KI:Ag^+$ and $MnF_2:E_u^{2+}$ systems in the far-infrared absorption. They could satisfactorily explain the temperature dependent characteristics in terms of various anharmonic interaction mechanisms coupling the resonant modes to lattice phonons.

We have made temperature dependent studies of the half-width and frequency shift of the gap mode of the NO_3^- ion in KI single crystals for the first time as it has not been possible in past to undertake such studies on gap modes as the difference band absorption of the host lattice at temperatures above 10 K dominates the spectral region near the gap. This will be discussed in detail in chapter VI.

REFERENCES

1. Alderman D.W. and Cotts R.M 1970 Phys. Rev. B1, 2870

2. Alexander R.W. Jr. Hughes A.E. and Sievers A.J. 1970 Phys. Rev. B1, 1563.

3. Barker A.S. Jr. and Sievers A.J. 1975 Rev. Mod. Phys. 47, Suppl. 2, S1.

4. Barker E.F. 1929 Phys. Rev. 33, 684.

5. Bauerle D. 1973 Springer Tracts in Modern Physics 68, 76.

6. Becker C.R. and Martin T.P. 1972 Phys. Rev. B5, 1604.

7. Beyler H.U. 1972 Phys. Status Solidi (b) 52, 419.

8. Bridges F. 1972 Phys. Rev. B8, 3321.

9. Bridges F. 1973 Solid State Commun. 13, 1877.

10. Bron W.E. and Dreyfus R.W. 1966 Phys. Rev. Lett. 16, 165.

11. Brugger K. and Mason W.P. 1961 Phys. Rev. Lett 7, 270.

12. Brugger K., Fritz T.C. and Kleinman D.A. 1967 J. Acoust. Soc. Am. 41, 1015.

13. Chau C.K., Klein M.V. and Wedding B. 1967 Phys. Rev. Lett. 17, 371.

14. Cleeton C.E. and William N.H. 1934 Phys. Rev. 45, 234.

15. De Jong C., Wegdam G.H. and Van der Elsken J. 1973 Phys. Rev. B8, 4868.

16. De Souza M. and Luty F. 1973 Phys. Rev. B8, 5866.

17. De Souza M., Gongora A., Aegerter M. and Luty F. 1970 Phys. Lett 25, 1426.

18. Devonshire A.F. 1936 Proc. Roy. Soc. A153, 601.

19. Dienes G.J., Hatcher R.D., Smoluchowski R. and Wilson W. 1966 Phys. Rev. Lett 16, 25.

20. Dotsch H. 1969 Phys. Status Solidi 31, 649.

21. Dreybrodt W. and Fussgaenger K. 1966 Phys. Status Solidi 18, 133.

22. Dreyfus R.W. 1969 Phys. Rev. 188, 1340.

23. Eisenmenger W. and Dayen A.H. 1967 Phys Rev. Lett 18, 125.

24. Elliot R.J., Hayes W., Jones G.D. and Macdonald H.F. 1965 Proc. Roy. Soc. A289, 1.

25. Evans A.R. and Fitchen D.B. 1970 Phys. Rev. B2, 1074.

26. Fritz B. 1968 in Localized Excitation in Solids edited by R.F. Wallis (Plenum, New York) p 480.

27. Gomez M., Bowen S.P. and Krumhansl J.A. 1967 Phys. Rev. 153, 1009.

28. Gupta R.K. and Mathur P. 1976 Solid State Commun. 18, 835.

29. Gupta R.K. and Mathur P. 1980 J. Phys. Chem. Solid 41, 385.

30. Haridasan T.M., Gupta R.K. and Ludwig W. 1973 Solid State Commun 12, 1205.

31. Hartel H. and Luty F. 1965 Phys. Status Solidi 12,347.

32. Hartel H and Luty F. 1968, International Color Center Conference, Rome (unpublished).

33. Hetzler M.C. and Walton D. 1970 Phys. Rev. Lett. 24, 505.

34. Hetzler M.C. and Walton D. 1973a Phys. Rev. B8, 4801.

35. Hetzler M.C. and Walton D. 1973b Phys. Rev. B8, 4812.

36. Hund F. 1927 Z. Physik 43, 805.

37. Ishigama M., Becker C.R., Martin T.P. and Prettle W. 1972 Phys. Status Solidi (b) 54, K81.

38. Jaswal S.S. 1965 Phys. Rev. 140, A687.

39. Jaswal S.S. 1972 Phys. Lett. 42A, 309.

40. Kalyani S. and Haridasan T.M. 1976 Chem. Phys. Lett. 44, 184.

41. Kapphan S. 1974 J. Phys. Chem. Solids 35, 621.

42. Kapphan S. and Luty F. 1968 Solid State Commun. 6, 907.

43. Kapphan S. and Luty F. 1972 Phys. Rev. B6, 1537.

44. Kapphan S. and Luty F. 1973 J. Phys. Chem. Solids 34, 969 .

45. Kinder H. 1972 Phys. Rev. Lett. 27, 410.

46. Kirby R.D., Hughes A.E. and Sievers A.J. 1970 Phys. Rev. B2, 481.

47. Klein M.V. 1961 Phys. Rev. 122, 1393.

48. Kuhn U. and Luty F. 1964 Solid State Commun. 2, 281.

49. Kuhn U. and Luty F. 1965 Solid State Commun. 4, 31.

50. Larson T.R. and Silsbee R.H. 1972 Phys. Rev. B5, 778.

51. Lombardo G. and Pohl R.O. 1965 Phys. Rev. Lett. 15,291.

52. Luty F. 1974a Phys. Rev. B10, 3667.

53. Luly F. 1974b Phys. Rev. B10, 3677.

54. Maradudin A.A. 1966 in Solid State Physics edited by F. Seitz, D. Turnbull (Academic, New York) Vol.19 p 1.

55. Matthew J.A.D. 1965 Solid State Commun. 3, 365.

56. Merzbacher E. 1970 Quantum Mechanics (John Wiley, New York) Chapter 5.

57. Moller W., Kaiser R. and Bilz H. 1970 Phys. Lett. 32A, 171.

58. Narayanamurti V. and Pohl R.O. 1970 Rev. Mod. Phys. 42, 201.

59. Narayanamurti V., Seward W.D. and Pohl R.O. 1966 Phys. Rev. 148, 481.

60. Nolt I.G. 1967 Ph.D. Thesis, Cornell University (unpublished).

61. Pauling L. 1930 Phys. Rev. 36, 430.

62. Peierls R.E. 1974 Quantum Theory of Solids (University Press, Oxford) Chapter 2 p 39.

63. Pompi R.L. and Narayanamurti V. 1968 Solid Commun. 6, 645.

64. Quigley R.J. and Das T.P. 1969 Phys. Rev. 177, 1340.

65. Robert R and de Souza M. 1974 Phys. Rev. B9, 5257.

66. Rollefson R.J. 1972 Phys. Rev. 135, 3235.

67. Rosenbaum R.L., Chau C.K. and Klein M.V. 1969 Phys. Rev. 186, 852.

68. Sack H.S. and Moriarty M.C. 1965 Solid State Commun. 3, 93.

69. Sauer P. 1966 Zeit fur Physik 194, 360.

70. Sauer P. 1967 Zeit fur Physik 199, 280.

71. Scott R.S. and Flygare 1969 Phys. Rev. 182, 445.

72. Seward W.D. and Narayanamurti V. 1966 Phys. Rev. 148, 463.

73. Shepherd I.W. and Feher G. 1965 Phys. Rev. Lett. 15, 194.

74. Shore H.B. 1966 Phys. Rev. Lett 17, 1142.

75. Shore H.B. and Sander L.M. 1975 Phys. Rev. B12, 1546.

76. Sievers A.J. and Lytle C.D. 1965 Phys. Lett 14, 271.

77. Templeton T.L. and Clayman B.P. 1971 Solid State Commun. 9, 697.

78. Timusk T. and Staude W. 1964 Phys. Rev. Lett 13, 373.

79. Verma A.L. 1980 J. Phys. C: Solid State Phys. 13, 2009.

80. Ward R.W. and Clayman B.P. 1974a Can. J. Phys. 52, 1502.

81. Ward R.W. and Clayman B.P. 1974b Phys. Rev. B9, 4455.

82. Ward R.W. and Clayman B.P. 1974c Solid State Commun. 14, 1335.

83. Wilson W.D., Hatcher R.D., Dienes G.J. and Smoluchowski R. 1967 Phys. Rev. 161, 888.

84. Windheim R. 1976 Solid State Commun. 18, 1183.

85. Windheim R. and Kinder H. 1975 Phys. Lett 51A, 475.

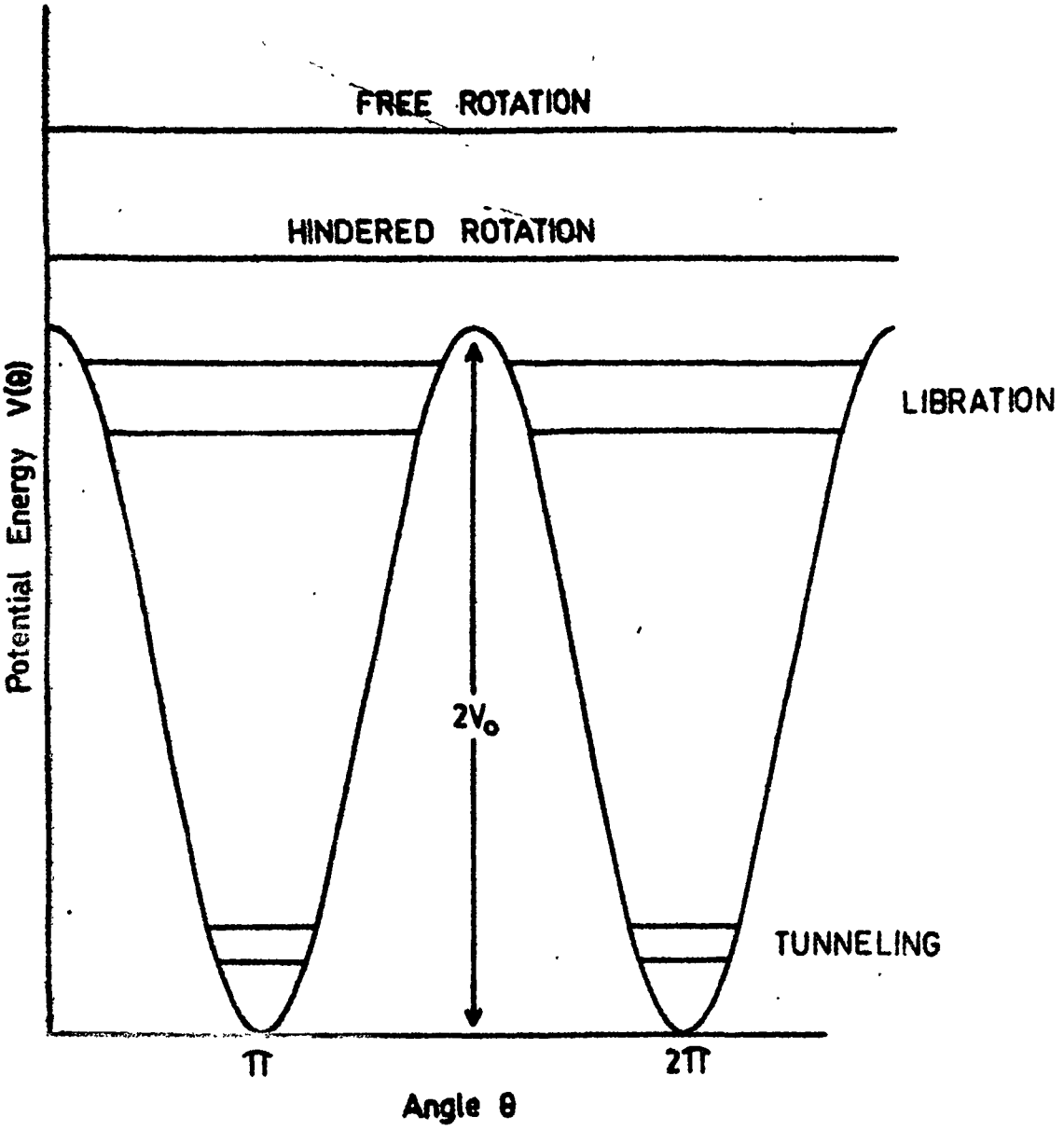

Figure 2.1 The Pauling's potential function $V=V_0(1-\cos 2\theta)$. The tunneling, librational, hindered rotational, and free rotational states are indicated in the figure.

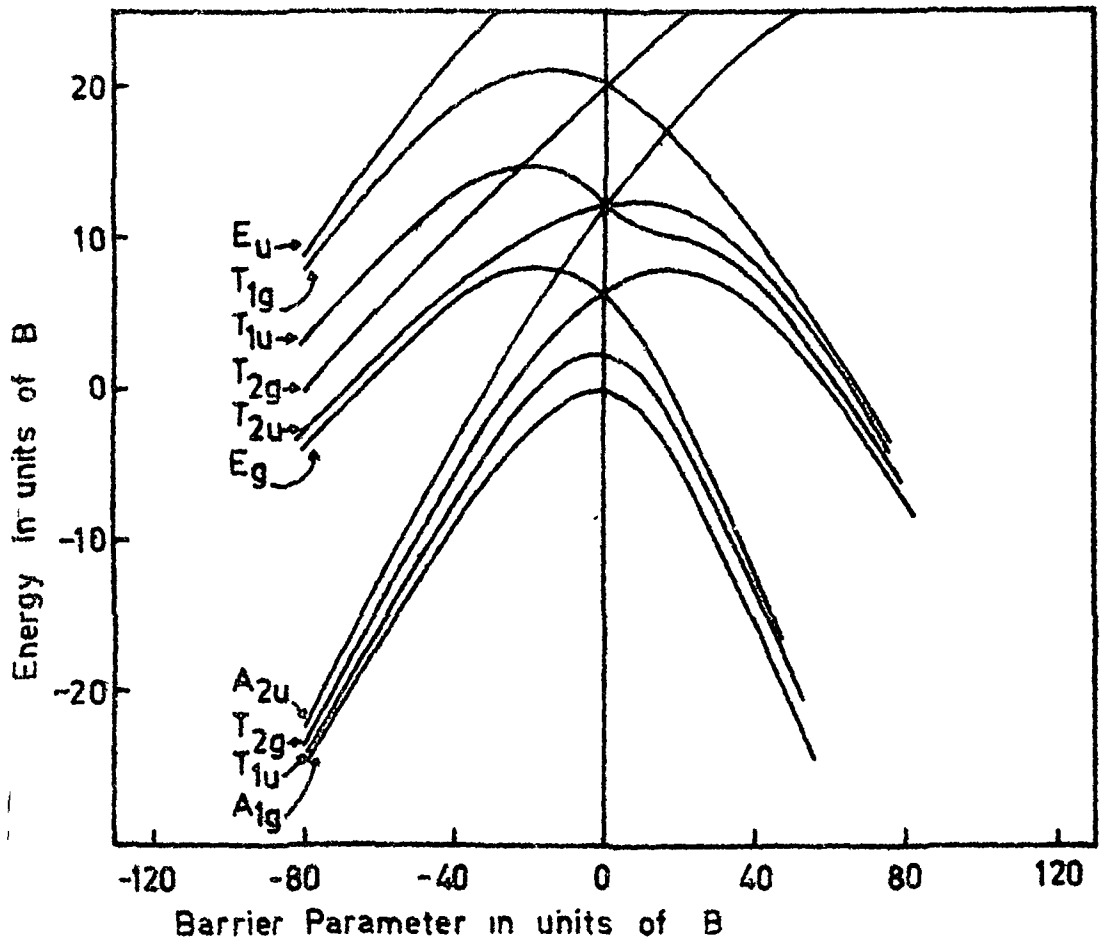

Figure 2.2 Influence of the Devonshire potential on the low lying rotational states of a molecule of rotational constant B. Energies and barrier parameter K are in units of B. With increasing barrier height the librational frequencies increase and tunnel splittings decrease. In the limit of large negative K, the librational ground state is split into four states and for large positive K, the ground state splits into three states.

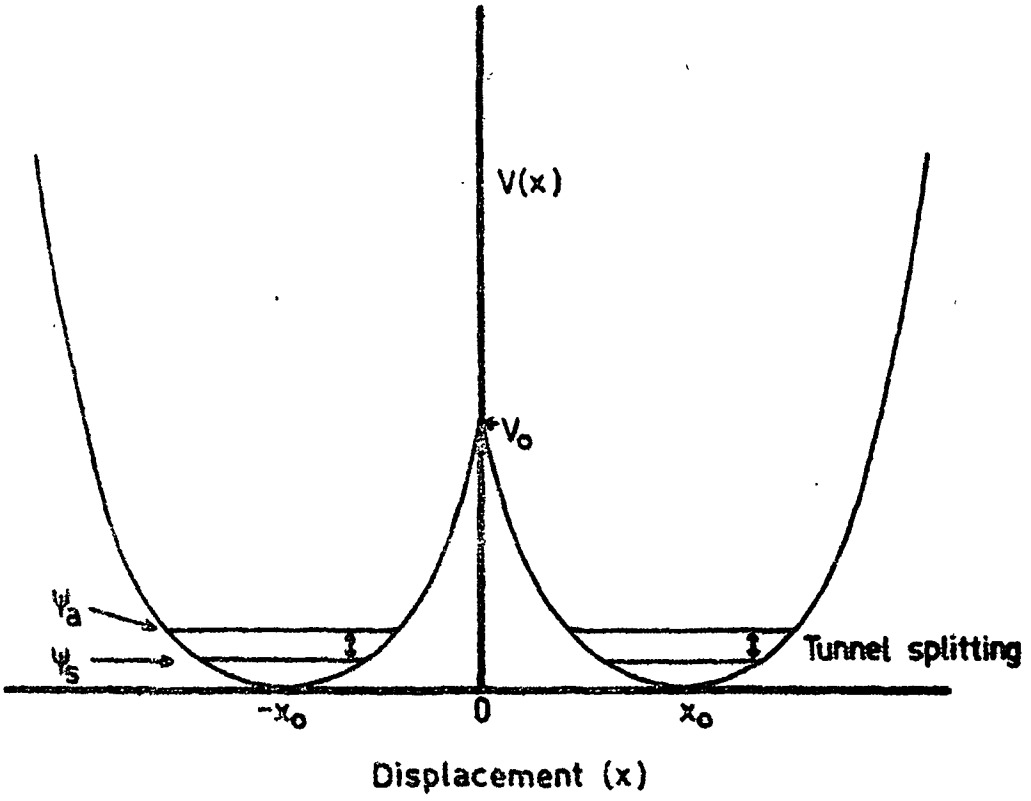

Figure 2.3 Model potential of the one-dimensional double-well harmonic oscillator.

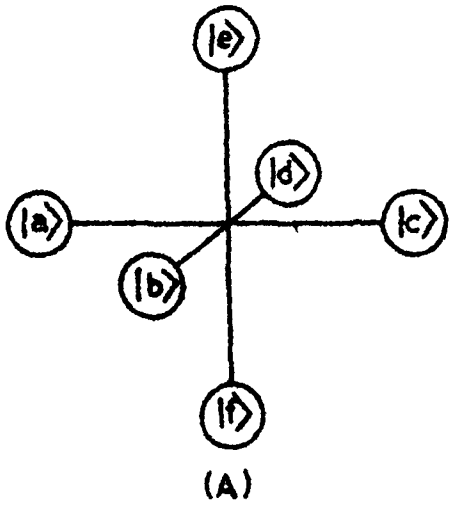

(A)

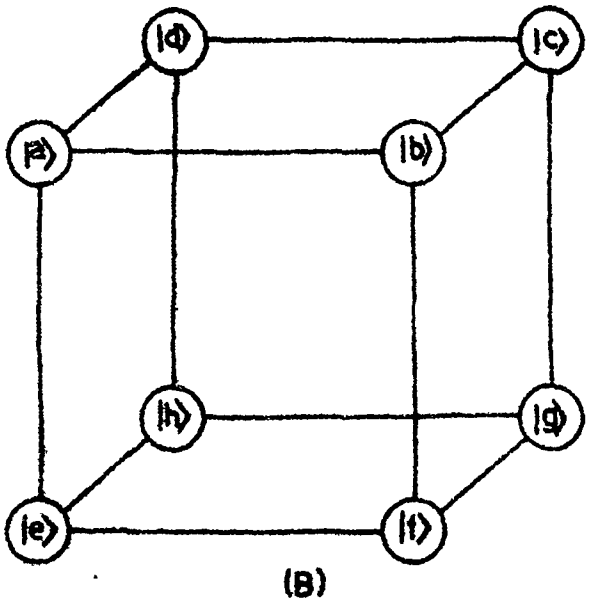

(B)

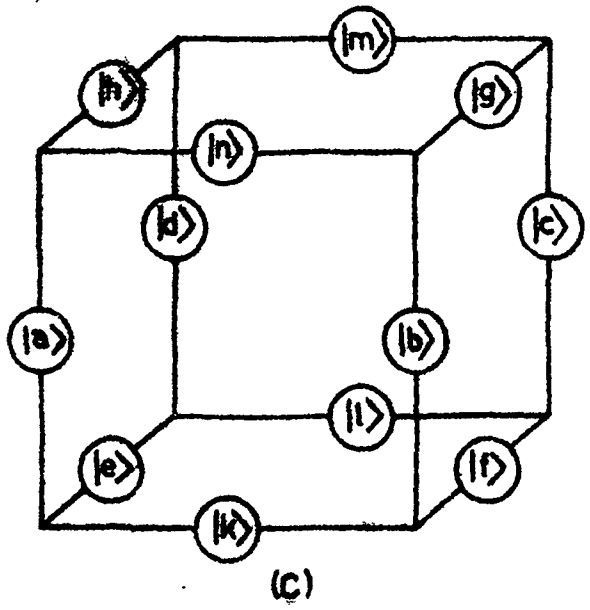

(C)

Figure 2.4 Minima positions and labeling of the localized harmonic oscillator basis states ($|a\rangle, |b\rangle, |c\rangle, |d\rangle, \cdots$, etc.) for (A) XY_6, (B) XY_8, and (C) XY_{12} models.

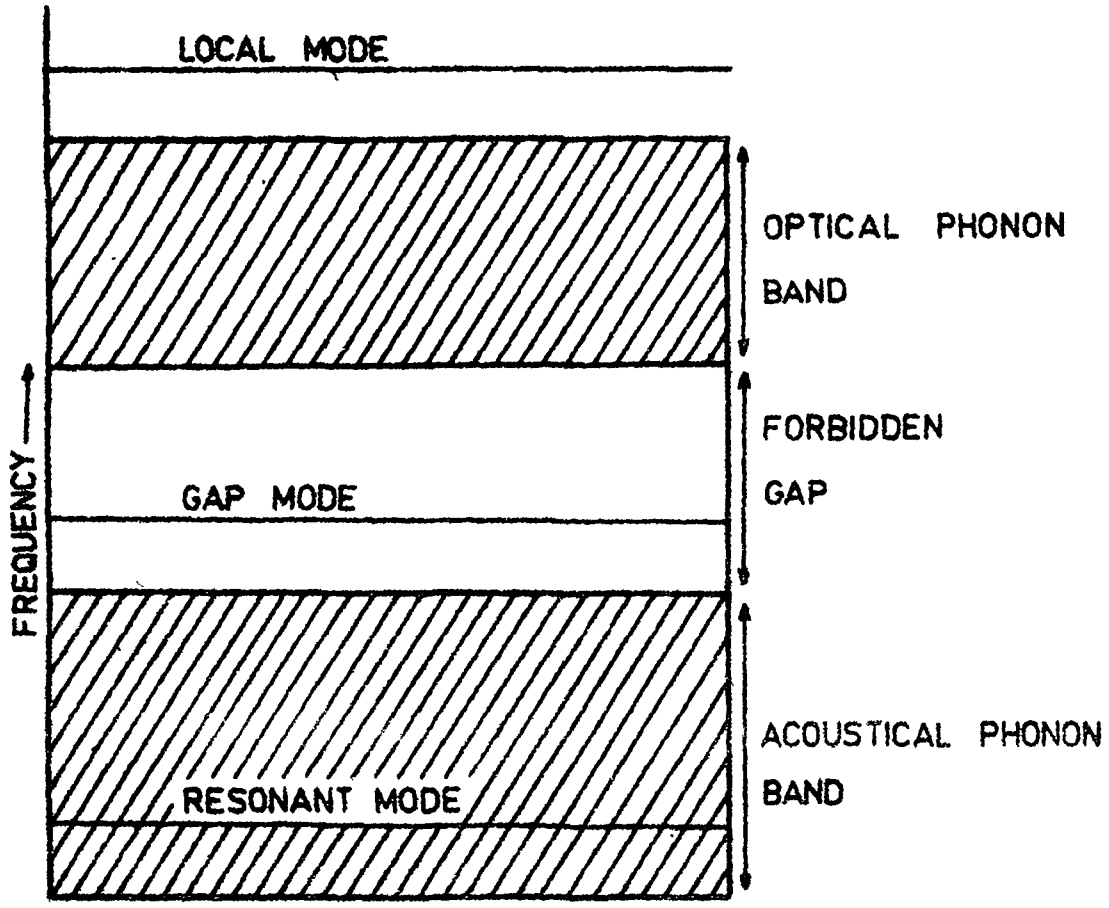

Figure 2.5 Schematic diagram showing resonant mode, gap mode and local mode due to impurity ions substituted in otherwise pure crystals.

CHAPTER III

EXPERIMENTAL PROCEDURE

Single crystals of potassium iodide doped with potassium nitrite were grown by pulling from the melt using the Kryopolous technique. The starting materials were high purity reagent grade substances. To prevent OH^- contamination, potassium iodide was baked at $\sim 400^\circ C$ in nitrogen atmosphere for few days after grinding repeatedly. After being pulled from the melt the crystals were cooled slowly in about a week to room temperature to avoid any inhomogenieties. The resulting crystals always contain both the nitrite and nitrate ions in comparable concentrations but by growing under nitrogen atmosphere, more than 95% nitrate ions can be converted into nitrite ions. The NO_3^- and NO_2^- concentrations in doped KI crystals were determined by spectrophotometric methods. For small concentration studies, crystals containing $\sim 10^{17}$ ions cm^{-3} and upto 20 mm thickness were used in the experiments. For high concentration studies, crystals containing $\sim 10^{18}$ to $\sim 10^{19}$ ions cm^{-3} and of $\sim$ 1 mm thickness were used. Single crystals of nitrate-doped KI were obtained by the same method as for the $KI:NO_2^-$ crystals by adding 0.02 to 0.05% KNO_3 by weight in KI. The $KI:NO_3^-$ crystals were grown under the atmosphere of dry oxygen gas. The concentration of the nitrate ions in

the resulting crystals was of the order of 10^{17} to 10^{18} ions cm^{-3}. Samples of $\sim 10 \times 10 \times 8$ mm^3 were cut from the boules and polished properly. To avoid interaction effect among impurities, samples of large thickness and lower concentration were used.

The high resolution infrared absorption measurements were made on a Perkin-Elmer Ebert-14 spectrometer equipped with a helium-cooled copper-doped germanium bolometer as a detector. This detector has a 1mm x 1mm sensitive area. The infrared radiation after absorption by the sample has to be focussed at this area of the detector. The detector is not background limited when operated above 77K. Reduction of operating temperature results in background limited operation with increase in detectivity and time constant. At these conditions the detector has almost uniform detectivity over a range 1000 to 5000 cm^{-1}. The gratings used in the monochromator had 144 lines per mm. Filters were used to remove infrared radiation of higher frequencies. The spectrometer was flushed with dry nitrogen to remove the atmospheric water vapour. Nernst glower was used as a source. The infrared radiation after dispersion from the monochromator was chopped mechanically and then focussed at the sample held in a cryostat in a modified optical arrangement between the exit slit of the monochromator and the detector. This arrangement allows only monochromatic infrared radiation to fall on the sample and not the whole

range of it. Thus the use of monochromatic radiation reduces the infrared heating of the sample. Low temperature absorption measurements were made with a resolution of 0.03 to 0.05 cm^{-1}, All spectra were recorded at a rate of two to four wavenumbers per hour. At sample temperatures above 25 K, absorption lines become relatively broad and spectra were recorded with a resolution between 0.1 and 0.15 cm^{-1}. The resolution of the instrument was checked with the water vapour bands very carefully. Variable temperature measurements between 1.7 and 4.2 K were made with the help of an immersion cryostat by pumping on the liquid helium and temperatures were determined from the vapour pressure of the helium gas. Temperatures below 4.2 K were obtained by using an immersion cryostat. The sample holder is immersed in the refrigerant. The main part of the cryostat is the copper can in which the sample is immersed. The copper can was soldered to the stainless steel helium container by means of indium. The copper can has provisions for sealing two optical windows. CaF_2 windows were sealed using a special type of epoxy. CaF_2 is preferred because it has an expansion coefficient at room temperature almost identical to that of the copper. CaF_2 can be used effectively at or above about 1000 cm^{-1}. The sample holder having threaded base was attached to stainless steel rod. Its height was adjustable and it could be rotated as well. The helium container was surrounded by a nitrogen radiation shield of

copper which is connected to a liquid nitrogen container of copper surrounding the upper part of the stainless steel helium container. The whole system was enclosed in a vacuum can of stainless steel which had two room temperature windows of Irtran IV. For measurements between 5 and 77 K, a variable temperature conduction cryostat of convensional design was used. Sample temperature was adjusted by passing a regulated current through a nichrome wire heater wrapped around the sample holder. The temperature was measured by determining the resistance of a 1/10 W Allen-Bradley carbon resistor of either 1000 or 4700 Ω nominal resistance which were calibrated at boiling temperatures of liquid helium and nitrogen at atmospheric pressure. Temperature measurements above 5 K are accurate to better than $\pm$ 0.50 K.

The spectrometer gives the absorption spectrum of a sample in terms of its transparency. Transparency of a layer of material is defined as the ratio of the intensity of the transmitted light (I_t) to that of the incident light (I_i). Thus the transparency of a sample is recorded on a non-linear scale. We have to reduce it to linear scale, i.e., in terms of optical density. Optical density is defined as the common logarithm of the opacity where opacity is the reciprocal of the transiparency. Thus

$$\text{Transparency} = \frac{I_t}{I_i}$$

$$\text{Opacity} = \frac{I_i}{I_t}$$

and

$$\text{Optical density} = \log_{10}\left(\frac{I_i}{I_t}\right)$$

The absorption peaks of interest as recorded by the spectrometer were divided into small bins of frequency interval and percent transimittance was measured at these points. With the help of standard tables, this was converted into optical density and plotted on a linear scale. The spectra shown in different figures in this thesis are the replotted figures showing optical density on a linear wavenumber scale.

Most of the experimental measurements were made by Prof. A.L. Verma when he was working at the University of Amsterdam. We are grateful to Prof. J. Van der Elsken of the University of Amsterdam for providing facilities for experimental work.

CHAPTER IV

TUNNELING MOTION OF THE NO_2^- ION IN KI SINGLE CRYSTALS.*

ABSTRACT

Motional states of the NO_2^- ion doped in KI single crystals have been investigated using high resolution infrared technique. At very low concentrations of the impurity, the antisymmetric stretching vibration (ν_3) of the NO_2^- ion shows multiplet structure at 1.7 K. This structure can be understood in terms of contributions of different type of tunneling motions of the NO_2^- ion among the twelve equivalent potential wells in KI lattice. An attempted has been made to give an estimate of the potential barriers hindering reorientation of the ion in the KI lattice.

---

* Paper based on this study is going to appear:
S.S. Khatri and A.L. Verma 1983.
J. Phys. C: Solid State Phys. 16 (in press)

4.1. INTRODUCTION AND REVIEW OF WORK DONE ON THE NO_2^- ION DOPED IN ALKALI HALIDES.

The nitrite ion is a bent dipolar molecule of C_{2v} point group symmetry having three axes of rotation as shown in figure 4.1. It is almost a prolate symmetric top with the rotational constants A = 4.22 cm^{-1}, B = 0.45 cm^{-1} and C = 0.43 cm^{-1} about the three principal axes passing through the centre of mass of the ion (Narayanamurti et al 1966). The nitrite ion in various alkali halide hosts has been studied by a number of workers. Its gap modes in KI have been studied by Timusk and Staude (1964), Sievers and Lytle (1965), Renk (1965) and many others. Renk (1965) suggested that the NO_2^- ion in alkali halide lattices may have several equilibrium positions with the possibility of tunneling. From a study of the fine structure associated with the normal modes and thermal conductivity measurements, Narayanamurti et al (1966) concluded that this ion must have several low lying tunneling states in the potassium halides. They interpreted their results on the basis of Pauling's model (1930). For the NO_2^- ion in KBr and KI, the situation becomes more complex because of evidence for simultaneous rotational motions and the motion associated with displacement of the centre of mass of the ion in its cavity (Narayanamurti and Pohl 1970). The NO_2^-

ion in NaCl appeared to be immobile at low temperatures. Avarma and Rebane (1969) observed the luminescence spectra of the NO_2^- ion in potassium halides which gave the evidence of hindering effect of the crystal field on the rotation of the ion. On the basis of stress-induced dichroism of the ν_1 and ν_3 fundamental vibrations of the NO_2^- ion in KCl at 2 K, Narayanamurti et al (1966) concluded that the equilibrium orientation of the NO_2^- dipole (which is also the C_2 axis of the ion) was along the $\langle 110 \rangle$ direction and (110) was the molecular plane. These measurements were not performed for KBr and KI host lattices but were assumed to give similar effects. Evans and Fitchen (1970) confirmed these findings by their stress-induced dichroism in the UV absorption of the NO_2^- ions in potassium halides and deduced that the O-O axis of the ion points along the $\langle 001 \rangle$ direction (figure 4.2). The Raman spectra and polarization measurements on these systems by Rebane and Rebane (1973) and Rebane et al (1974) were consistent with the findings of Evans and Fitchen (1970). The $\langle 110 \rangle$ orientation of the NO_2^- ion and O-O axis along the $\langle 001 \rangle$ direction is consistent with the C_{2v} symmetry of the ion and also is electrostatically favoured, since in this orientation, the negatively charged oxygen atoms of the ion make their closest approach to the positively charged nearest-neighbour K^+ ions. Dielectric relaxation measurements by Sack and Moriarty (1965) indicated a larger dipole moment of 0.97 Debye for the

KI:NO_2^- system compared to 0.21 Debye for the KCl:NO_2^- system which is expected for the dipole moment of the ion situated at the centre of the cavity. The large dipole moment for the KI:NO_2^- system implies that the NO_2^- ion may take off-centre position in the cavity with its centre of mass displaced along the $\langle 110 \rangle$ direction because of the high polarizability of the I^- ion which would tend to attract the positive nitrogen ion. Therefore the dynamics of the NO_2^- ion in KI should be similar to that of an off-centred ion with twelve potential wells for the orientation of its dipole moment.

In this chapter we present our high resolution infrared measurements on the KI:NO_2^- system for low concentrations of the NO_2^- ions in KI. At low ($\sim 10^{17}$ ions cm^{-3}) concentration, a very complex and temperature dependent structure (at least six components) with the antisymmetric stretching vibration ν_3 is observed which is interpreted as arising from the tunneling motion of the NO_2^- ion among the twelve $\langle 110 \rangle$ equivalent equilibrium orientations of the ion in the KI lattice at 1.7 K. From the observed unequal spacings of the tunnel-split levels, we have attempted to calculate potential barriers for different types of tunnelings.

4.2 EXPERIMENTAL RESULTS

Infrared spectra of the NO_2^- ion in alkali halides in the fundamental vibration region have been reported by

Narayanamurti et al (1966). The strongest bands for the KI:NO_2^- system are found in the region of the ν_3 fundamental vibration centred around 1253 cm^{-1} while much weaker bands are observed corresponding to the symmetric stretching ν_1 at nearly 1308 cm^{-1} and bending mode ν_2 at 805 cm^{-1}. The ν_3 fundamental vibration band shows a half-width of about 0.6 cm^{-1} without any apparent structure with crystals containing $\sim 10^{18}$ ions cm^{-3} at 1.7 K. When crystals of $\sim$ 20 mm thickness containing $\sim 10^{17}$ ions cm^{-3} are used, the ν_3 fundamental band at 1.7 K shows a splitting into six prominant closely-spaced components at 1252.41, 1252.57, 1252.75, 1252.83, 1252.97 and 1253.24 cm^{-1} with instrumental resolution of $\sim$ 0.03 cm^{-1}. The splitting of the ν_3 fundamental band has been explained due to the tunneling of the NO_2^- ion in KI among the twelve $\langle 110 \rangle$ equilibrium orientations (Khatri and Verma 1983). The relative intensities of the components show temperature dependence between 1.7 and 4.2 K. These measurements were repeated with several crystal specimen containing varying impurity concentrations and after annealing them extensively. All the observations on these different crystals were in general agreement. The temperature dependent studies of the components were made qualitatively to confirm that they arise due to the tunneling of ions, and were not due to pair modes, interstitial sites,etc. A typical spectrum at 1.7 K is shown in figure 4.3. Above 4.2 K the width of the lines becomes large and it becomes

difficult to identify the individual components separately.

4.3 DISCUSSION

The complicated structure associated with the ν_3 fundamental vibration of the NO_2^- ion in KI can be understood in terms of tunneling of the ion among the twelve equivalent positions displaced along the $\langle 110 \rangle$ directions. There are basically two theories to understand three dimensional tunneling behaviour of atoms and molecules in crystals. They are the Devonshire model and the GBK model as discussed in chapter II. The small spacings between the components of the ν_3 band of the NO_2^- ion in KI suggests that the potential barriers for tunneling are large and hence, the GBK model should be a good approximation for this system. The Devonshire model is good for small and medium potential barriers. Moreover, in this model, the centre of mass of molecular impurities coincide with the centre of the cavity formed by replacement of the host ion. The molecule then rotates about an axis passing through the centre of mass of the ion in octahadral potential and the motion of the ion is a function of angular coordinates only. But in case of the NO_2^- ion in KI, the centre of mass of the NO_2^- ion is displaced owing to its large dipole moment of 0.97 Debye (Sack and Moriarty 1965)) and so, its motion includes centre of mass movement alongwith angular motions. It becomes difficult to explain this in terms of the Devonshire

model. The centre of mass of the off-centred NO_2^- ion moves from one potential well to another by tunneling through the potential barriers. Therefore, it can be better understood in terms of the GBK model. The dipole moment of the NO_2^- ion in KI points along the $\langle 110 \rangle$ direction with its centre of mass displaced along the same direction. The orientation of the NO_2^- ion in KI is shown in figure 4.2. The NO_2^- ion has twelve equilibrium configurations and corresponds to the XY_{12} model (figure 2.4C).

Measurements were made on the ν_3 fundamental vibration of the $\langle 110 \rangle$ oriented dipolar NO_2^- ion doped in KI. In the absence of tunneling, the ground and excited states of the ν_3 fundamental of the NO_2^- ion in KI will be 12-fold degenerate. The symmetries of the ground and excited states are A_1 and B_1 in the C_{2v} point group which corresponds to the A_{1g} and A_{2u} symmetries in the O_h point group for the NO_2^- ion in KI. Tunneling among different equivalent wells leads to the splitting of the 12-fold orientational degeneracy of both these levels producing $E(A_{1g})$, $E(E_g)$, $E(T_{1u})$, $E(T_{2u})$ and, $E(T_{2g})$ ground vibrational levels and $E(A_{2u})$, $E(E_u)$, $E(T_{2g})$, $E(T_{1g})$ and, $E(T_{1u})$ excited vibrational levels. The symmetries of the excited vibrational levels are different from those of the ground vibrational levels. This is because of the A_{2u} symmetry of the excited state of the ν_3 fundamental in the

octahedral environment. Therefore, the state A_{1g} becomes A_{2u}, E_g becomes E_u, T_{1u} becomes T_{2g}, T_{2u} becomes T_{1g} and T_{2g} becomes T_{1u} in the excited vibrational state of the ion. However, the expressions for the eigen values remain the same. From the unequal splitting of the ν_3 fundamental, it is evident that the energy levels do not have equal spacings. Transitions between these levels give rise to the multiplet structure in the ν_3 fundamental region. The energy level scheme and electric dipole allowed transitions are shown in figure 4.4. Observed and calculated line positions are given in table IV.1.

The wave functions and eigen values for the XY_{12} model have been worked out by Gomez et al (1967) which are given in chapter II. The eigen values are obtained in terms of the matrix elements and overlap integrals. In the large barrier height limit, the overlap integrals can be neglected and the eigen values can be written in terms of matrix elements only as

$$E(A_{1g}) = E_o + 4\eta + 2\mu + 4\nu + \sigma \qquad (4.1)$$

$$E(E_g) = E_o - 2\eta + 2\mu - 2\nu + \sigma \qquad (4.2)$$

$$E(T_{1u}) = E_o + 2\eta - 2\nu - \sigma \qquad (4.3)$$

$$E(T_{2u}) = E_o - 2\eta + 2\nu - \sigma \qquad (4.4)$$

$$E(T_{2g}) = E_o - 2\mu + \sigma \qquad (4.5)$$

These matrix elements are related to the 60° (η) (nearest-neighbour), 90° (μ) (next nearest-neighbour),

120° (υ) (third nearest-neighbour) and 180° (σ) (fourth nearest-neighbour) tunnelings of the NO_2^- ion. From the observed separation of the lines, it can be inferred that other matrix elements than η (60° tunneling) are also important. In fact the best fitting to the experimental observations is obtained when the matrix elements satisfy the condition $\mu > \sigma > \eta > \upsilon$ and the energy of the $E(T_{2g})$ state is equal to that of $E(T_{2u})$ of the ground vibrational state and the energy of the $E(T_{1u})$ state is equal to the energy of the $E(T_{1g})$ state of the excited vibrational state. Under these conditions, the electric dipole allowed transitions between the ground and excited vibrational levels agree quite satisfactorily with the experimentally observed line positions. The relative intensities of the predicted lines calculated on the basis of the Boltzmann distribution of population and degeneracies of various components of ground state agree well with the experimental observations (table IV.1), which of course give only the qualitative features. The actual intensities will depend on the transition dipole moments. The lowest energy transition predicted at 1252.14 cm^{-1} has not been observed presumably due to its weak intensity. Spacings between the levels of the ground vibrational states can be found from equations 4.1 - 4.5 and we get

$$E(E_g) - E(A_{1g}) = 6\,(\eta + \upsilon) = \Delta \qquad (4.6)$$

$$E(T_{1u}) - E(E_g) = 2\mu + 2\sigma - 4\eta = \Delta' \qquad (4.7)$$

$$E(T_{2u}) - E(T_{1u}) = 4(\eta - \upsilon) = \Delta'' \qquad (4.8)$$

$$E(T_{2g}) - E(T_{2u}) = 0$$

which gives $\sigma - \mu = \upsilon - \eta$ (4.9)

We have assumed same level structures in the ground and excited vibrational levels. The spacings between the observed lines and those obtained from the GBK model are as follows

$$1253.24 - 1252.97 = 0.27\ cm^{-1} = \Delta$$

$$1252.97 - 1252.83 = 0.14\ cm^{-1} = \Delta'$$

$$1252.83 - 1252.75 = 0.08\ cm^{-1} = \Delta''$$

$$1252.75 - 1252.57 = 0.18\ cm^{-1} = \Delta''$$

$$1252.57 - 1252.41 = 0.16\ cm^{-1} = \Delta'$$

using $\Delta = 0.27\ cm^{-1}$ and the average values of $\Delta' = 0.15\ cm^{-1}$ and $\Delta'' = 0.13\ cm^{-1}$ in equations 4.6 - 4.9 and solving for η, μ, υ and σ we get

$$\mu = 0.093\ cm^{-1}$$

$$\sigma = 0.060\ cm^{-1}$$

$$\eta = 0.039\ cm^{-1}$$

$$\upsilon = 0.006\ cm^{-1}$$

These results suggest that the tunneling of the NO_2^- dipoles among next nearest-neighbours (90° tunneling) is the primary mode of tunneling and 180° tunneling also contributes significantly, whereas the 60° tunneling probability is less important and 120° tunneling contributes very little to the

observed energies. The observed and calculated values of transition energies of the tunnel-split levels of the NO_2^- ion in KI are given in table IV.1 which are in reasonable agreement.

From these matrix elements, an estimate of barrier heights for the four types of tunnelings can be made with the help of simple model of a double harmonic oscillator (Gomez et al 1967) in which tunneling occurs between two wells only (figure 2.3). The matrix element δ relating two states is given by equation 2.15 in chapter II. The barrier height in this model is the potential energy of the particle at the origin. From equation 2.11 for x = o we get an expression for the barrier height as

$$V_o = \frac{1}{2} m \omega^2 x_o^2 \qquad (4.10)$$

For known values of m, x_o, and the matrix element δ ; ω can be obtained from equation 2.15 and the barrier height V_o can be calculated from equation 4.10. Equation 2.15 gives two values of ω : one is very small and the others is large. The barrier height corresponding to the small value of ω comes out to be smaller than the splitting and hence this value cannot be taken as it is unphysical. Therefore, the higher value of ω is considered. The barrier heights for four types of tunnelings corresponding to η , μ , ν and σ can be calculated if the distance $2x_o$ between the

two minima positions of the nearest-neighbour wells, next nearest-neighbour wells, third nearest-neighbour wells and fourth nearest-neighbour wells are known. These can be calculated from the knowledge of the dipole moment of the NO_2^- ion in KI. From the model, the value x_o is equal to d for η , is equal to $\sqrt{2}$d for μ , is equal to $\sqrt{3}$d for υ and is equal to 2d for σ where 2d is the displacement of the ion from the cavity centre. The procedure to find out the value of 2d is given here.

The NO_2^- ion in KI has an effective dipole moment of 0.97 Debye (Sack and Moriarty 1965) directed from the centre of mass of the ion towards the centre of the cavity, whereas its intrinsic dipole moment is 0.21 Debye in the opposite direction. Therefore the net dipole moment due to its displacement is 1.18 Debye directed towards the cavity centre. The absence of the negatively charged I^- ion from the cavity is equivalent to a positive charge with magnitude equal to that of the I^- ion. The effective ionic charge of the I^- ion in KI has been found to be $e^* = 0.71e$ (Mitra 1969), where e is the electronic charge. This effective charge forms a dipole with the negatively charged NO_2^- ion. These two charges must have a separation of $2d = 0.346\text{Å}$. Using this value of 2d, the barrier heights corresponding to η , μ , υ and σ come out to be

$V_{o\eta} = 1027.74\ cm^{-1}$

$V_{o\mu} = 322.33\ cm^{-1}$

$V_{o\upsilon} = 409.65\ cm^{-1}$

and $V_{o\sigma} = 146.90\ cm^{-1}$ respectively.

The corresponding librational frequencies $\frac{\omega}{2\pi}$ corresponding to η , μ , υ and σ tunnelings are:-

$\nu_{\eta\,lib} = 223.5\ cm^{-1}$

$\nu_{\mu\,lib} = 88.5\ cm^{-1}$

$\nu_{\upsilon\,lib} = 81.5\ cm^{-1}$

$\nu_{\sigma\,lib} = 42.25\ cm^{-1}$

These calculated librational frequencies should give rise to side bands to the ν_3 fundamental vibration of the NO_2^- ion in KI at 1476.25, 1341.25, 1334.25 and 1295 cm^{-1} respectively. We have not studied the infrared spectra in this region but Narayanamurti et al (1966) have made observations in this region. One of their observed lines at 1333.5 cm^{-1} (80.5 cm^{-1} higher satellite) corresponds quite closely to our calculated frequency at 1334.5 cm^{-1} (81.5 high satellite). Considering that we have used a simple one-dimensional double-well harmonic oscillator model for the tunneling of the NO_2^- ion in KI, our results are quite satisfactory. The search for all these librational frequencies may lend further support for our proposed model and the calculated barrier heights; although the librational frequencies do not depend solely on barrier height but are functions of

detailed nature of the potential function.

In this study we could explain the tunneling of the NO_2^- ion in KI in terms of the GBK model satisfactorily. Since the NO_2^- ion takes off-centred position in the KI lattice, it makes the tunneling motions of the ion very much complicated compared with that in other alkali halides. The reorientation of the ion in KI cannot be explained solely in terms of rotation of the ion about its a, b or c axes but it is a combination of rotational and translational motions. The 90° (α) and 180° (σ) tunneling motions can be understood in terms of rotations about the a and c axes respectively together with translational motion. The 60°(η) and 120° (ν) tunneling motions are much more complicated. Barrier heights obtained for different types of tunneling motions are large. This is mainly due to the complex nature of tunneling motions of the NO_2^- ion in KI.

REFERENCES

1. Avarma R. and Rebane L. 1969 Phys. Status Solidi 35, 107.

2. Evans A.R. and Fitchen D.B. 1970 Phys. Rev. B2 1074.

3. Gomez M., Bowen S.P. and Krumhansl J.A. 1967 Phys. Rev. 153, 1009.

4. Khatri S.S. and Verma A.L. 1983. J. Phys. C: Solid State Physics 16 (in press).

5. Mitra S.S. 1969, in Optical properties of Solid, edited by S. Nudelman and S.S. Mitra, Plenum Press (New York) p413.

6. Narayanamurti V. and Pohl R.O. 1970 Rev. Mod. Phys. 42, 201.

7. Narayanamurti V., Seward W.D. and Pohl R.O. 1966 Phys. Rev. 148, 481.

8. Pauling L. 1930 Phys. Rev. 36, 430.

9. Rebane K.K. and Rebane L.A. 1973 Proc. XIth European Congress on Molecular Spectroscopy (Lallin, USSR), edited by O. Sild (London, Butterworths).

10. Rebane L.A., Khal'dre T. Yu., Novik A.E. and Gorokhovskii A.A. 1974 Sov. Phys-Solid State 15, 2129.

11. Renk K.F. 1965 Phys. Lett. 14, 281.

12. Sack H.S., Moriarty M.C. 1965 Solid State Commun. 3, 93.

13. Sievers A.J. and Lytle C.D. 1965 Phys. Lett 14, 271.

14. Timusk T. and Staude W. 1964 Phys. Rev. Lett. 13, 373.

Table IV.1 Tunnel split lines for the KI:NO_2^- system (in cm^{-1}) as observed experimentally and calculated. The relative intensities of these lines, calculated on the basis of Boltzmann distribution and degeneracy of various components of the ground state levels, are given in the last column.

Observed line position	Calculated line position	relative intensity (calculated) in arbitrary units
-	1252.14	1.88
1252.41	1252.41	1.88
1252.57	1252.56	1.88
1252.75	1252.69	5.87
1252.83	1252.82	2.10
1252.97	1252.97	1.59
1253.24	1253.24	1.00

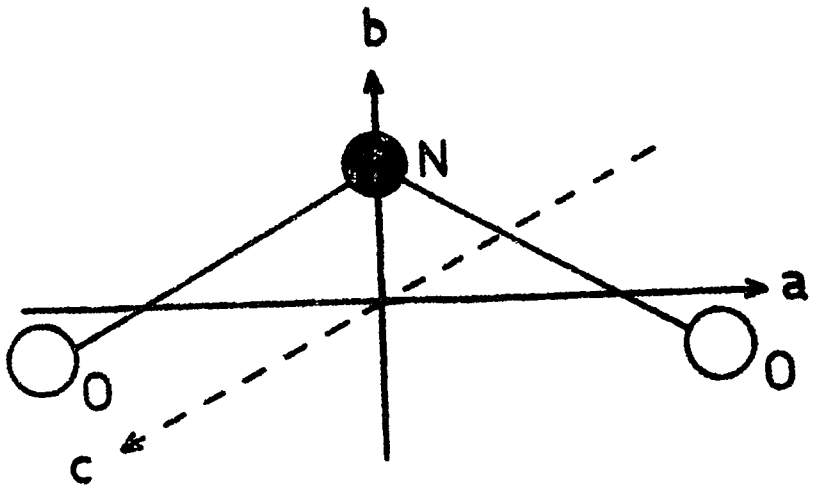

Figure 4.1 The three principal axes of rotation a, b and c of the NO_2^- ion.

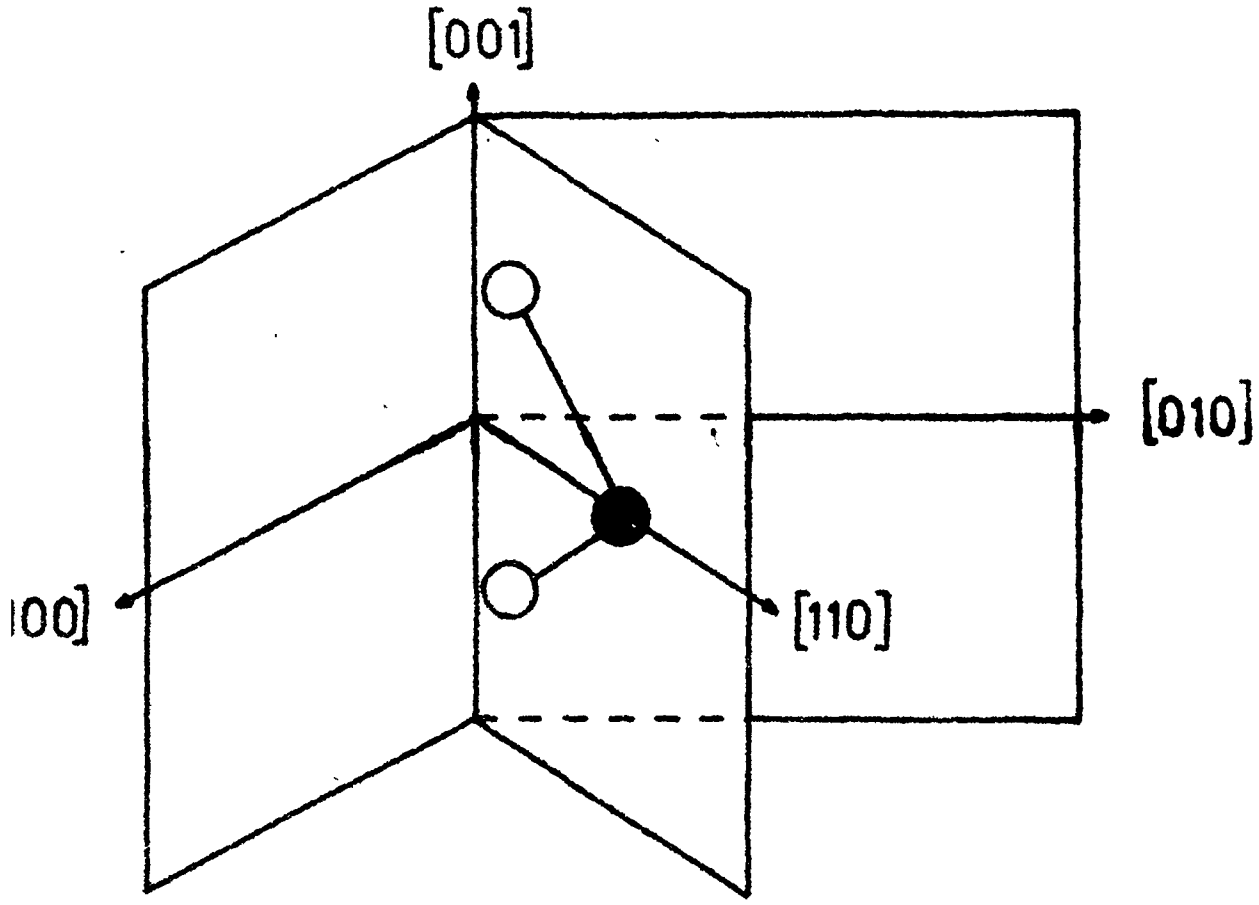

Figure 4.2 Equilibrium orientation of the off centred NO_2^- ion in KI at low temperatures, displaced towards I^- ion nearest to the nitrogen atom.

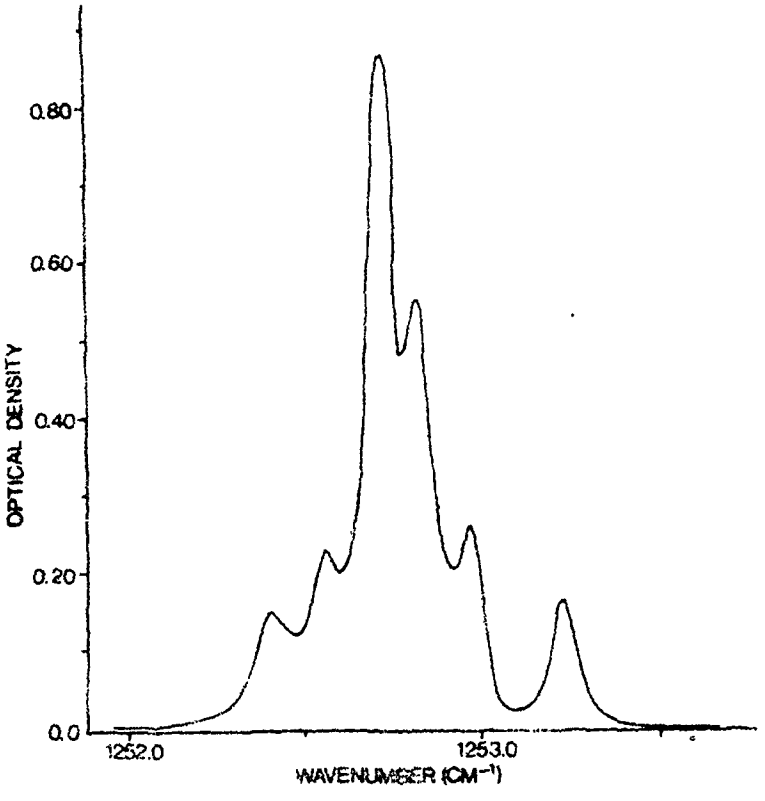

Figure 4.3 Infrared absorption spectrum of a 20mm thick KI crystal containing approximately 10^{17} NO_2^- ions cm^{-3} at 1.7 K in the ν_3 fundamental region; spectral resolution is about $0.03 cm^{-1}$.

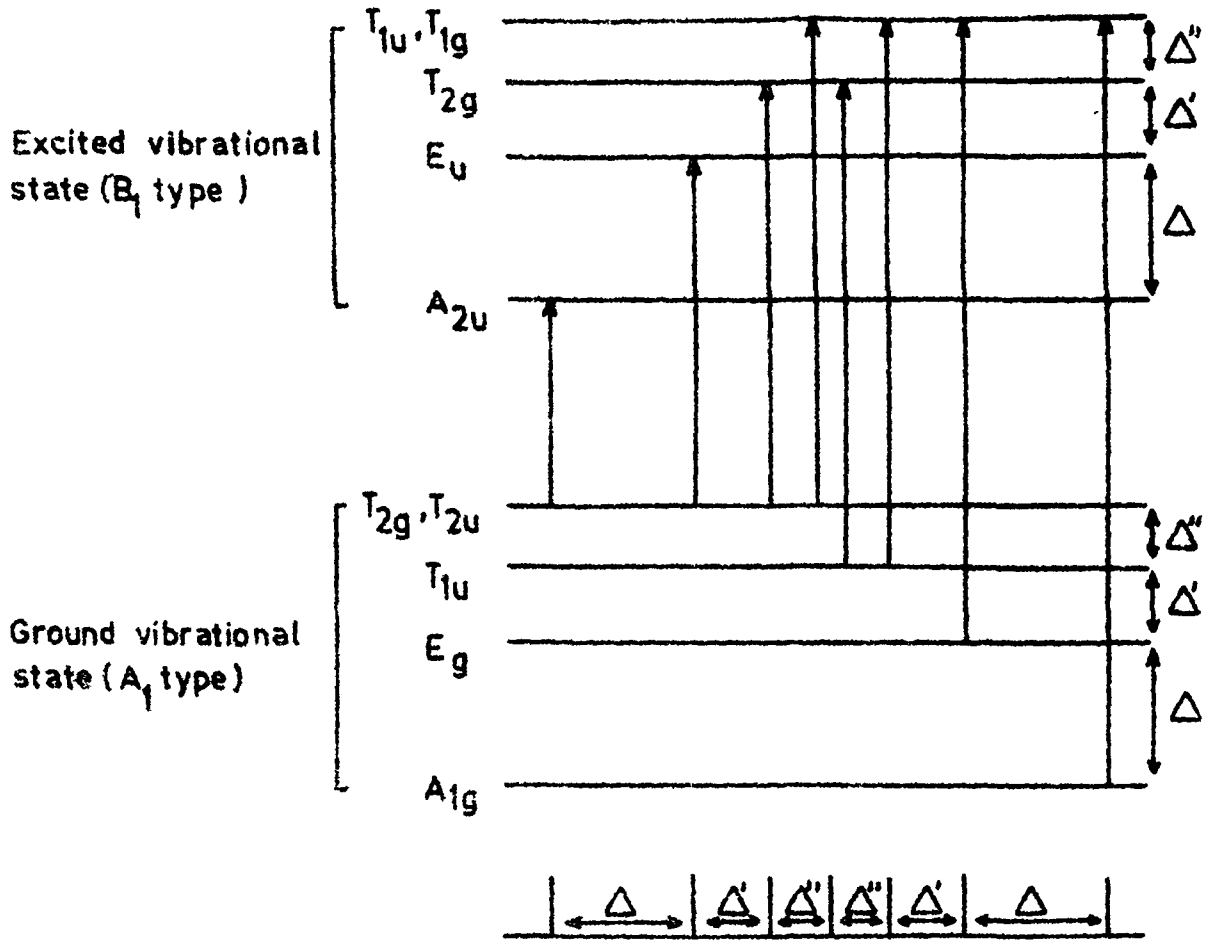

Figure 4.4 Tunneling levels of the vibrational ground and excited states for the [110] oriented dipoles (assuming the same structure in the ground and excited vibrational levels). The arrows indicate allowed optical transitions; resulting absorption lines are given in the lower part of the figure. Here $\Delta = 6(\eta+\upsilon) = 0.27\text{cm}^{-1}$, $\Delta' = (2\mu+2\sigma-4\eta) = 0.15\text{cm}^{-1}$, and $\Delta'' = 4(\eta-\upsilon) = 0.13\text{cm}^{-1}$.

CHAPTER V

LOCALIZED VIBRATIONS DUE TO PAIRS AND TRIPLET CLUSTERS OF THE NO_2^- IONS IN KI*

ABSTRACT

Several sharp bands in the vicinity of the anti-symmetric stretching vibration of the NO_2^- ion doped in KI single crystals containing $\sim 10^{19}$ ions cm^{-3} have been observed in the high resolution infrared studies at 1.7 K. These extra features have been explained as arising due to interactions between the transition dipole moments during the ν_3 vibrations of the nearby nitrite ions in pairs and triplet clusters. From these studies, we have obtained the magnitude of the transition dipole moment during ν_3 vibration of the NO_2^- doped in KI which is $\mu_t = 0.248$ Debye.

---

* A short version of this work has been accepted for publication:
S.S. Khatri and A.L. Verma 1983 Phys. Lett. (accepted for publication).

5.1 INTRODUCTION

The KI:NO_2^- system has been studied previously by Narayanamurti et al (1966) for relatively high concentrations of the NO_2^- ions ($\sim 10^{19}$ ions cm^{-3}) in KI. They reported closely-spaced lines near the ν_3 fundamental vibration band and suggested that they may be associated with the librational modes of the NO_2^- ions. In the present work we have studied high resolution infrared spectra of the KI:NO_2^- system containing high concentrations of the NO_2^- ions in KI single crystals. We have observed several temperature independent and closely-spaced distinct bands near the antisymmetric stretching vibration ν_3 of the NO_2^- ion at 1252.75 cm^{-1}. These satellite bands appear due to mutual interaction effects among the NO_2^- ions in KI. The coupling between them is provided by the transition dipole moments during the ν_3 fundamental vibration of the NO_2^- ions. We have considered several pairs and triplet clusters of the ions which are favoured energetically and have calculated their mode frequencies on the basis of coupled-harmonic oscillator model.

5.2 EXPERIMENTAL RESULTS

With relatively higher concentrations of the NO_2^- ions in KI, we have observed several temperature independent and closely-spaced distinct bands near the antisymmetric

stretching vibration ν_3 of the NO_2^- ion at 1252.75 cm^{-1}, at 1.7 K with $\sim$ 1mm thick crystals containing $\sim 10^{18}$ to 10^{19} ions cm^{-3}. At these concentrations, the main ν_3 band becomes saturated and many additional bands appear on the high and low frequency sides of the ν_3 band with spacings ranging from ~ 0.1 cm^{-1} to 1.2 cm^{-1} as shown in the figure 5.1. The bands on the low frequency side of the ν_3 vibration are much stronger compared to those on the high frequency side and the relative intensities of these bands between 1.7 and 10 K were found temperature independent. In order to check the concentration dependence, crystals containing varying concentrations of the NO_2^- ions were used. The intensities of these components relative to the intensity of the ν_3 fundamental band at 1227 cm^{-1} due to the $^{15}NO_2^-$ ions in natural abundance in the same crystal showed non-linear, roughly quadratic, dependence upon the impurity concentration. The measurements were made with the instrumental resolution of $\sim$ 0.05 cm^{-1}.

5.3 DISCUSSION

Earlier studies on this KI:NO_2^- system by Narayanamurti et al (1966) reported broad bands at 1240, 1248.5, 1245.5, 1261.0 and 1265.0 cm^{-1} near the ν_3 band at 1253 cm^{-1}. They interpreted the appearance of the high frequency satellite at 1254.5 cm^{-1} due to almost a free rotation of the ion around its b-axis, while other bands

were speculated to arise from librations of the ion. This possibility can be ruled out on the basis of our concentration dependent studies on the band observed by us at 1254 cm^{-1} and other bands. For concentrations of $\sim 10^{18}$ ions cm^{-3} used by Narayanamurti et al (1966), the mutual interactions between the NO_2^- ions in KI cannot be neglected, and such interactions should give rise to side bands. We have made observations in KI crystals containing varying concentrations of $\sim 10^{18}$ to 10^{19} NO_2^- ions cm^{-3}. At such high concentrations, formations of pairs and triplet clusters of the NO_2^- ions in KI are favoured (Behringer 1958) and mutual interaction effects become important. We have studied these interaction effects and explained the origin of various satellite bands observed near the ν_3 band in terms of these interactions. As discussed earlier, at higher concentrations of the NO_2^- ions in KI ($\sim 10^{18}$ to $\sim 10^{19}$ ions cm^{-3}), many satellite bands appear near the ν_3 fundamental band (figure 5.1). These bands were not observed with crystals containing lower concentration of the ions. Behringer (1958) has calculated the probability of occurance of pairs and triplet clusters for a random distribution of atoms in a cubic lattice. The non-linear, roughly quadratic, dependence of the intensities of these bands on the concentration of the ions suggests that these bands arise due to interacting ions in pairs and triplet clusters. The coupling between the two localized harmonic oscillators is provided by the interaction

between the transition dipole moments during the ν_3 vibration of the NO_2^- ions in KI (Khatri and Verma 1983). We have considered nearest-neighbour pairs, second nearest-neighbour pairs, open-triplets, closed-triplets and a third type of triplets which will be referred to as triplet clusters of third type. The NO_2^- ion does not occupy the normal lattice site but is displaced in the direction of its C_2 axis in KI along the $\langle 110 \rangle$ direction. Therefore, the centre of mass of one of the NO_2^- ions in the nearest-neighbour pairs may be near the origin, which is taken as one of the normal anion site, and the centre of mass of the other ion may be near the $(\frac{a}{2}, \frac{a}{2}, 0)$ position in the lattice (figure 5.2a) where a is the lattice constant. For the nearest-neighbour pairs in which the C_2 axes of the NO_2^- ions point along the $[110]$ and $[1\bar{1}0]$ directions the coordinates of the centre of mass of the first ion will be $(\sqrt{2}d, \sqrt{2}d, 0)$ and that of the second ion will be $(\frac{a}{2} + \sqrt{2}d, \frac{a}{2} - \sqrt{2}d, 0)$ where 2d is the displacement of the centre of mass of the ion from the normal lattice site. Since there are twelve possibilities for each NO_2^- ion, there will be altogether 144 types of pairs, out of which many will be identical. Similarly coordinates of the centre of mass of the ions in the second nearest-neighbour pairs, open-triplet clusters, closed-triplet clusters and triplet clusters of third type can be found. In the case of second nearest-neighbours, the position of one of the ions will be

near the origin and of the other ion will be near (a,0,0) (figure 5.2b). The positions of the ions in the open-triplets would be near the origin, ($\frac{a}{2}$, $\frac{a}{2}$, 0) and near (a,a,0) (figure 5.2c); in the closed-triplets they would be near (0,0,0), ($\frac{a}{2}$, $\frac{a}{2}$, 0) and (0, $\frac{a}{2}$, $\frac{a}{2}$) (figure 5.2d); and in the triplet clusters of third type, they would be near (0,0,0), ($\frac{a}{2}$, $\frac{a}{2}$,0) and (0,a,0) (figure 5.2e).

The dipole interaction varies as R^{-3}, the interaction effect will be negligible for dipoles situated at larger distances from each other. Therefore, we have considered only the pairs and triplet clusters of the types mentioned above and have neglected contributions due to other distant pairs and clusters. Moreover, for large distances ($R \gg a$), there should be correction factor in the dipole-dipole interaction but it is close to unity for smaller distances as discussed in chapter II.

For the NO_2^- ions in KI there are two types of interactions. One is between the permanent dipoles and the other is between the transition dipoles during the ν_3 vibration of the NO_2^- ions. The interactions between the permanent dipoles of the NO_2^- ions determines the relative orientations of the NO_2^- dipoles while the second type of interaction is responsible for the coupling between the NO_2^- localized oscillations during their ν_3 vibration and give rise to satellite bands. The transition dipole moment

of the NO_2^- ion during its ν_3 vibration lies in the plane of the ion and is perpendicular to the permanent dipole direction, i.e., it is along the a axis of the ion as shown in figure 4.1. The NO_2^- ion has a permanent dipole moment of 0.97 Debye along the $\langle 110 \rangle$ direction. Because of the twelve equilibrium orientations possible for the NO_2^- ions in KI lattice there will be various possible configurations of pairs and triplet clusters. For pairs there are $12^2 = 144$ possibilities and for triplet clusters there are $12^3 = 1728$ possibilities and hence for dipole-dipole interactions. But the number of distinct possibilities are not so large. There will be positive and negative interaction energies between permanent dipoles. Because of the possibility of tunneling, the ions will align in those configurations in which a pair or a triplet cluster will have large negative interaction energy. The pairs and triplet clusters with positive interaction energies are very unlikely energetically and their population would be negligible. We have considered the mutual interaction between the transition dipole moments of only those pairs and triplets clusters which have large negative interaction energies between permanent dipoles.

If $\vec{\mu}_i$ and $\vec{\mu}_j$ are the two permanent dipoles and $\vec{R}_{ij}$ is the distance between them then the interaction energy is given by:

$$W_{pair} = \frac{\mu^2}{R_{ij}^3}\left[\hat{\mu}_i \cdot \hat{\mu}_j - 3(\hat{\mu}_i \cdot \hat{R}_{ij})(\hat{\mu}_j \cdot \hat{R}_{ij})\right] \cdots (5.1)$$

where $\hat{\mu}_i$, $\hat{\mu}_j$ and $\hat{R}_{ij}$ are the unit vectors along the $\vec{\mu}_i$, $\vec{\mu}_j$ and $\vec{R}_{ij}$ respectively. $\mu^2 = |\vec{\mu}_i||\vec{\mu}_j|$ since, $|\vec{\mu}_i| = |\vec{\mu}_j|$ and $|\vec{R}_{ij}| = |\vec{R}_{ji}|$. For triplet clusters, the interaction energy is given by:

$$W_{trip} = \frac{\mu^2}{2} \sum_{\substack{i,j=1 \\ i \neq j}}^{3} \frac{(\hat{\mu}_i \cdot \hat{\mu}_j) - 3(\hat{\mu}_i \cdot \hat{R}_{ij})(\hat{\mu}_j \cdot \hat{R}_{ij})}{R_{ij}^3} \quad \cdots (5.2)$$

the factor of $1/2$ comes to avoid double counting. We have calculated the interaction energies from expressions (5.1) and (5.2) for all possible configurations and have taken into account only the large negative interaction energies which are given in tables V.1, V.2, V.3, V.4 and V.5,. For nearest-neighbour pairs we have considered nine negative interaction energies, for second nearest-neighbours five, for open-triplets five, for closed-triplets only three, since this type of clusters are the least probable, and for the third type of triplets, we have considered five largest negative energies between the permanent dipoles. The orientations of the C_2 axes of the NO_2^- ions in pairs and triplet clusters considered are given in tables V.1 -V.5.

The ν_3 vibration of the NO_2^- ion is the localized harmonic oscillator. In pairs two such harmonic oscillators are coupled to each other as mentioned earlier. The equation

of motion for such a coupled harmonic oscillator is given by the expression (2.16). But in case of the NO_2^- ions, $m_1=m_2=m$ and $\omega_1 = \omega_2 = \omega$ which is equal to the frequency of the ν_3 vibration. The equation of motion of two such coupled harmonic oscillators can be written as:

$$H = \frac{1}{2} m(\dot{q}_i^2 + \dot{q}_j^2 + q_i^2\omega^2 + q_j^2\omega^2) + Bq_iq_j \quad \cdots (5.3)$$

q_i and q_j are the normal coordinates of the NO_2^- ions during the ν_3 vibration and B is the coupling constant. The last coupling term can be written in terms of dipole-dipole interaction as:

$$Bq_iq_j = \frac{\mu_t^2}{r_{ij}^3}\left[\hat{\mu}_{ti}\cdot\hat{\mu}_{tj} - 3(\hat{\mu}_{ti}\cdot\hat{r}_{ij})(\hat{\mu}_{tj}\cdot\hat{r}_{ij})\right] \quad \cdots (5.4)$$

where $\vec{\mu}_{ti}$ and $\vec{\mu}_{tj}$ are the transition dipole moments of the two ions, $|\vec{r}_{ij}| = |\vec{r}_{ji}|$ is the distance between the centres of two dipoles and $\mu_t^2 = |\vec{\mu}_{ti}|\cdot|\vec{\mu}_{tj}|$, since $|\vec{\mu}_{ti}| = |\vec{\mu}_{tj}| = \mu_t$. $\hat{\mu}_{ti}$, $\hat{\mu}_{tj}$ and $\hat{r}_{ij}$ are the unit vectors along $\vec{\mu}_{ti}$, $\vec{\mu}_{tj}$ and $\vec{r}_{ij}$ respectively. A triplet cluster is equivalent to three pairs of coupled harmonic oscillators. The coupling is the sum of the

interactions of transition dipoles of the three pairs, which can be written as:

$$B' \sum_{\substack{i,j=1 \\ (i\neq j)}}^{3} q_i q_j = \frac{\mu_t^2}{2} \sum_{\substack{i,j=1 \\ (i\neq j)}}^{3} \left[\frac{\hat{\mu}_{ti}\cdot\hat{\mu}_{tj} - 3(\hat{\mu}_{ti}\cdot\hat{r}_{ij})(\hat{\mu}_{tj}\cdot\hat{r}_{ij})}{r_{ij}^3} \right] \quad \ldots (5.5)$$

The distance between the centres of two dipoles can be calculated from the coordinates of the centre of mass of the two ions which can be found from the displacement ($2d=0.346\text{Å}$) of the ion in KI and direction of displacement. These factors are known for the NO_2^- ions embedded in KI lattice as explained earlier.

We have calculated the coupling terms using expressions (5.4) and (5.5) for all possible orientations of the NO_2^- ions having negative interaction energies between permanent dipoles which are given in various tables (V.1 - V.5). For a particular pair, for instance, nearest-neighbour pairs, whose C_2 axes are along the [110] and [101] directions; $\vec{\mu}_t$ can be either in the [001] or [00$\bar{1}$] direction for the first ion and in the [010] or [0$\bar{1}$0] direction for the second ion. Therefore there are $2^2 = 4$ possibilities for such interactions which can be schematically represented as (1) $\uparrow\uparrow$ (2) $\downarrow\downarrow$ (3) $\uparrow\downarrow$ and (4) $\downarrow\uparrow$. These can be grouped into two sets depending on the values of interaction

energies between the induced dipole moments (transition dipole moment) μ_t of the ions. First and second configurations are identical and third and fourth configurations are identical as far as the interaction between the induced dipoles are concerned. Therefore, there are only two distinct possibilities for interaction between the induced dipole moments of the NO_2^- ions in a pair. For the pairs whose μ_t are along the same direction, for instance, pairs with their C_2 axes along the [110] and [1$\bar{1}$0] directions, the configuration in which the induced dipole moments are in opposite phase will not show any infrared absorption because of total cancellation of the varying dipole moments. They may show Raman scattering due to changing polarizability of the system. Such possibilities are not there for triplet clusters. For triplet clusters there are $2^3 = 8$ possibilities for interaction between the induced dipoles because of the same reasons as mentioned above. These eight possibilities can be schematically represented as (1)$\uparrow\uparrow\uparrow$,(2) $\downarrow\downarrow\downarrow$, (3)$\uparrow\uparrow\downarrow$,(4)$\downarrow\downarrow\uparrow$,(5) $\uparrow\downarrow\uparrow$,(6)$\downarrow\uparrow\downarrow$,(7) $\uparrow\downarrow\downarrow$ and (8)$\downarrow\uparrow\uparrow$. These can be grouped into four sets depending on the values of the interaction energies between the three induced dipole moments. First and second configurations are identical, third and fourth are identical, fifth and sixth are identical and seventh and eighth configurations are identical as far as the interaction between the induced

dipole moments are concerned. Therefore there are only four distinct possibilities for the interaction between the induced dipole moments of the NO_2^- ions in a triplet cluster. We have calculated the interaction energies which are given in tables V.1 - V.5. The position of a satellite band is obtained by adding the interaction energy of the induced dipoles to the ν_3 band calculated in cm^{-1}. Interactions with negative sign give satellite bands on the low frequency side of the ν_3 band and those with positive sign give satellite bands on the higher frequency side. Here the transition dipole moment μ_t is an adjustable parameter. We have calculated the interaction energies for various values of μ_t, but μ_t= 0.248 Debye gave best agreement with the experimental observations. Since there are numerous possibilities of interaction energies, several calculated line positions correspond to a single observed line. We have given the calculated and observed lines in tables V.6 and V.7,. The agreement between the calculated and observed lines is quite satisfactory. The line calculated at 1263.76 cm^{-1} (11.01 cm^{-1} higher satellite) was not observed by us since our observation did not extend beyond 1261 cm^{-1} but Narayanamurti et al(1966) have observed this line at 1265 cm^{-1} which may correspond to our calculated value.

The transition dipole moment is related to the

dipole derivative by the relation

$$\mu_t = \frac{\partial \mu}{\partial q} \delta q \qquad \cdots \quad (56)$$

where q is the normal coordinate of the NO_2^- ion associated with its ν_3 vibration. Decius (1955) calculated the dipole derivative for the NO_3^- ion in KNO_3 and CO_3^{-2} ions in $CaCO_3$, $SrCO_3$ and $BaCO_3$. He considered the coupling between the nearest-neighbour NO_3^- ions in KNO_3, and the CO_3^{-2} ions in $CaCO_3$, $SrCO_3$ and $BaCO_3$ during the out-of-plane bending modes of these ions. He considered the interactions between the induced dipole moments of the ions in pairs during their out-of-plane bending vibrations. From his data the induced dipole moment of the NO_3^- ions in KNO_3 comes out to be 1.43 Debye and for the CO_3^{-2} ions in $CaCO_3$, $SrCO_3$ and $BaCO_3$ induced dipole moments come out to be 1.48, 1.69 and 1.90 Debye respectively. For the NO_2^- ion in KI the magnitude of the transition dipole moment comes out to be 0.248 Debye which is small compared to the above mentioned systems. This suggests that the coupling between the nearby NO_2^- ions in KI should be weak which is confirmed by the closely-spaced lines observed by us with the ν_3 fundamental vibration of the NO_2^- ion in KI. Small value of μ_t will give small interaction energies for pairs and triplet clusters of the NO_2^- ions in KI and hence the closely-spaced lines with the ν_3 fundamental vibration of the ion.

Our high resolution studies on this system have resolved the earlier controversies regarding the origin of these well defined sharp bands. Our studies confirm that these bands arise due to mutual interactions between the nearby NO_2^- ions in KI and are not due to free rotations or librations of the ions.

REFERENCES

1. Behringer R.E. 1958 J. Chem. Phys. 29, 537.

2. Decius J.C. 1955 J. Chem. Phys. 23, 1290.

3. De Souza M. and Luty F. 1973 Phys. Rev. B 8, 5866.

4. Khatri S.S. and Verma A.L. 1983 Phys. Lett (accepted for publication)

5. Narayanamurti V., Seward W.D. and Pohl R.O. Phys. Rev. 148, 481.

Table V.1 Interaction energies of permanent dipoles and transition dipoles of the NO_2^- ions in nearest-neighbour pairs. Types of the pairs giving same interaction energy are given in the last column. The pairs are characterized by the directions of the permanent dipoles near (0,0,0) and (a/2,a/2, 0) positions.

Interaction energy (cm^{-1}) (permanent dipoles)	Interaction energy (cm^{-1}) (transition dipoles)	Orientation of permanent dipole moments in the nearest-neighbour pairs
-15.37	± 0.20	$[1\bar{1}0][011]$, $[1\bar{1}0][01\bar{1}]$, $[\bar{1}10][101]$, $[\bar{1}10][10\bar{1}]$, $[\bar{1}01][1\bar{1}0]$ $[\bar{1}0\bar{1}][\bar{1}\bar{1}0]$, $[0\bar{1}1][\bar{1}10]$, $[0\bar{1}\bar{1}][\bar{1}10]$
-34.16	± 0.24	$[\bar{1}\bar{1}0][\bar{1}01]$, $[\bar{1}\bar{1}0][\bar{1}0\bar{1}]$, $[\bar{1}\bar{1}0][0\bar{1}1]$, $[\bar{1}\bar{1}0][0\bar{1}\bar{1}]$, $[101][110]$, $[10\bar{1}][110]$, $[011][110]$, $[01\bar{1}][110]$
-44.46	± 0.30	$[110][101]$, $[110][10\bar{1}]$, $[110][011]$, $[110][01\bar{1}]$, $[\bar{1}01][\bar{1}\bar{1}0]$, $[\bar{1}0\bar{1}][\bar{1}\bar{1}0]$, $[0\bar{1}1][\bar{1}\bar{1}0]$, $[0\bar{1}\bar{1}][\bar{1}\bar{1}0]$
-23.52	± 0.33	$[1\bar{1}0][\bar{1}01]$, $[1\bar{1}0][\bar{1}0\bar{1}]$, $[\bar{1}10][0\bar{1}1]$, $[\bar{1}10][0\bar{1}\bar{1}]$, $[101][\bar{1}10]$, $[10\bar{1}][\bar{1}10]$, $[011][1\bar{1}0]$, $[01\bar{1}][1\bar{1}0]$
-29.03	-1.22	$[101][10\bar{1}]$, $[10\bar{1}][101]$, $[\bar{1}01][\bar{1}0\bar{1}]$, $[\bar{1}0\bar{1}][\bar{1}01]$, $[011][01\bar{1}]$, $[01\bar{1}][011]$, $[0\bar{1}1][0\bar{1}\bar{1}]$, $[0\bar{1}\bar{1}][0\bar{1}1]$.

continued.....

Interaction energy (cm^{-1}) (permanent dipoles)	Interaction energy (cm^{-1}) (transition dipoles)	Orientation of permanent dipole moments in the nearest-neighbour pairs
-17.64	+ 2.19	$[10\bar{1}][\bar{1}0\bar{1}]$, $[10\bar{1}][\bar{1}01]$, $[0\bar{1}1][0\bar{1}\bar{1}]$, $[01\bar{1}][0\bar{1}1]$.
-48.21	$\pm$ 3.67	$[10\bar{1}][01\bar{1}]$, $[10\bar{1}][011]$, $[\bar{1}01][0\bar{1}\bar{1}]$, $[\bar{1}0\bar{1}][0\bar{1}1]$, $[01\bar{1}][10\bar{1}]$, $[01\bar{1}][101]$, $[0\bar{1}1][\bar{1}0\bar{1}]$, $[0\bar{1}\bar{1}][\bar{1}01]$.
-38.27	+ 2.48	$[1\bar{1}0][\bar{1}10]$, $[\bar{1}10][1\bar{1}0]$.
-78.67	+ 2.55	$[110][\bar{1}\bar{1}0]$, $[\bar{1}\bar{1}0][\bar{1}\bar{1}0]$.

Table V.2 Interaction energies of permanent dipoles and transition dipoles of the NO_2^- ions in second nearest-neighbour pairs. Types of the pairs giving same interaction energy are given in the last column. The pairs are characterized by the directions of the permanent dipoles near (0,0,0) and (a,0,0) positions.

Interaction energy (cm^{-1}) (Permanent dipoles)	Interaction energy (cm^{-1}) (transition dipoles)	Orientation of permanent dipole moment in second nearest-neighbour pairs
-8.41	± 0.11	$[\bar{1}10][0\bar{1}1]$, $[110][0\bar{1}\bar{1}]$, $[1\bar{1}0][011]$, $[1\bar{1}0][01\bar{1}]$, $[101][01\bar{1}]$, $[\bar{1}01][0\bar{1}\bar{1}]$, $[10\bar{1}][011]$, $[10\bar{1}][0\bar{1}1]$, $[011][\bar{1}\bar{1}0]$, $[011][\bar{1}0\bar{1}]$, $[01\bar{1}][\bar{1}\bar{1}0]$, $[01\bar{1}][\bar{1}01]$, $[0\bar{1}1][\bar{1}10]$, $[0\bar{1}1][\bar{1}0\bar{1}]$, $[0\bar{1}\bar{1}][\bar{1}10]$, $[0\bar{1}\bar{1}][\bar{1}01]$,
-13.68	-1.75	$[01\bar{1}][0\bar{1}\bar{1}]$, $[\bar{0}1\bar{1}][0\bar{1}1]$, $[0\bar{1}1][01\bar{1}]$, $[0\bar{1}\bar{1}][011]$
-20.66	+ 0.90	$[\bar{1}10][1\bar{1}0]$, $[1\bar{1}0][\bar{1}10]$, $[\bar{1}10][\bar{1}\bar{1}0]$, $[\bar{1}\bar{1}0][\bar{1}10]$, $[101][10\bar{1}]$, $[10\bar{1}][\bar{1}01]$, $[\bar{1}01][\bar{1}0\bar{1}]$, $[\bar{1}0\bar{1}][\bar{1}01]$.
-6.92	+ 0.90	$[110][110]$, $[1\bar{1}0][1\bar{1}0]$, $[\bar{1}10][\bar{1}10]$, $[\bar{1}\bar{1}0][\bar{1}\bar{1}0]$, $[101][101]$, $[10\bar{1}][10\bar{1}]$, $[\bar{1}01][\bar{1}01]$, $[\bar{1}0\bar{1}][\bar{1}0\bar{1}]$.

Table V.3 Interaction energies of permanent dipoles and transition dipoles of the NO_2^- ions in open-triplet clusters. Types of the triplet cluster giving same interaction energy are given in the last column. The triplet clusters are characterized by the directions of the permanent dipoles near (0,0,0) (a/2,a/2,0) and (a,a,0) positions. Each triplet cluster gives four interaction energies between transition dipole moments as given in this table.

Interaction energy(cm^{-1}) (permanent dipoles)	Interaction energy (cm^{-1}) (transition dipoles)	Orientation of permanent dipole moments in the open-triplet clusters
-95.21	-7.50 0.16 7.18 0.16	$[0\bar{1}\bar{1}][\bar{1}01][0\bar{1}\bar{1}]$, $[0\bar{1}1][\bar{1}0\bar{1}][0\bar{1}1]$, $[01\bar{1}][101][01\bar{1}]$, $[011][10\bar{1}][011]$, $[\bar{1}0\bar{1}][0\bar{1}1][\bar{1}0\bar{1}]$, $[\bar{1}01][0\bar{1}\bar{1}][\bar{1}01]$,$[10\bar{1}][011][10\bar{1}]$, $[101][01\bar{1}][101]$.
-97.90	-3.39 -3.95 3.36 3.98	$[011][\bar{1}01][\bar{1}\bar{1}0]$, $[0\bar{1}1][\bar{1}0\bar{1}][\bar{1}\bar{1}0]$, $[\bar{1}0\bar{1}][0\bar{1}1][\bar{1}\bar{1}0]$, $[\bar{1}01][0\bar{1}\bar{1}][\bar{1}\bar{1}0]$, $[110][10\bar{1}][011]$, $[\bar{1}10][\bar{1}01][01\bar{1}]$.
-127.95	2.87 2.24 -2.83 -2.27	$[0\bar{1}\bar{1}][\bar{1}\bar{1}0][\bar{1}\bar{1}0]$, $[0\bar{1}\bar{1}][\bar{1}\bar{1}0][\bar{1}\bar{1}0]$, $[\bar{1}0\bar{1}][\bar{1}\bar{1}0][\bar{1}\bar{1}0]$, $[101][\bar{1}\bar{1}0][\bar{1}\bar{1}0]$, $[110][110][01\bar{1}]$, $[\bar{1}10][\bar{1}10][011]$, $[\bar{1}10][\bar{1}10][10\bar{1}]$ $[\bar{1}10][\bar{1}10][\bar{1}01]$

continued.....

Interaction energy (cm^{-1}) (permanent dipoles)	Interaction energy (cm^{-1}) (transition dipoles)	Orientation of permanent dipole moments in the open-triplet clusters
-117.00	2.3 -2.78 -2.33 2.81	$[01\bar{1}][110][110]$, $[011][110][110]$, $[10\bar{1}][110][110]$, $[101][110][110]$, $[\bar{1}\bar{1}0][\bar{1}\bar{1}0][0\bar{1}\bar{1}]$, $[\bar{1}\bar{1}0][\bar{1}\bar{1}0][0\bar{1}1]$, $[\bar{1}\bar{1}0][\bar{1}\bar{1}0][\bar{1}0\bar{1}]$, $[\bar{1}\bar{1}0][\bar{1}\bar{1}0][\bar{1}01]$.
-166,31	5.42 -0.32 -4.78 -0.32	$[\bar{1}\bar{1}0][\bar{1}\bar{1}0][\bar{1}\bar{1}0]$, $[110][110][110]$

Table V.4 Interaction energies of permanent dipoles and transition dipoles of the NO_2^- ions in closed-triplet clusters. Types of the triplet clusters giving same interaction energy are given in the last column. The triplet clusters are characterized by the directions of permanent dipoles near (0,0,0), (a/2,a/2,0) and (0, a/2,a/2) positions. Each triplet cluster gives four interaction energies between transition dipole moments as given in this table.

Interaction energy (cm^{-1}) (Permanent dipoles)	Interaction energy (cm^{-1}) (transition dipoles)				Orientation of permanent dipole moments in the closed-triplet clusters.
-126.84	-3.13	-4.21	3.61	3.73	$[001][10\bar{1}][110]$, $[01\bar{1}][10\bar{1}][110]$, $[\bar{1}01][\bar{1}\bar{1}0][011]$, $[\bar{1}\bar{1}0][0\bar{1}\bar{1}][10\bar{1}]$, $[110][011][\bar{1}01]$, $[10\bar{1}][110][0\bar{1}\bar{1}]$.
-110.31	1.19	-5.56	-1.78	6.15	$[01\bar{1}][0\bar{1}\bar{1}][110]$, $[\bar{1}01][0\bar{1}\bar{1}][10\bar{1}]$ $[\bar{1}01][\bar{1}\bar{1}0][\bar{1}10]$, $[10\bar{1}][011][0\bar{1}\bar{1}]$ $[10\bar{1}][\bar{1}01][\bar{1}\bar{1}0]$, $[110][01\bar{1}][\bar{1}\bar{1}0]$.
-144.64	-3.67	-3.67	-3.67	11.01	$[\bar{1}01][0\bar{1}\bar{1}][110]$, $[10\bar{1}][011][\bar{1}\bar{1}0]$.

Table V.5 Interaction energies of permanent dipoles and transition dipoles of the NO_2^- ions in triplet clusters of third type. Type of the triplet clusters giving same interaction energy are given in the last column. The triplet clusters are characterized by the directions of the permanent dipoles near (0,0,0), (a/2, a/2, 0) and (0,a,0) positions. Each triplet cluster gives four interaction energies between transition dipole moments as given in this table.

Interaction energy (cm^{-1}) (Permanent dipoles)	Interaction energy (cm^{-1}) (transition dipoles)				Orientation of permanent dipoles in the triplet clusters of third type.
-102.04	-2.24	-2.65	-2.46	2.86	$[\bar{1}0\bar{1}]$ $[1\bar{1}0]$ $[1\bar{1}0]$, $[\bar{1}0\bar{1}]$ $[1\bar{1}0]$ $[1\bar{1}0]$, $[1\bar{1}0]$ $[110]$ $[\bar{1}0\bar{1}]$, $[110]$ $[110]$ $[\bar{1}0\bar{1}]$.
-107.29	2.96	-2.3	-2.8	2.14	$[\bar{1}\bar{1}0]$ $[\bar{1}\bar{1}0]$ $[10\bar{1}]$, $[\bar{1}\bar{1}0]$ $[\bar{1}\bar{1}0]$ $[10\bar{1}]$, $[10\bar{1}]$ $[\bar{1}10]$ $[\bar{1}10]$, $[10\bar{1}]$ $[\bar{1}10]$ $[\bar{1}10]$.
-110.53	6.14	-1.19	-3.92	-1.04	$[\bar{1}10]$ $[\bar{1}10]$ $[\bar{1}\bar{1}0]$, $[\bar{1}10]$ $[1\bar{1}0]$ $[1\bar{1}0]$.
-109.04	5.76	-0.81	-4.30	-0.66	$[1\bar{1}0]$ $[\bar{1}10]$ $[\bar{1}10]$, $[\bar{1}\bar{1}0]$ $[\bar{1}\bar{1}0]$ $[110]$.
-103.67	-1.49	-4.80	-0.30	6.59	$[\bar{1}\bar{1}0]$ $[\bar{1}\bar{1}0]$ $[1\bar{1}0]$, $[\bar{1}10]$ $[\bar{1}10]$ $[110]$.

Table V.6 Observed and calculated satellite bands due to nearby interacting transition dipoles during ν_3 vibration of the NO_2^- ions in KI on the low frequency side of the ν_3 band.

Observed	Calculated	corresponding interaction energies (cm^{-1}) transition dipole	type of cluster
1252.06	1252.09	-0.66	triplet (3rd type)
1251.78	1251.94	-0.81	triplet (3rd type)
	1251.71	-1.04	triplet (3rd type)
	1251.56	-1.19	triplet (3rd type)
	1251.53	-1.22	n.n. pair
1250.97	1251.00	-1.75	2nd n.n. pair
	1250.97	-1.78	closed triplet
1250.56	1250.56	-2.19	n.n. pair
	1250.48	-2.23	open triplet
	1250.42	-2.33	open triplet
	1250.51	-2.24	triplet (3rd type)
	1250.45	-2.30	triplet (3rd type)
1250.12	1250.10	-2.65	triplet (3rd type)
	1250.29	-2.46	triplet (3rd type)
1249.14	1249.08	-3.67	n.n. pair
	1249.08	-3.67	closed triplet
1248.76	1248.80	-3.95	open triplet
	1248.83	-3.92	triplet (3rd type)
1248.25	1247.97	-4.78	open triplet
	1248.54	-4.21	closed triplet
	1247.95	-4.80	triplet (3rd type)
	1248.45	-4.32	triplet (3rd type)

continued...

Observed cm^{-1}	Calculated cm^{-1}	Corresponding interaction energy (cm^{-1}) (transition dipoles)	type of cluster
1247.23	1247.19	-5.56	closed triplet
1246.15	-		
1245.25	1245.25	-7.50	open triplet
-	1252.64	-0.11	2nd n.n. pair
	1252.55	-0.20	n.n. pair
	1252.51	-0.24	n.n. pair
	1252.45	-0.30	n.n. pair
	1252.42	-0.33	n.n. pair
	1252.43	-0.32	open triplet
-	1251.26	-1.49	triplet(3rd type)
-	1249.92	-2.83	open triplet
	1249.97	-2.78	open triplet
	1249.95	-2.80	triplet (3rd type)
-	1249.36	-3.39	open triplet
	1249.62	-3.13	closed triplet

Table V.7 Observed and calculated satellite bands due to nearby interacting transition dipoles during ν_3 vibration of the NO_2^- ions in KI on the high frequency side of the ν_3 band.

Observed (cm^{-1})	Calculated (cm^{-1})	Corresponding interaction energy (cm^{-1}) (transition dipoles)	type of cluster
1253.01	1252.95	0.20	n.n. pair
	1252.99	0.24	n.n. pair
	1253.05	0.30	n.n. pair
	1253.08	0.33	n.n. pair
	1252.91	0.16	open triplet
1254.00	1253.94	1.19	closed triplet
1255.06	1255.23	2.48	n.n. pair
	1255.30	2.55	n.n. pair
	1254.99	2.24	open triplet
	1255.05	2.30	open triplet
	1254.89	2.14	triplet (3rd type)
1256.07	1256.11	3.36	open triplet
1257.16	-		
1258.97	1258.90	6.15	closed triplet
	1259.34	6.59	triplet (3rd type)
	1258.89	6.14	triplet (3rd type)
1259.92	1259.93	7.18	open triplet
	1252.86	0.11	2nd n.n. pair
	1253.65	0.90	2nd n.n. pair

continued ....

Observed (cm^{-1})	Calculated (cm^{-1})	Corresponding interaction energy (cm^{-1}) (transition dipoles)	type of cluster
-	1255.62	2.87	open triplet
	1255.56	2.81	open triplet
	1255.61	2.86	triplet(3rd type)
	1255.71	2.96	triplet(3rd type)
-	1256.42	3.67	n.n. pair
	1256.36	3.61	closed triplet
	1256.48	3.73	closed triplet
-	1256.76	4.01	open triplet
-	1263.76	11.01*	closed triplet

* Observed by Narayanamurti et al (1966) at 1265 cm^{-1}.

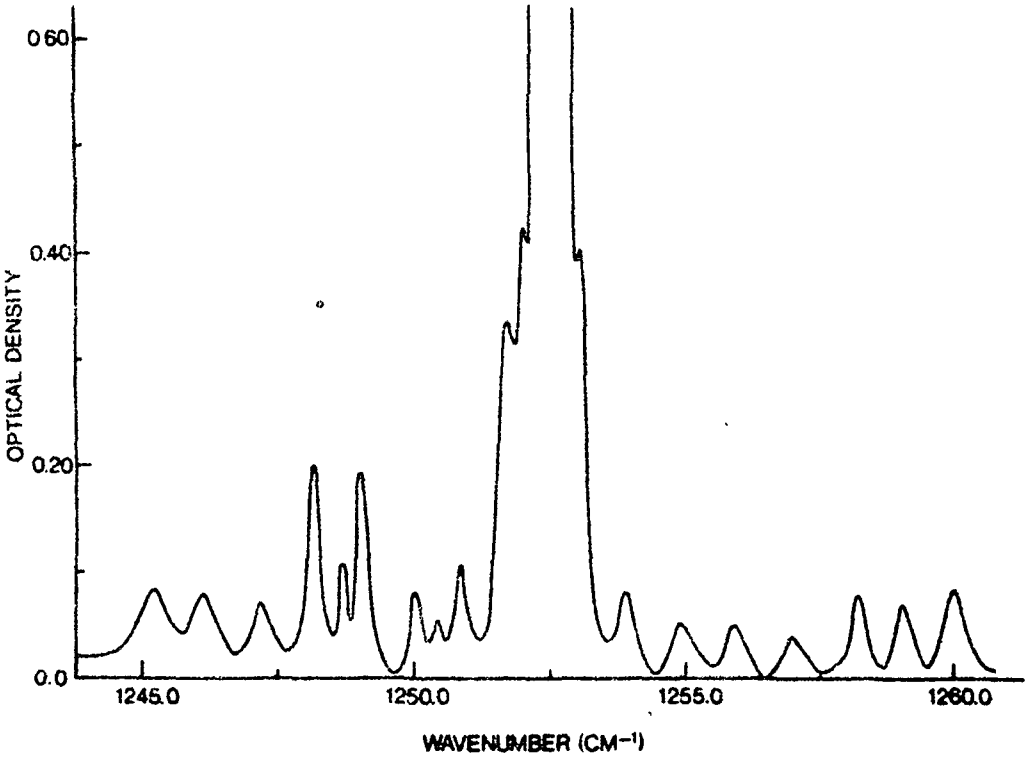

Figure 5.1 Infrared absorption spectrum of a 1mm thick KI crystal containing approximately 10^{19} NO_2^- ions cm^{-3} at 1.7 K in the ν_3 fundamental region; spectral resolution is about 0.05 cm^{-1}.

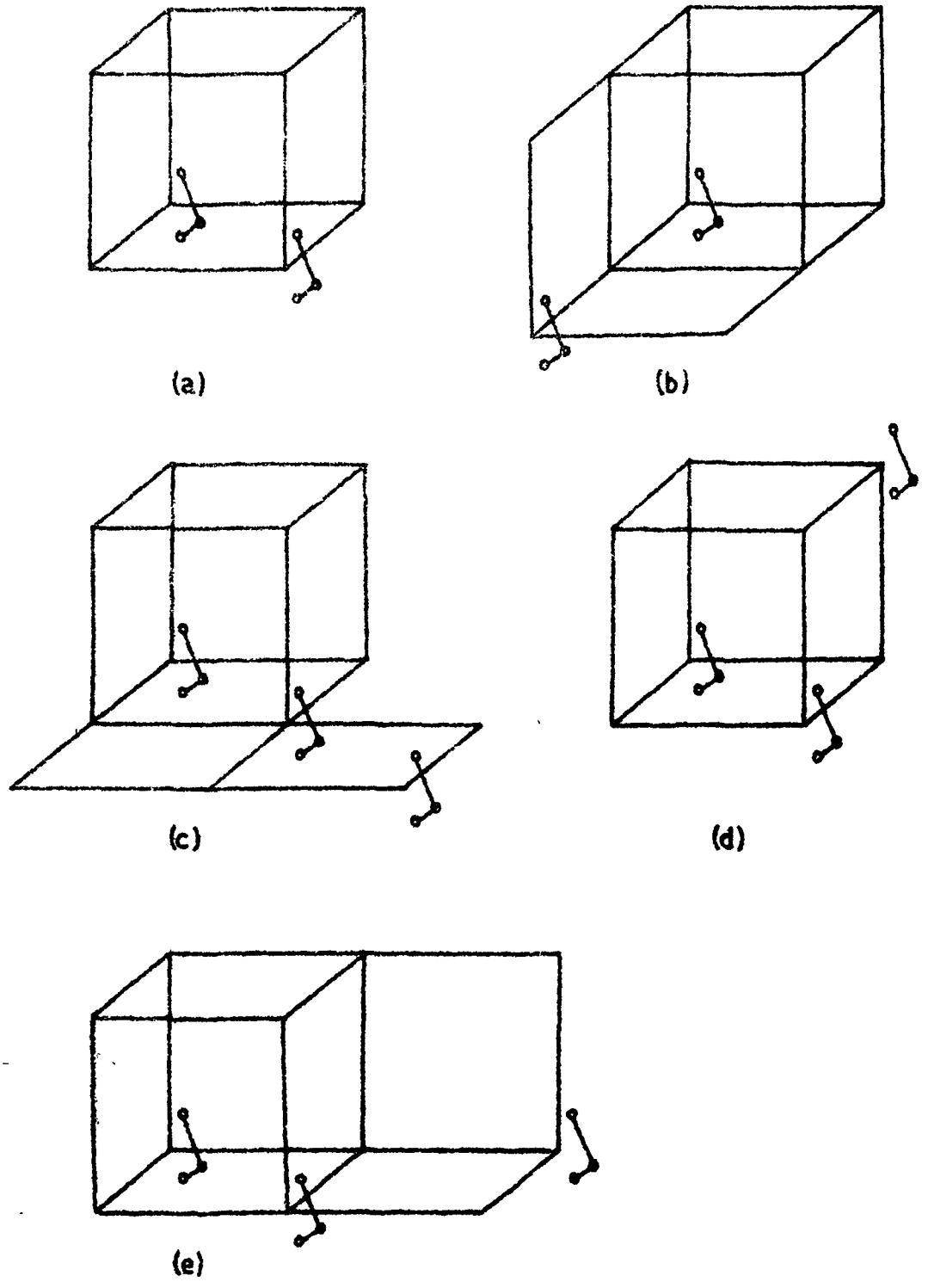

Figure 5.2 Different types of pairs and triplet clusters of the NO_2^- ions in KI single crystal. (a) n.n. pair, (b) second n.n. pair, (c) open-triplet cluster, (d) closed-triplet cluster, and (e) triplet cluster of third type.

CHAPTER VI

TEMPERATURE DEPENDENCE OF HALF-WIDTH AND FREQUENCY SHIFT OF THE GAP MODE OF THE NO_3^- ION IN KI.*

ABSTRACT

The temperature dependence of the half-width and centre frequency of the ν_3 fundamental vibration and its combination with the low frequency gap mode of the NO_3^- ion doped in KI single crystals has been investigated from 1.7 to 77 K. From this study, detailed information about the variation of the half-width and centre frequency of the gap mode as a function of temperature has been obtained which can be satisfactorily explained in terms of anharmonic interactions of the gap mode with the host lattice phonons.

---

* Paper based on this study has appeared: S.S. Khatri and A.L. Verma 1982 J. Phys. C: Solid State Phys. 15, 1143.

6.1 INTRODUCTION

There has been considerable amount of work done, both experimental and theoretical, on the temperature dependence of the width, position and intensities of local and resonant modes of several substitutional impurities in alkali halides as reviewed in chapter II (Barker and Sievers 1975). Such studies can provide useful information about the interactions between the localized modes and the lattice phonons. In contrast, hardly any such studies have been reported on gap modes, although gap modes have been observed by several workers in the past. The reason as mentioned in chapter I is that the difference band absorption of the host lattice dominates the spectral region near the gap and thus filling this region at temperatures above around 10 K. Therefore it is extremely important to explore the temperature dependent characteristics of gap modes in suitable systems and see whether similar anharmonic interactions (which are responsible for such properties of local and resonant modes) could explain the observed phenomenon.

6.2 EXPERIMENTAL RESULTS

The infrared spectrum of nitrate ion in KI between 1300 and 1500 cm^{-1} at 4.2 K has been reported and its complicated structure has been interpreted satisfactorily

(Eijnthoven and Vander Elsken 1969). For the present studies, the important features of the spectra are the ν_3 fundamental of the $^{14}NO_3^-$ ion at 1372.50 cm^{-1}, that of the $^{15}NO_3^-$ ion at 1340.60 cm^{-1}, appearing in the spectrum due to natural accurance of the ^{15}N isotope, and the combination of the former band with the 72.92 cm^{-1} gap mode at 1445.42 cm^{-1}. The frequencies of all these bands are reported as measured at 4.2 K. We have measured the temperature dependence of the last two bands mentioned above from 1.7 to 77 K. The low intensity sharp band due to the ν_3 fundamental of the $^{15}NO_3^-$ isotopic species monitors the frequency shift and width of the internal vibration especially when the 1372.5 cm^{-1} band of the $^{14}NO_3^-$ isotope is too intense to be measured accurately with the same crystal. Figure 6.1 shows the spectrum of the NO_3^- ion in KI in the combination band region at 4.2K recorded with an instrumental resolution of 0.05 cm^{-1}. The water vapour band at 1465.01 cm^{-1} was used to monitor the frequency shift of the combination band. Both combination and internal vibration bands show Lorentzian lineshapes and gap modes are known to give Lorentzian lineshapes.

The temperature dependent characteristics of the combination band has been attributed to the sum of such characteristics of the ν_3 fundamental and the gap mode. The band-width and frequency shift of the ν_3 fundamental

of the $^{15}NO_3^-$ ion were substracted from those of the combination band at the same temperature to get these quantities for the gap mode. The frequency shift and band-width of the ν_3 fundamental of the $^{15}NO_3^-$ ion at a particular temperature are taken as the zero point for the frequency shift and band-width of the combination band at the same temperature and the difference is taken as arising from the temperature-dependent effects of the gap mode. With increasing temperatures, band-width of the gap mode increases whereas its frequency decreases. We have assumed that the residual band-width at 0 K is also Lorentzian and the temperature-dependent characteristics of the ν_3 fundamentals of the $^{14}NO_3^-$ and $^{15}NO_3^-$ species are identical.

6.3 DISCUSSION

Pure potassium iodide crystal has a gap between acoustical and optical phonon branches and lattice vibrations of frequencies between 69.7 and 95.6 cm^{-1} do not occur. When the I^- ion is replaced by the NO_3^- ion, two gap modes at 72.92 $\pm$ 0.05 and 87.95 $\pm$ 0.05 cm^{-1} appear but no temperature-dependent studies were ever made on this or any other system. In this work we have studied the temperature dependence of half-width and frequency shift of the 72.92 cm^{-1} gap mode in KI and have attempted to explain these properties in terms of various anharmonic

interactions of the gap mode with lattice phonons. These anharmonic interactions give rise to scattering of phonons by the gap mode and its decomposition into lattice phonons, and anharmonic interactions between the lattice phonons itself causing thermal expansion of the lattice (Khatri and Verma 1982).

6.4 HALF-WIDTH

We have considered basically two mechanisms responsible for increase in the band-width of the gap mode at higher temperatures' decomposition processes and scattering processes as discussed in chapter II. In the decomposition process the gap mode excited state decays into one or more lattice phonons. Decay into one lattice phonon is not possible for the 73 cm^{-1} gap mode from requirements of conservation of energy. The most probable mode of decay for the low frequency gap mode (72.92 cm^{-1}) of the NO_3^- ion in KI will involve two phonons. The temperature dependence of the half-width due to two phonon decay will have the form given by expression 2.21. For all possible two phonon decays, it can be written as a sum (Bauerle 1973)

$$\Delta\Gamma_g = 18\pi \sum_{i,j} |V_3(g,i,j)|^2 (n_i + n_j + 1)\,\delta(\omega_g - \omega_i - \omega_j) \qquad \cdots (6.1)$$

where delta function expresses the necessary energy conservation. The above expression can also be written as

$$\Delta\Gamma_g = A \sum_{i,j} \omega_i \omega_j (n_i + n_j + 1)\, \delta(\omega_g - \omega_i - \omega_j) \quad \cdots (6.2)$$

A is a constant. In Debye approximation for lattice phonons, it can be written as

$$\Delta\Gamma_g = \left[\frac{kT}{\nu_m ch}\right]^5 C \int_0^{\nu_m ch/kT} x^3 \left(\frac{\Omega ch}{kT} - x\right)\left(\frac{1}{e^x - 1} + \frac{1}{\exp\left(\frac{\Omega ch}{kT} - x\right) - 1} + 1\right) dx \quad \cdots (6.3)$$

where $\nu_m = 69.7\ cm^{-1}$ is the maximum frequency of the acoustic band, $\Omega = 72.92\ cm^{-1}$ is the gap mode frequency and $X = \frac{h\nu}{kT}$. This process predicts a constant value at low temperatures and a linear dependence on T at higher temperatures. We have calculated the contribution of two phonon decay processes to the width from equation (6.3) in terms of constant C which gave a significant contribution to the half-width in the temperature range of interest.

At slightly higher temperatures, another fourth order process takes over which may be described as scattering

of lattice phonons by the gap mode leading to fluctuations in the gap mode state (Elliot et al 1965 and Alexander et al 1970). Scattering processes give a contribution to the half-width in Debye approximation, this is given by expression (2.24) which is:

$$\Delta\Gamma_g' = \beta \left[\frac{T}{\theta_D}\right]^7 \int_0^{\theta_D/T} \frac{x^6 e^x}{(e^x - 1)^2} \, dx$$

where β is a coupling constant and is positive and θ_D is the effective Debye cut off frequency as explained in chapter II. This process predicts a T^2 dependence in the high temperature limit and T^7 dependence in the low temperature limit. The total half-width is given by the sum of (6.3) and (2.24). The constants C, β , and θ_D were adjusted by non-linear parameterization in the least square fitting. Values of C = 0.191 cm^{-1}, β = 0.275 cm^{-1}, and θ_D= 24 K gave the best fit to the experimentally determined half-width which are shown in figure 6.2.

6.5 FREQUENCY SHIFT

Here again, we considered thermal expansion of the lattice and the elastic scattering of phonons by gap modes as major contributions to the frequency shift of the gap mode

as a function of temperature. The temperature dependent frequency of the gap mode arising from thermal expansion of the lattice is given by an expression (2.26) which is:

$$\Delta\nu_{th} = 3\frac{\Delta a}{a(o)}\alpha_{gap}(A_{1g})$$

The meanings of the symbols are already explained in chapter II. Data for lattice parameter a(T) was taken from Landolt-Bornstein (1973). The hydrostatic strain coupling constant $\alpha_{gap}(A_{1g})$ can be calculated from the frequency-stress derivatives for the ν_3 fundamental of the $^{15}NO_3^-$ in KI and the combination band $[\nu_3(^{14}NO_3^-)$ + gap mode$]$ under uniaxial stress (Bruining and Van der Elsken 1975, Bauerle 1973). The lattice parameter was fitted to the expression

$$a(T) = a(o) + a_1T + a_2T^2$$

or

$$a(T)-a(o) = a = a_1T + a_2T^2 \quad \ldots \quad (6.4)$$

where a(o) =6.994 Å, $a_1 = 1.016 \times 10^{-5}$ Å K^{-1} and $a_2 = 1.573 \times 10^{-6}$ Å K^{-2}. For calculating $\alpha_{gap}(A_{1g})$ the equations relating frequency-stress derivatives $\frac{\Delta\nu}{\Delta P}$ and various strain coupling constants for various directions of applied stress and polarization of radiation are used (Bauerle 1973). The two equations for determining

$\alpha_{gap}(A_{1g})$ are

$$-\frac{\Delta\nu}{\Delta P}(\vec{P}\,[111]\;\vec{E}\,[111]) = \alpha(A_{1g})(S_{11}+2S_{12})+\frac{2}{3}\gamma(T_{2g})S_{44} \quad \ldots \quad (6.5)$$

$$-\frac{\Delta\nu}{\Delta P}(\vec{P}\,[111]\;\vec{E}[1\bar{1}0]) = \alpha(A_{1g})(S_{11}+2S_{12})-\frac{2}{3}\gamma(T_{2g})S_{44} \quad \ldots\ldots \quad (6.6)$$

$\alpha(A_{1g})$ is as defined above for gap mode which is $\alpha_{\nu_3}(A_{1g})$ for the fundamental and $\alpha_{(\nu_3+gap)}(A_{1g})$ for the combination band and $\gamma(T_{2g})$ is the strain coupling constant related to the distortion of T_{2g} symmetry of the lattice in the O_h point group of KI crystal. $S_{11} = 38.3 \times 10^{-13}cm^2$ $dyne^{-1}$, $S_{12} = -5.4 \times 10^{-13}cm^2dyne^{-1}$ and $S_{44}=270 \times 10^{-13}cm^2$ $dyne^{-1}$ are the elastic bulk compliances (Landolt-Bornstein 1969) for pure KI. Equation (6.5) is for the stress $\vec{P}$ in the [111] direction and electric vector $\vec{E}$ of light in the [11$\bar{1}$] direction and equation (6.5) is for $\vec{P}$ in the [1$\bar{1}$1] direction and $\vec{E}$ in the [1$\bar{1}$0] direction. $\frac{\Delta\nu}{\Delta P}(\vec{P}[111], \vec{E}[111])$ is $2cm^{-1}$/Kbar and 1.67 cm^{-1}/Kbar for the ν_3 fundamental and the combination band (ν_3 + gap mode) respectively (Bruining and Van der Elsken 1975) and $\frac{\Delta\nu}{\Delta P}(\vec{P}[11\bar{1}], \vec{E}[1\bar{1}0])$ is $1cm^{-1}$/Kbar and 1.29 cm^{-1}/Kbar for the ν_3 fundamental and the combination band respectively (Bruining and Van der Elsken 1975). Using these values, $\alpha_{(\nu_3+ gap)}(A_{1g})$ and

and $\alpha_{\nu_3}(A_{1g})$ can be found from equations (6.5) and (6.6). We get

$$\alpha_{(\nu_3 + gap)}(A_{1g}) = - 538.182 \text{ cm}^{-1}$$

and $$\alpha_{\nu_3}(A_{1g}) = - 545.455 \text{ cm}^{-1}$$

therefore $$\alpha_{gap}(A_{1g}) = \alpha_{(\nu_3 + gap)}(A_{1g}) - \alpha_{\nu_3}(A_{1g}) = 7.273 \text{cm}^{-1}$$

using these values, the contribution of lattice thermal expansion to the frequency shift of the 73 cm^{-1} gap mode has been calculated from equation (2.26) and is shown as a broken curve in figure 6.3. This shows a decrease in the frequency of the gap mode with increasing temperature.

The major contribution to shift in the centroid frequency of the gap mode with temperature can be attributed to the elastic scattering of the lattice phonons by the gap mode which in Debye approximation is given by expression (2.25) as:

$$\Delta\nu_{sc} = \delta\left[\frac{T}{\theta_c}\right]^4 \int_0^{\theta_c/T} \frac{x^3}{e^x - 1}\, dx$$

This varies as T^4 in the low temperature limit and as T in the high temperature limit. The values of the coupling coefficient δ, and the effective Debye temperature θ_c needed to predict the additional frequency shift (shown by the dotted curve in figure 6.3) to agree with experimental

results are $\delta = 0.51$ cm^{-1} and θ_C comes out to be very close to 24 K as we have obtained for θ_D. Therefore, we have taken θ_C = 24 K. The full curve (figure 6.3) shows the sum of the contributions due to scattering and thermal expansion, i.e., the total frequency shift $[\Delta\nu = \nu_{gap}(0) - \nu_{gap}(T)]$ which is in reasonable agreement with the experimentally observed behaviour. Therefore similar anharmonic processes are responsible for the temperature-dependent effects for the gap modes which are responsible for local modes.

The increase in the half-width of the gap mode at higher temperatures can be explained in terms of the scattering and decomposition processes. The scattering mechanism dominates at higher temperatures but the two phonon-decay process contributes significantly at low temperatures. The decrease in the frequency of the gap mode with increase in temperature can be explained in terms of the scattering processes and thermal expansion of the lattice. The contribution of lattice thermal expansion is quite small compared to that of the scattering processes at all temperatures.

We have obtained the values of θ_D and θ_C as 24 K. This implies similar phonon distributions active in the contributing physical processes. The value 24 K for θ_D and θ_C indicates coupling to only long wavelength acoustic phonon modes. The values of the coupling constants β and δ are obtained as 0.275 cm^{-1} and 0.51 cm^{-1} respectively.

These are small compared to those obtained for in-band resonant modes. This indicates that the gap modes couple weakly to the lattice phonons compared to the in-band resonant modes.

REFERENCES

1. Alexander R.W. Jr., Hughes A.E. and Sievers A.J. 1970 Phys. Rev. B1, 1563.

2. Barker A.S. Jr. and Sievers A.J. 1975 Rev. Mod. Phys. 47, Suppl. 2, S1.

3. Bauerle D. 1973 Springer Tracts in Modern Physics 68, 76.

4. Bruining J. and Van der Elsken J. 1975 Phys. Rev. B11, 5123.

5. Eijnthoven R.K. and Van der Elsken J. 1969 Phys. Rev. Lett. 23, 1455.

6. Elliot R.J., Hayes W., Jones G.D., Macdonald H.F. and Sennett C.T. 1965 Proc. Roy. Soc. A289, 1.

7. Khatri S.S. and Verma A.L. 1982. J. Phys. C: Solid State Phys. 15, 1143.

8. Landolt-Bornstein New Series 1969 Group III Vol. 2 ed. K-H Hellwege (Berlin:Springer) p5.

9. Landolt-Bornstein New Series 1973 Group III Vol. 7a ed. K-H Hellwege (Berlin:Springer) p585.

able VI.1. Half-width $\Delta\Gamma$ of the 73 cm^{-1} gap mode of the O_3^- ion in KI.

emperature T(K)	Half-width in cm^{-1}	Temperature T(K)	Half-width in cm^{-1}
1.7	0.15	43.0	0.35
4.2	0.16	43.5	0.36
5.5	0.17	50.5	0.40
7.0	0.18	52.5	0.38
10.0	0.185	55.0	0.45
11.0	0.19	58.0	0.48
14.5	0.20	60.0	0.55
16.0	0.195	60.5	0.57
20.5	0.21	62.5	0.575
21.5	0.225	65.0	0.58
25.0	0.25	67.5	0.65
27.5	0.24	70.0	0.70
31.0	0.27	74.0	0.715
32.0	0.26	75.0	0.74
36.0	0.32	77.5	0.775
37.5	0.29		

Table VI.2. Frequency shift $\Delta\nu$ of the 73 cm^{-1} gap mode of the NO_2^- ion in KI.

Temperature T(K)	Frequency shift in cm^{-1}	Temperature T(K)	Frequency shift in cm^{-1}
1.7	0.00	50.5	0.31
4.2	0.02	52.5	0.28
5.0	0.04	55.0	0.34
10.0	0.05	58.0	0.38
14.5	0.06	60.0	0.395
20.5	0.08	62.5	0.45
25.0	0.105	65.0	0.40
32.0	0.20	70.0	0.49
37.5	0.22	74.5	0.52
43.0	0.25	77.0	0.475

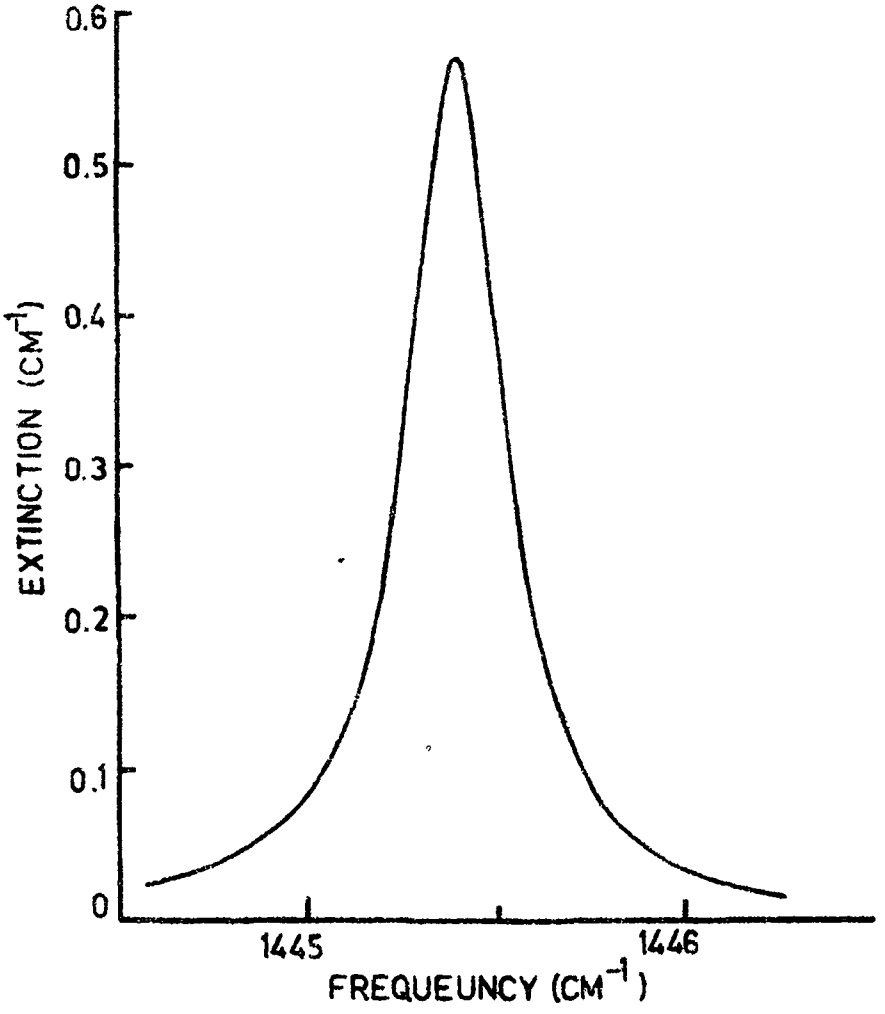

Figure 6.1 Infrared absorption spectrum of a 10 mm thick crystal containing approximately 10^{17} NO_3^- ions cm^{-3} at 4.2 K in the ν_3 and gap mode region; spectral resolution is about 0.05 cm^{-1}.

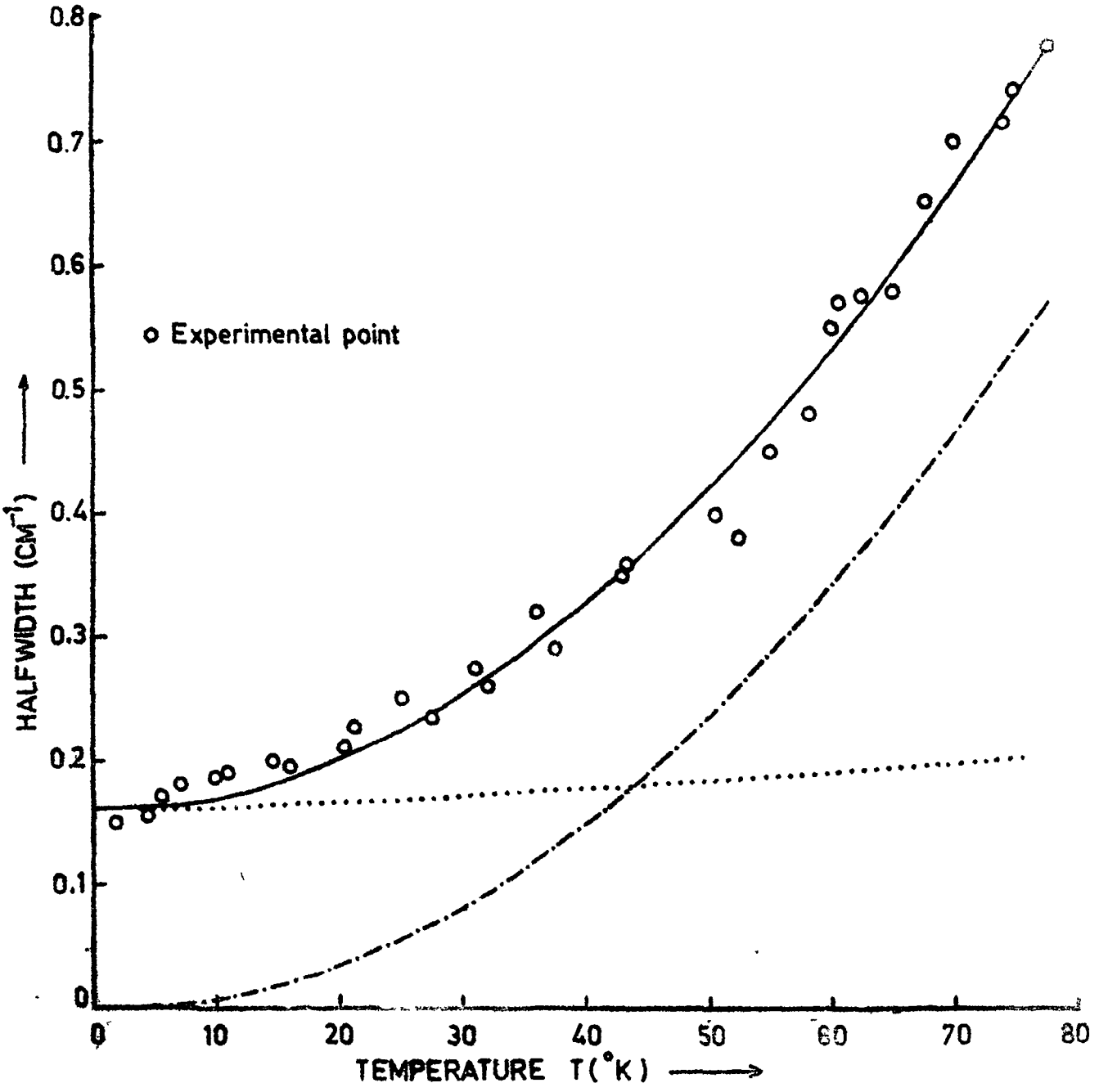

Figure 6.2 Temperature dependence of the halfwidth of the gap mode. The dotted curve represnts the calculated contribution of the two-phonon decay along with the temperature independent contributions due to local strain etc. The chain curve represents the contribution from the phonon scattering process with $\theta_D = 24$ K. The full curve is the resultant of the other two curves.

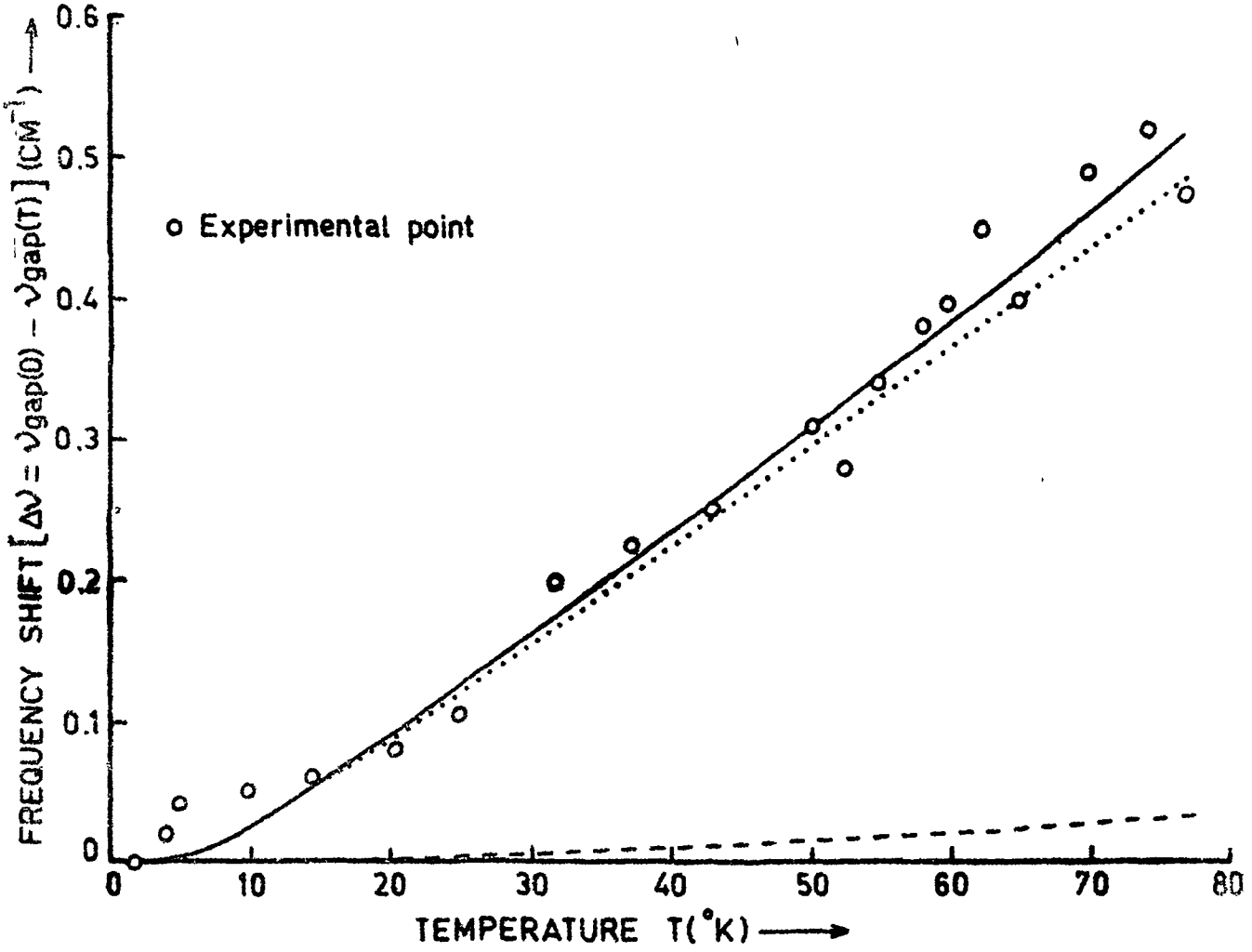

Figure 6.3 Temperature dependence of the frequency shift $\Delta\nu = \nu_{gap}(0) - \nu_{gap}(T)$ for the 73cm^{-1} gap mode. The broken curve represents the contribution from lattice thermal expansion. The dotted curve represents the contribution from the phonon scattering process with $\theta_c = 24$ K. The full curve is the resultant of the other two curves.

CHAPTER VII

CONCLUSIONS

In chapter I, we have outlined the unresolved controversies about the motional states of the NO_2^- and NO_3^- ions doped in KI single crystals. In spite of several studies made on the KI:NO_2^- system, the motional states and pair modes of the NO_2^- ion in KI could not be resolved experimentally by earlier workers and therefore this system was very poorly or wrongly understood. Moreover, there was no temperature-variation study reported earlier on the gap modes of any system and therefore the mechanism of interaction of gap modes with host lattice phonons was unclear. In this chapter, we have outlined the importance of the studies undertaken in this dissertation and have been able to understand these systems rather satisfactorily.

We have given general experimental and theoretical background in chapter II in order to understand the different kind of motional states and localized modes of ions substituted in alkali halides. Different theoretical models have been described and important experimental techniques to probe these motional states have been discussed. By and large, the infrared techniques have yielded much more information than any other technique in this field.

Chapter III deals with the techniques of sample preparation, modified instrumental arrangement to attain higher resolution and the helium cooled detector etc. It is evident that in order to resolve the closely-spaced lines and probe subtle effects, a very careful preparation and choice of samples and use of proper experimental arrangement is extremely important.

In chapter IV we have studied the tunneling motion of the NO_2^- ion in KI. Our studies show that the experimental result for the tunneling of the NO_2^- ion in KI host can be understood quite satisfactorily on the basis of the GBK model. From the present study, it is evident that the motional states of the NO_2^- ion in KI lattice are very complex compared to that in other alkali halide hosts. In other alkali halide hosts, such as KCl (Narayanamurti et al 1966), motional states of the NO_2^- ion can be understood in terms of rotations of the ion about the three principal axes (a,b,c) since the centre of mass of the NO_2^- ion coincides with the centre of the cavity. However, in the KI lattice, because of the displacement of the centre of mass of the ion, the picture appears more complicated. The tunneling motion of the ion in KI is not merely rotational in character but is a combination of translation and rotation. The tunneling of the NO_2^- ion among various equivalent wells in KI is similar to that of monatomic off-centred ions. The tunneling motions

of the ion associated with the matrix elements μ and σ can be understood in terms of rotations about the a and c axes respectively along with translational motion, but in case of η and ν , it is much more complex.

In the present studies we have found that the matrix element μ (90° tunneling) is the largest, σ (180° tunneling) also contributes significantly whereas η (60° tunneling) is less important and the contribution from ν (120° tunneling) is almost negligible. In these calculations we have not considered the effect of lattice distortions around the NO_2^- ion in KI. The effect of distortion is to renormalize the tunneling matrix elements (Shore and Sander 1975). During the tunneling motion the distortions must follow the impurity motion. In case of the NO_2^- ion in KI it is possible that for the 60° and 120° tunnelings the distortion may not follow the impurity motion and hence making these tunnelings less probable .

Using one-dimensional approximation for tunneling, barrier heights associated with different types of tunneling motions have been calculated. The barrier heights obtained here are large compared to those obtained for the NO_2^- ion in other alkali halides by Narayanamurti et al (1966) which is mainly due to the complex nature of tunneling motion of the NO_2^- ion in KI. In the present study, our aim was to understand the tunneling behaviour of the ion

in KI and could understand this complex behaviour quite satisfactorily with the available experimental data. Higher frequency librational modes for the KI:NO_2^- system are predicted and their observation could lend further support for the model used in this study.

In chapter V, we saw the effect of increasing the concentration of the NO_2^- ions in KI. Many sharp bands appear near the ν_3 fundamental of the NO_2^- ion in KI. The origin of these bands was satisfactorily explained on the basis of a model of coupled harmonic oscillators where the coupling is brought about by the interactions between the transition dipole moments of the ions during their ν_3 vibration. From this study we could estimate the magnitude of the transition dipole moment of the NO_2^- ion during ν_3 vibration to be μ_t = 0.248 Debye which is small compared to those obtained for other systems like the NO_3^- ion in KNO_3 and CO_3^{-2} ion in $CaCO_3$, $SrCO_3$ and $BaCO_3$. In these systems the value of the induced dipole moments range from 1.48 to 1.9 Debye. The small value of transition dipole moment of the NO_2^- ion in KI can be correlated with weaker intensity of the ν_3 fundamental vibration of the NO_2^- ion compared to other ions quoted above. Small value of μ_t for the NO_2^- ion in KI would also provide rather weaker coupling between nearby ions in pairs and triplet clusters giving rise to closely-spaced lines.

In the earlier studies on the KI:NO_2^- system with large concentrations of the NO_2^- ions in KI ($\sim 10^{19}$ ions cm^{-3}), Narayanamurti et al (1966) were not able to oberve these bands. However, they observed few bands at higher frequencies but could not understand the origin of those bands. From the present studies, it is evident that these well-resolved bands arise due to mutually interacting ions in pairs and triplet clusters. From this study, the importance of high resolution work is evident for proper understanding of the often observed broad bands and complicated structures near fundamental vibrations of molecular ions in solids.

In chapter VI we have studied the temperature dependence of the half-width and frequency of the 73 cm^{-1} gap mode of the NO_3^- ion in KI. We could explain these effects in terms of various anharmonic interactions of the gap mode with lattice phonons. From the present studies it is evident that out of the two line-broadening mechanisms for the gap mode, the scattering mechanism dominates at higher temperatures while the two-phonon decay mechanism contributes significantly at low temperatures. Major contribution to the frequency shift of the gap mode comes from scattering mechanism at all temperatures while contribution from thermal expansion is very small upto 77 K. Both of the processes decrease the frequency of the gap mode with increase in temperature.

The effective Debye temperatures needed to fit the calculated values of different contributions to the line-width and frequency shift with the experimental data indicates a limit to the distribution of phonons taking part in the particular mechanism under consideration. The best value of the effective Debye temperature to explain the frequency shift and half-width of the gap mode is obtained as 24 K. This implies a participation of similar type of phonon distribution of the host lattice in the contributing physical processes. The values of the coupling coefficients to explain the data for the gap mode of the NO_3^- ion in KI are $\beta = 0.275\ cm^{-1}$ and $\delta = 0.51\ cm^{-1}$. For comparison purposes with the in-band resonant modes in systems like $KBr:Li^+$, $NaCl:Cu^+$, $KI:Ag^+$ etc. (Alexander et al 1970), the values of effective Debye temperatures for these systems vary from 25 to 33 K, coupling constant β from 2 to 12 cm^{-1} and δ from 1 to 3 cm^{-1}. Smaller values of the coupling constants β and δ for the gap mode of the NO_3^- ion in KI compared with the in-band resonant modes of these quoted systems indicate that the resonant modes couple more strongly to the lattice phonons than the gap modes. Near similarity of the effective Debye temperatures in all these systems for gap and resonant modes suggests that they couple to nearly a similar type of distribution of long wavelength acoustic phonons of the host lattice.

REFERENCES

1. Alexander R.W. Jr. Hughes A.E. and Sievers A.J. 1970 Phys. Rev. B1, 1563.

2. Narayanamurti V., Seward W.D. and Pohl R.O. 1966, Phys. Rev. 148, 481.

3. Shore H.D. and Sander L.M. 1975 Phys. Rev. B12, 1546.